Studies of E2s Related to Unconventional Ubiquitination in *Arabidopsis thaliana*

A Thesis Submitted to the College of

Graduate and Postdoctoral Studies

In Partial Fulfillment of the Requirements

For the Degree of Doctor of Philosophy

In the Department of Biochemistry, Microbiology and Immunology

University of Saskatchewan

Saskatoon

By

Sheng Wang

PERMISSION TO USE

In presenting this thesis in partial fulfilment of the requirements for a Postgraduate degree from the University of Saskatchewan, I agree that the Libraries of this University may make it freely available for inspection. I further agree that permission for copying of this thesis in any manner, in whole or in part, for scholarly purposes may be granted by the professor or professors who supervised my thesis work or, in their absence, by the Head of the Department or the Dean of the College in which my thesis work was done. It is understood that any copying or publication or use of this thesis or parts thereof for financial gain shall not be allowed without my written permission. It is also understood that due recognition shall be given to me and to the University of Saskatchewan in any scholarly use which may be made of any material in my thesis. Requests for permission to copy or to make other use of material in this thesis in whole or part should be addressed to:

Dean
College of Graduate and Postdoctoral Studies
University of Saskatchewan
116 Thorvaldson Building, 110 Science Place
Saskatoon, Saskatchewan S7N 5C9
Canada

Head
Department of Biochemistry, Microbiology and Immunology
University of Saskatchewan
107 Wiggins Road
Saskatoon, Saskatchewan, S7N 5E5
Canada

ABSTRACT

Protein ubiquitination, a fundamental protein modification cascade, is catalyzed by three types of enzymes referred to as E1 for ubiquitin (Ub) activation, E2 for Ub conjugation and E3 for Ub ligation. Arabidopsis has 37 E2 genes and functions for most of them remain largely unknown. Further, although the conventional Lys48-linked protein ubiquitination is well known for its function in protein degradation, functions for protein ubiquitination linked through other lysine residues of Ub, e.g. Lys11 and Lys63 are poorly understood in plants. This study aims to advance the understanding of the functions of Arabidopsis E2s involved in the unconventional ubiquitination. Previously, UBC13A/B have been identified as the E2 for Lys63-linked polyubiquitination, and *ubc13* mutant plants display strong phenotypes in root development. In this study, a family of six E3s that can interact with UBC13 were identified, and when a subgroup of three genes were inactivated, the T-DNA mutants showed a glucose-sensitive phenotype suggesting their possible role in sugar signaling. It has been proposed that in root development UBC13 may control the level of Aux/IAA (Auxin/indole-3-acetic acid) proteins which regulate the activity of auxin response factors (ARFs). Several *ARFs* were evaluated, and overexpression of *ARF6* enhanced the root hair growth in WT plants and partially rescued the root phenotypes of the *ubc13* mutant. A major part of this study was on Arabidopsis UBC22, a sole member of an Arabidopsis E2 subfamily. Results from the phylogenetic analysis and *in vitro* ubiquitination assay indicate that UBC22 is an E2 for Lys11-linked ubiquitination in plants. The *ubc22* knockout mutant had much reduced seed setting, and further analysis showed that UBC22 plays a critical role in the formation of

functional megaspore and female gametophyte. Moreover, certain *ubc22* mutant plants showed distinct phenotypes in vegetative development. The RNA-seq analysis revealed that genes of different pathways were differentially affected in different subtypes of plants. Plants of one subtype had increased expression of genes in pathogen defense and showed an enhanced resistance to a plant pathogen. Therefore, the present results have provided a new understanding on the function of UBC13, identified UBC22 as a novel E2, and revealed its multiple functions in plants.

ACKNOWLEDGEMENTS

I would like to sincerely thank my supervisor Dr. Hong Wang for his continuous support and encouragement during my study. Dr. Wang guided me all through these years and provided me with inspiration and direction for my research.

I would like to thank my committee members, Dr. Patrick Covello, Dr. Raju Datla, Dr. Jeremy Lee, Dr. Yangdou Wei and Dr. Yuliang Wu as well as the external examiner, Dr. Rongming Zhao, for their valuable feedback and suggestions.

I would like to thank the members of Dr. Wang's laboratory: Dr. Ling Cao for the help with some of the microscopic work; Liang Zhao for helping with real-time quantitative PCR analysis for Figure 5.4; Keke Li for the help with the work for Figure 3.10B and C; Feng Hui, as well as the lab members, for the help of taking care of my plants when I was away from the lab.

I would like to thank Dr. Qiang Li for the help of analyzing RNA-seq data for Figure 5.4B and C; Dr. Yangdou Wei for providing the plant pathogen strains; and Dr. Xinliang Ma for the initial help with the CRISPR system.

I would like to thank the Department of Biochemistry, College of Medicine for the financial support for my study.

Finally, my special thanks would go to my parents and my wife Yuting Luo, for their loving considerations, constant encouragement, and great patience during my graduate studies.

TABLE OF CONTENTS

LIST OF TABLES

LIST OF FIGURES

LIST OF ABBREVATIONS

AD	DNA-activation domain
APC/C	anaphase-promoting complex/cyclosome
ARF	auxin response factor
At	*Arabidopsis thaliana*
ATP	adenosine 5'-triphosphate
BD	DNA-binding domain
CBB	Coomassie Brilliant Blue
CHIP	C-terminus of HSC70 interacting protein
CRISPR	clustered regularly interspaced short palindromic repeats
CRL	cullin RING E3 ligase
Cys	cysteine
Da	Dalton
DIC	differential interference contrast
DUB	de-ubiquitinating enzyme
E1/Uba	ubiquitin activating enzyme
E2/Ubc	ubiquitin conjugating enzyme
E3	ubiquitin ligase
ER	endoplasmatic reticulum
ERAD	ER-associated degradation
ERF	ethylene response factor
FM	functional megaspore
GFP	green florescent protein
Gly	glycine
GUS	β-glucuronidase
HA	human influenza hemagglutinin
HECT	homologous to the E6AP carboxyl terminus

His	Histidine
Lys	lysine
MMC	megaspore mother cell
MS	Murashige and Skoog
NF-κB	nuclear factor kappa-light-chain-enhancer of activated B cells
NLS	nuclear localization signal
OD	optical density
PCNA	proliferating cell nuclear antigen
PCR	polymerase chain reaction
PR	pathogenesis-related
PUB	plant U-box E3
PVDF	polyvinylidene difluoride
RBR	RING-BetweenRING-RING
RING	really interesting new gene
RUB	related to Ub
SCF	SKP-CUL1-F-box protein
SDS-PAGE	sodium dodecyl sulfate polyacrylamide gel electrophoresis
SUMO	small Ub-related modifier
Ub	ubiquitin
UBC	Ub-conjugating catalytic
UBD	Ub-binding domain
UBL	Ub-like protein
UEV	Ub-conjugating enzyme variant
UPL	Ub-protein ligase
YFP	yellow florescent protein

1. CHAPTER ONE - INTRODUCTION AND LITERATURE REVIEW

1.1. Overview of ubiquitin and ubiquitination

It is critically important for a cell or an organism that the levels of proteins particularly regulatory proteins are controlled according to temporal and spatial needs, and unnecessary or damaged proteins are removed in a timely fashion. Therefore, active and complex systems for protein degradation and removal have evolved. Studies on proteolysis in early 1980 revealed some of the key components in ATP-dependent proteolysis, referred to as APF1 (ATP-dependent Proteolysis Factor 1) and APF2, which were identified later as ubiquitin and the 26S proteasome, respectively (Wilkinson, 2005). The small protein, ubiquitin (Ub), can be attached to substrate proteins through a process called protein ubiquitination, rendering the substrates recognizable by the 26S proteasome for degradation. Since then, this protein modification process has attracted tremendous attention due to a very broad range of functions it plays in eukaryotic cells.

Ubiquitination is a process in which one or more units of Ub are attached to a substrate protein (Figure 1.1). It typically consists of three steps in forming an isopeptide bond between Ub and the substrate (Komander and Rape, 2012; Pickart, 2001). First, Ub is activated by a Ub-activating enzyme (Uba or E1) in the presence of ATP to form an E1-Ub thioester bond between an E1 cysteine (Cys) residue and the carboxyl-terminal glycine (Gly) of Ub. Then the activated Ub is transferred to a specific member of the Ub-conjugating enzyme (UBC or E2) family on its Cys residue to form an E2-Ub thioester bond. Finally, the E2-Ub conjugate donates its Ub to the target protein either by itself or through a Ub ligase

(E3). The number of E1, E2, and E3 in eukaryotic species displays a pyramid structure: one or two E1s, tens of E2s, and hundreds of E3s. The substrate specificity is generally believed to be conferred by E3 ligases. The product, in the end, is a Ub conjugate in which the C-terminal Gly carboxyl group of Ub is linked through an isopeptide bond to an amino group in the target protein. Typically a Lys ε-amino group serves as the target site. Ub can also be attached to serine and threonine residues through an ester bond, or the N-terminal amino group of a substrate protein through a peptide bond (Pickart and Eddins, 2004).

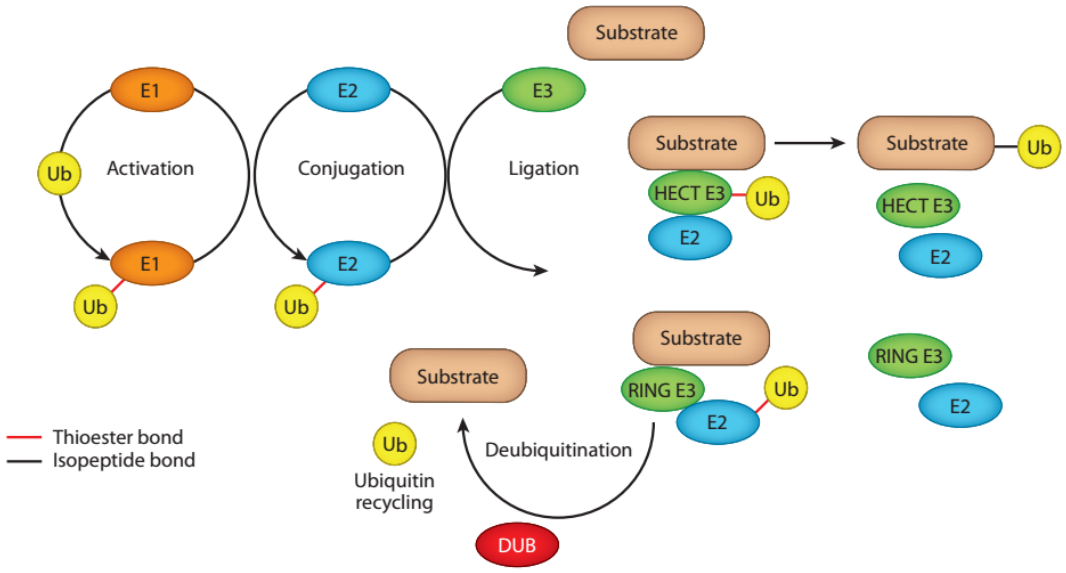

Figure 1.1 Enzymatic processes involved in the ubiquitination cascade. The coordinated activity of three types of enzymes: Ub-activating (E1), Ub-conjugating (E2), and Ub-ligating enzyme (E3 ligase) are required for Ub attachment to a substrate protein. Two different groups of E3 ligases (RING and HECT) are shown. The Ub can be transferred to the substrate directly by RING-type E3 and indirectly by HECT-type E3, in which a HECT E3-Ub intermediate conjugate is formed. Deubiquitinating enzymes (DUBs) can remove Ub from modified proteins to recycle Ub. The figure is from (Husnjak and Dikic, 2012) and used with permission.

A substrate protein can be ubiquitinated in several different ways. In mono ubiquitination, only one Ub is attached to a Lys residue of the target protein. The same target protein can be further ubiquitinated at additional sites, which is referred to as multi-monoubiquitination. In polyubiquitination, ubiquitination can occur repetitively at one site of the target protein, resulting in the formation of a Ub chain. After the substrate is ubiquitinated, it can be recognized by one of the many Ub-binding proteins which contain one or multiple Ub-binding domains (UBD) (Dikic et al., 2009). The well-known fate of a ubiquitinated protein is targeted degradation through the 26S proteasome. However, non-proteolytic functions of ubiquitination have been well documented, for instance in protein translocation and signal transduction (Adhikari and Chen, 2009). Ub or a Ub chain can also be removed from the substrate protein by de-ubiquitinating enzymes (DUBs) for another round of attachment.

1.2. Key components in the ubiquitination cascade

1.2.1. Ubiquitin protein

Ub is a small protein of 76 amino acids with a molecular weight of 8.5 kDa. The name "ubiquitin" (originally ubiquitous immunopoietic polypeptide) reflects its wide distribution in cells and also highly conserved nature among all eukaryotes (Wilkinson, 2005). The differences between animal, plant and fungal Ub are only two or three residues (Callis et al., 1995). This high degree of sequence similarity indicates functional conservation of the Ub protein throughout evolution and indeed Ub from distant species seem interchangeable. For instance, Arabidopsis Ub appears able to function normally in yeast (Ling et al., 2000). Ub is

highly stable with a compact β-grasp fold which has five β-strands grasping an α-helix diagonally and a flexible C-terminal tail (Figure 1.2A) (Vijay-Kumar et al., 1987). This compact arrangement explains the stable property of Ub, especially its resistance to heat.

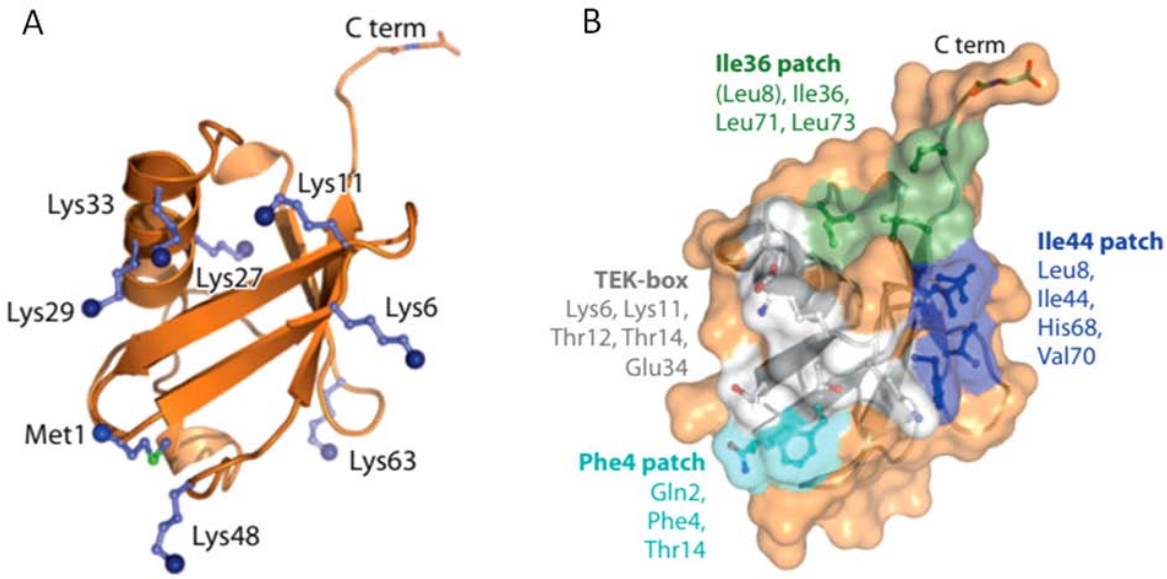

Figure 1.2 Structure of Ub. (A) A Ub structure showing the seven Lys and Met1 residues. The amino groups used in Ub chain are indicated by blue spheres. It has a core secondary structure consisting of five β-strands grasping an α-helix diagonally. (B) Different patches are shown on a Ub surface. Ile44 (blue), Ile36 (green), Phe4 patches (cyan), and TEK-box (white) are highlighted. The figure is modified from (Komander and Rape, 2012) and used with permission.

In addition, there are a number of Ub-like proteins (UBL) with a folded structure similar to Ub, and they can also be attached to substrate proteins. Two of the UBLs, NEDD8 (neuronal precursor cell-expressed developmentally downregulated protein 8) and SUMO (small Ub-related modifier) are the best known and studied, both of which play critical roles in eukaryotes. Similar to ubiquitination, NEDD8 and SUMO are attached to substrates through their own E1-E2-E3 reaction cascades and processes are referred to as neddylation or

sumoylation (Hay, 2005; Rabut and Peter, 2008).

The residues on Ub surfaces are highly conserved, suggesting that these residues may be critical for protein-protein interactions. Alanine scanning mutagenesis of yeast Ub revealed that 16 out of 63 Ub surface residues are essential (Sloper-Mould et al., 2001). These essential residues localize to three hydrophobic regions. One is the Phe4 hydrophobic patch containing Gln2, Phe4, and Thr12, and required for endocytosis (Figure 1.2B). The other one is the Ile44 hydrophobic patch including Leu8, Ile44, His68, and Val70, required for both endocytosis and proteasome degradation (Figure 1.2B). The Ile44 hydrophobic patch is bound by the 26S proteasome and most Ub-binding proteins. The third one, the Ile36 hydrophobic patch involving Leu71 and Leu73, can be recognized by Ub-binding proteins and also mediate interactions between Ub in a chain (Komander and Rape, 2012). There are other essential residues located in or near the C-terminal tail region, which are important for the attachment of Ub to substrates. The TEK-box of Ub, a motif including Lys6, Lys11, Thr12, Thr14, and Glu34, plays a key role in the mitotic degradation of cell cycle regulators (Jin et al., 2008).

The most important feature of Ub is that its seven lysines (Lys6, Lys11, Lys27, Lys29, Lys33, Lys48, and Lys63) and the N-terminus (Met1) can function as the sites for Ub attachment or Ub chain formation (Figure 1.2A). The C-terminus of a “donor” Ub can be covalently linked to a “receptor” Ub through the ε-amino group of one of the lysine residues or N-terminal amino group. Sequential attachment of Ub results in a Ub chain. Since each of the lysine residues can be used in forming the links, the complexity of Ub chain assembly is

extremely high. Different Ub-Ub linkages have distinct conformations and could be recognized by different Ub-binding proteins, possibly leading to diverse outcomes of ubiquitinated proteins. Ub linkage types involving all seven Lys and the N-terminal Met residues have been identified in yeast and mammalian cells (Meierhofer et al., 2008; Xu et al., 2009b). All lysine residues except for Lys27 are found to be located on the surface of Ub (Figure 1.2A). Since Lys27 is buried, Ub chain assembly through this residue may require conformation changes in Ub structure to expose the site.

1.2.2. Ub activation-enzyme (E1)

The E1 enzyme first binds to ATP and Ub, catalyzes C-terminal acyl-adenylation of Ub and then forms a thioester bond with Ub. Eventually, one of the E2 conjugating enzymes is recruited for further steps (Schulman and Harper, 2009).

Normally, there are only one or two E1s in each eukaryotic species. For instance, one E1 in yeast is encoded by the essential gene *UBA1*. The *uba1-206* mutant showed rapid depletion of Ub conjugates and other phenotypes (Ghaboosi and Deshaies, 2007). In human, UBA1 had been considered as the only E1 in the ubiquitination cascade for many years, but the study of UBA6 revealed it as a second E1 protein (Jin et al., 2007). While UBA1 can transfer an activated Ub to a broader range of E2s, UBA6 only transfers a Ub to UBE2Z, a UBA6 specific E2 (Jin et al., 2007). These results indicate that the UBA6-mediated ubiquitination may have much more specific protein targets compared to UBA1. It has been shown that the brain-specific depletion of UBA6 expression in mice leads to neuro-developmental and behavioral defects (Lee et al., 2013). In addition, in the human genome,

there are five other *UBA* genes, but they encode E1 enzymes for activating Ub-like proteins, but not Ub (Schulman and Harper, 2009).

Based on structural analysis of UBA1 proteins from yeast and mouse, UBA1 comprises five different domains starting at the N-terminus sequentially: an inactive adenylation domain (IAD), the first catalytic Cys half-domain (FCCD), the active adenylation domain (AAD), the second catalytic Cys half-domain (SCCD), and the C-terminal Ub fold domain (UFD) (Groen and Gillingwater, 2015). When UBA1 is properly folded, those domains are directly adjacent to each other to facilitate the transfer of Ub to E2s. Since UBA1 sits at the apex of the ubiquitination cascade and is required for protein ubiquitination, UBA genes are essential in many different species (Groen and Gillingwater, 2015). On the other hand, the functional specification of ubiquitination is normally determined by the downstream reactions and substrate proteins.

1.2.3. Ub conjugating-enzyme (E2)

Ub conjugating-enzyme (E2) sits at the middle of the ubiquitination cascade. An E2 first interacts with an E1 which has already been loaded with a Ub. After the activated Ub is transferred to a Cys residue of the E2 active site, the E2 has to dissociate from the E1, in order to further interact with a cognate E3. Thus, an E2 needs to perform two functions: receive a Ub from E1 and transfer the Ub either to Ub ligases (E3) or directly to substrates. Since extensive studies have been done on biochemical functions and structures of human E2s, these E2s will be discussed and used as examples. The E2s in other species will also be included and specified in the discussion.

All E2s contain a highly conserved UBC (Ub-conjugating catalytic) domain, which is composed of about 150 amino acids. This domain adopts an α/β-fold with four α-helices and four β-strands plus two E3-interacting loops, and serves as a platform of binding to E1, Ub, and E3. The highly conserved Cys residue is located in a shallow groove between two α-helices (Burroughs et al., 2008). In addition to the UBC domain, some E2s also have short extensions at the N- and/or C-terminus, which may play a role in the functional specificity of these E2s. Furthermore, several E2s have an additional domain, implying that these E2s may have other functions in addition to Ub conjugating.

While typically E2s function in Ub conjugation, some E2s catalyze the conjugation of UBLs. Since there are other E1s needed specifically for UBLs, the interaction of E2s with the E1 for activating Ub is important for receiving Ub. Adding to the complexity of interactions, the UBLs with a structure similar to Ub can compete for the same target site. For example, proliferating cell nuclear antigen (PCNA) can be monoubiquitinated or sumoylated. While monoubiquitinated PCNA recruits error-prone polymerases to bypass DNA repair, sumoylated PCNA at the same Lys residue blocks recombination between sister chromatids (Hoege et al., 2002). This specificity is due to the conformational changes when an E1 is loaded with a Ub or a UBL (Huang et al., 2007a; Lee and Schindelin, 2008). Several highly conserved Lys residues in E2s for Ub conjugation are responsible for a Ub-activating E1, which are absent in E2s specific for NEED8 and SUMO (Huang et al., 2007a; Lee and Schindelin, 2008).

The interaction between an E2 and E3 is also important for transferring Ub to substrates. Typically, an E2 can interact with more than one E3. For example, the human E2 UBE2D can interact with a large number of E3s. Also, one E3 may interact with different E2s (Ye and Rape, 2009). For instance, the human APC/C is capable of interacting with two E2s, UBE2C and UBE2S. Thus, the plural interactions between E2s and E3s increase the number of E2-E3 pairings while specific paring of E2-E3 can affect the outcome of ubiquitination on substrates. It is known that a structure involving an α-helix and two loops in the N-terminal region of the E2 is responsible for E3 recognition. The sequence variation in this region plays a key role in determining the specificity of E3 interactions (Ye and Rape, 2009).

Another key function of E2s is in regulating Ub chain formation. The assembly of a Ub chain starts with the attachment of the first Ub to a Lys residue on a substrate followed by addition of more Ub monomers to form a chain. The Ub chains can be linked through one of the seven Lys resides as well as the N-terminal Met of Ub, thus vastly increasing the complexity of Ub chains. Evidence so far suggests that E2s play a key role in determining the Ub chain linkage specificity as well as the chain length (Komander and Rape, 2012). The side chain of a conserved Asn residue close to the catalytic Cys residue in the E2 is proposed to play a key role in linking a donor Ub to a Lys residue of the acceptor Ub (Wu et al., 2003). It has been observed that different E2-E3 pairs may be needed for two stages of Ub chain assembly: chain initiation and chain elongation. One case is the Lys63-linked ubiquitination of PCNA in yeast (Hoege et al., 2002). The monoubiquitination of yeast PCNA during DNA repair is initiated by the E2 Rad6, and monoubiquitinated PCNA then recruits error-prone

DNA polymerases to bypass DNA damage. Further, the monoubiquitinated PCNA can be polyubiquitinated via a Lys63-linkage by another E2 complex, Ubc13-Mms2, and is involved in an error-free DNA repair pathway (Hoege et al., 2002). Mms2 is an E2 variant with a structure similar to Ubc13, but lacks a catalytic Cys residue. Another case is the activation of the NF-κB (Nuclear Factor kappa-light-chain-enhancer of activated B cells) pathway in immune responses. The E2 UBE2D is responsible for the initiation of the Ub chain while the E2 complex UBE2N-UBE2V1 is responsible for elongating the Lys63-linked Ub chain (Chen and Sun, 2009). A third example is the Lys11-linked Ub chain assembly in mammalian cells. The large E3 complex APC/C interacts with UBE2C to initiate the chain assembly, and then another E2, UBE2S, takes over the position of UBE2C to elongate the Lys11-linked Ub chain (Wickliffe et al., 2011a). On the other hand, there are known examples of E2s that are involved in both the initiation and elongation of Ub chains. The yeast E2 Ubc3 (Cdc34) together with its cognate E3 adds a Lys48-linked Ub chain to the inhibitor of cyclin-dependent kinases 1 (Sic1), leading to its degradation and allowing cells to enter into the S phase (Verma et al., 1997).

The specific functions of E2s in Ub chain initiation and elongation through specific linkages are indicative of their function in determining linkage specificity. In addition, experimental data have also shown that certain E2s can catalyze *in vitro* the formation of Ub chains through specific linkages without an E3. For instance, the Ubc13-Mms2 E2 complex of yeast can synthesize the formation of Lys63-linked Ub chain *in vitro*, whereas UBE2S of human can catalyze the formation of Lys11-linked Ub chains (Eddins et al., 2006; Wickliffe

et al., 2011a). It has been shown that the preference for a specific linkage by an E2 is mainly due to the way by which the E2 orients the acceptor Ub to expose a particular Lys residue to its active site (Figure 1.3) (Eddins et al., 2006). In the Ubc13-Mms2-Ub complex, the donor Ub is covalently linked to the catalytic Cys residue of Ubc13, while the acceptor Ub is non-covalently bound to Mms2. The interaction of Mms2 and Ub exposes the Lys63 residue of the acceptor Ub and positions it toward to Ubc13, thus facilitating the addition of the donor Ub specifically to the Lys63 residue of the acceptor Ub (Figure 1.3).

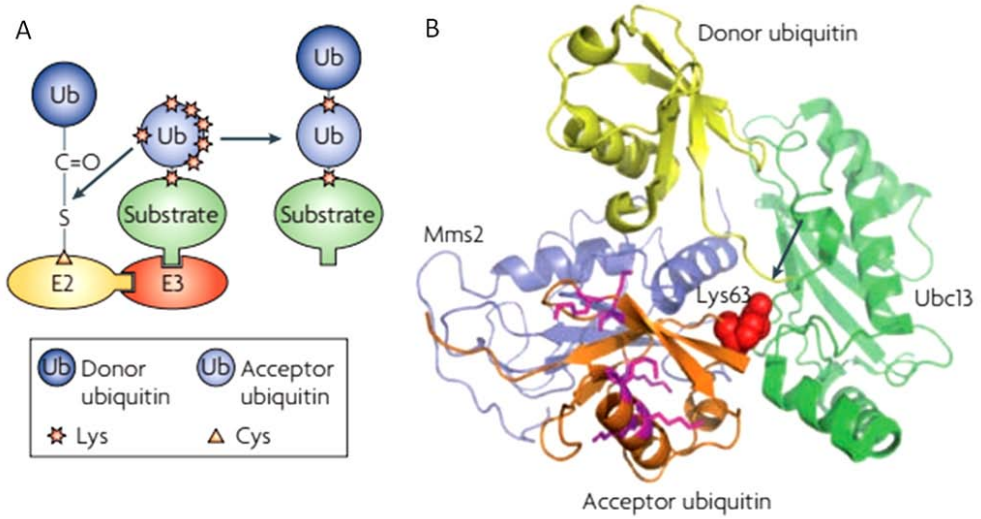

Figure 1.3 A model of Ub chain linkage selection during E2-Ub conjugation. (A) The E2 orients the acceptor Ub in a way which positions only one particular Lys residue to face the activate site of E2, and then attachs the acceptor Ub to the donor Ub through a specific linkage. (B) Structure of the yeast E2 complex Ubc13–Mms2 with bound Ub. In the complex, an acceptor Ub interacts with Mms2 in a way that only the Lys63 residue is aligned with the thioester (arrow) that links the donor Ub and Ubc13. The figure is from (Ye and Rape, 2009) and used with permission.

Therefore, E2s play a key role in the middle of the ubiquitination cascade and regulate this process at different levels: (1) to interact with an E1 to select Ub rather than a UBL; (2) to interact with an E3 to transfer Ub to the substrates specifically; (3) to initiate and elongate Ub chain assembly; and (4) to determine the specificity of Ub chain linkages.

1.2.4. Ub ligase (E3)

The Ub ligase (E3) mediates the transfer of Ub from an E2 to a substrate and is generally believed to play a key role in determining the substrate specificity. Consistent with the function in substrate specificity, a large number of E3s exist in every eukaryotic species, presumably serving the needs of interacting with many different substrates and functioning in different cellular processes.

Historically, E3 ligases are grouped into two major types: the RING (Really Interesting New Gene) type and the HECT (Homologous to the E6AP Carboxyl Terminus) type, depending on their mechanisms of transferring the Ub to a substrate. A RING-type E3 mediates the transfer of Ub from the E2-Ub conjugate directly to a substrate, whereas a HECT-type E3 forms an E3-Ub intermediate through a conserved Cys residue on the HECT domain, and then transfers the Ub to a substrate (Figure 1.4) (Deshaies and Joazeiro, 2009; Petroski and Deshaies, 2005). In humans, the majority of E3s belong to the RING-type, and only 28 belong to the HECT-type (Li et al., 2008). Some E3s can function alone as the E3 ligase. More commonly, a RING E3 exists as part of a large complex such as cullin-RING E3 ligases (CRL) which consist of a RING E3 and other subunits, and the additional subunits can function in substrate recognition and enzymatic regulation (Petroski and Deshaies, 2005).

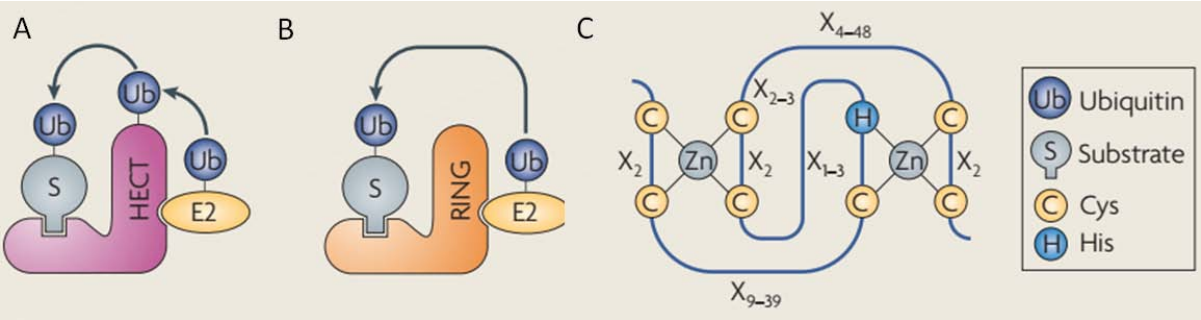

Figure 1.4 Two major types of E3 ligases. (A) The HECT E3s contain a conserved Cys residue which forms thioester linkage with a Ub. Then the Ub is transferred to the substrate which binds the N-terminus of HECT E3. (B) RING E3s facilitate the Ub transfer directly to the substrate without forming an intermediate conjugate with Ub. (C) A unique structure of RING domain sequences. The figure is modified from (Rotin and Kumar, 2009) and used with permission.

A key feature of an E3 is its binding to a specific E2. The RING and HECT domains have been shown to be responsible for the E2-E3 interaction specificity (Deshaies and Joazeiro, 2009; Petroski and Deshaies, 2005). A common RING domain has 40-60 amino acid residues and consists of a cluster of four pairs of Cys-Cys/His structures with a few amino acids between Cys and Cys/His in each pair, as well as some amino acids separating the pairs (Figure 1.4C). The consensus sequence can be described as follows: (Cys-X_2-Cys-$X_{(9\text{-}39)}$-Cys-$X_{(1\text{-}3)}$-His-$X_{(2\text{-}3)}$-Cys-X_2-Cys-$X_{(4\text{-}48)}$-Cys-X_2-Cys (X represents any amino acid). Structural analysis of RING domains showed that the conserved Cys and His residues are buried within the domain's core. This structure is stabilized through the binding to two atoms of zinc (Freemont, 1993). A small group of E3s contain a variant of the RING domain called U-box domain, which is similar to the RING domain but lacking most of the Cys-Cys/His residues (Hatakeyama and Nakayama, 2003). These E3s are also called U-box E3s. From the E2 perspective, the first α-helix and two loops in an E2 are mainly responsible for interacting

with a RING domain (Ye and Rape, 2009).

The HECT domain contains about 350 amino acids and is located at the C-terminus of the HECT E3s (Rotin and Kumar, 2009). It has a bilobal structure with a conserved Cys residue for thioester bond formation with Ub at the very end of C-terminus (C lobe). The N-terminal region (N lobe) of the HECT domain is responsible for the interaction with an E2 (Figure 1.4B). The substrate recognition is determined by regions outside the HECT domain of an E3. The two lobes are connected by a flexible loop, giving it an L-shape structure (Huang et al., 1999). In addition to RING and HECT domains, other domains also found in E3s may also be important for interacting with E2s (Scheffner and Kumar, 2014). For instance, the RING E3 Rad18 in yeast, together with its cognate E2 Rad6, is involved in the PCNA ubiquitination response to DNA damage. Rad18 can interact with Rad6 both through its RING domain and C-terminal domain (Hibbert et al., 2011).

In addition to RING and HECT E3s, another type called RBR (RING-BetweenRING-RING or RING1-BRcat-Rcat) E3s combines the features from both RING and HECT E3s to facilitate ubiquitination (Spratt et al., 2014). There are 12 RBR E3s in human, and all of them share a conserved structure with three domains: RING1, BRcat (Benign-catalytic) and Rcat (Required-for-catalysis). The RING1 is a RING domain for the interaction with an E2 while the Rcat domain is responsible for the formation of a thioester bond with Ub in a similar way to the C lobe of a HECT E3. The BRcat domain, sitting between RING1 and Rcat, has a similar structure to Rcat but lacks a catalytic Cys residue.

E3s are also involved in Ub chain assembly. Although E2s play a major role in

determining the Ub chain linkage specificity, the processivity of chain extension needs coordination of both E2 an E3. An example is the large E3 complex, APC/C, consisting of 11-13 subunits including a cullin APC2 and RING E3 APC11 subunits. APC11 recruits the E2 UBE2C via its RING domain for the E2-E3 interaction, to transfer a Ub to the substrate. Also, APC11 can move its position flexibly within the catalytic cavity of the large complex and works with the E2 UBE2C to promote multi-monoubiquitination. Moreover, another E2 UBE2S can be recruited to the APC/C complex to promote Lys11-linked polyubiquitination (Wickliffe et al., 2011a).

Another important and fundamental function of E3s is substrate recognition. An E3 may have multiple substrates, and different E3s can target the same substrate. Thus, the mechanisms of substrate recognition by E3s are highly diverse. The most common strategy is to utilize a specific region or domain for substrate recognition. For instance, the HECT-type E3s have a substrate binding region separated from its Ub reception region and E2 binding site. In a large E3 complex, substrate recognition may depend on other components of the complex (Petroski and Deshaies, 2005).

1.3. Diverse functions of Ub chain linkages

1.3.1. Overall introduction of Ub chain linkages

In a polyubiquitin chain, Ub can be linked through one of the seven Lys residues (Lys6, Lys11, Lys27, Lys29, Lys33, Lys48, and Lys63) or the Ub amino terminal Met1 residue, theoretically providing combinations of chain formation. Depending on the number of linkage type in the same polymer, the Ub chains can be grouped in two types: a homotypic

chain containing only one type of linkage and a heterotypic chain containing mixed linkages. The complexity increases further for a heterotypic chain when a Ub in the middle of Ub chain is attached by two donor Ub, forming a branched chain (Kulathu and Komander, 2012).

It has been shown that different Ub chain linkages have distinct conformations, allowing the interactions with different UBD proteins. As discussed earlier, Ub has several patches providing interacting surfaces for the UBD proteins. In a Ub chain, these patches are adjacent to each other in a characteristic manner to form unique binding surfaces allowing them to be recognized by certain UBD proteins (Kulathu and Komander, 2012). The specific recognition in the cell can lead to different outcomes. Since the Ub chain is very dynamic and difficult for structural analysis, Ub dimers of different linkages have been analyzed instead. The Ub dimers linked through Lys6, Lys11, Lys29, Lys33, and Lys48 have different interfaces, while the K63- and M1-linked dimers adopt an open conformation without contact sites except for the linkage (Figure 1.6) (Komander and Rape, 2012). These conformational differences increase the specificity of a Ub chain.

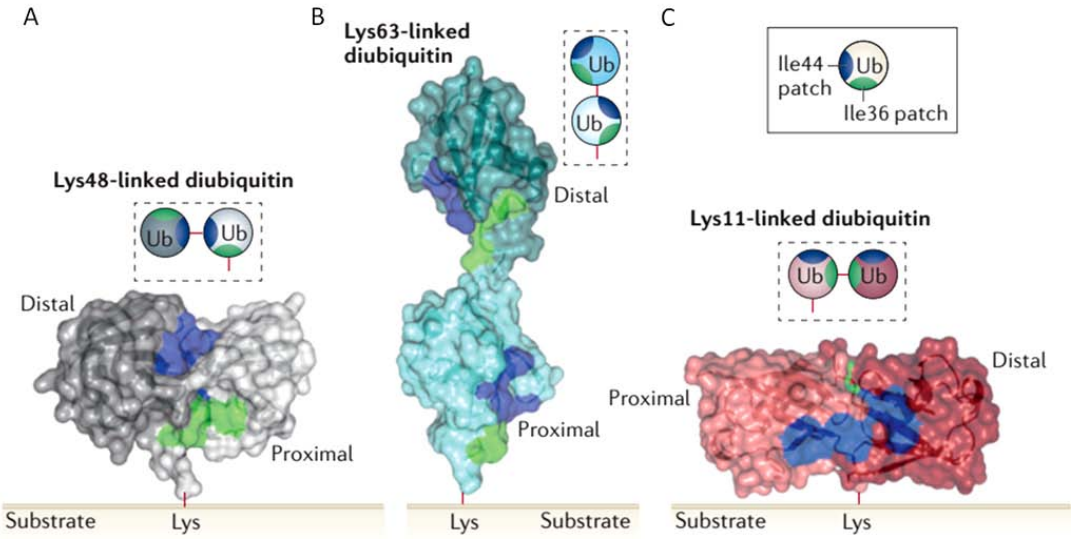

Figure 1.5 Crystal structures of Ub dimers through different linkages. Conformational differences are shown with (A) Lys48-linked, (B) Lys63-linked and (C) Lys11-linked Ub dimers. The Ile44 and Ile36 patches are highlighted in blue and green, respectively. Distal and proximal Ub moieties are indicated. The figure is modified from (Kulathu and Komander, 2012) and used with permission.

The Lys48-linked Ub chain was initially assumed to be the only linkage type in cells and function as a degradation signal targeting the substrates to the 26S proteasome. Later, studies of the Lys63-linked Ub chain revealed non-proteolytic functions of ubiquitination in DNA damage response in yeast (Spence et al., 1995) and immune response in mammalian cells (Wang et al., 2001). Studies over the years have generated considerable understanding on the functions of these two types of Ub chains. However, the functions of remaining six Ub chain types (Lys6, Lys11, Lys27, Lys29, Lys 33, and Met1) are less well defined; thus these chain types are normally called "atypical" chains. What this term refers to specifically may change with time depending on how much understanding we have on the structure and function of these Ub chain types. In plants, most studies are on the common type presumably Lys48-linked ubiquitination, while currently other types are considered atypical. For the

interests of this thesis, the function of Lys48-, Lys63-, and Lys11-linked polyubiquitination will be discussed.

1.3.2. Lys48-linked Ub chain

The function of the Lys48-linked Ub chain is generally believed to target substrates for degradation by the 26S proteasome. Genetic studies showed that yeast mutants with a point mutation of Lys48 to Arginine Ub (K48R) were lethal, but mutants with similar point mutations at other Lys residues were viable. The Ub-K48R mutation disrupts protein degradation and cell cycle progression, indicating that the K48-linked Ub chain is the principal targeting signal for proteasome degradation (Chau et al., 1989; Finley et al., 1994). Also, proteomic studies of different Ub linkages in affinity-purified protein samples from yeast showed that the Lys48 linkage is the most abundant, confirming the importance of this chain type in the cell (Xu et al., 2009b). Structural analysis shows that the Lys48-linked Ub chain binds to the 26S proteasome, more specifically to the regulatory 19S particle, which contains a Ub-binding subunit. Further, the minimal length for a Lys48-linked Ub chain to bind the 26S proteasome is about four Ub moieties (Thrower et al., 2000).

It is now known that the Lys48-linked Ub chain can also function in non-proteolytic processes. The first evidence came from the study of the Met4 transcription factor in yeast (Kaiser et al., 2000). Met4 can activate downstream genes in methionine biosynthesis. It can be polyubiquitinated and loses transcription activities when yeast cells grow on medium containing sufficient methionine. Intriguingly, although Met4 is modified by the Lys48-linked Ub chain, it is still long-lived and seems to escape from recognition by the 26S

proteasome. A further study revealed that a Ub-interacting motif in Met4 could bind to the Ub chain and protect Met4 from degradation by the 26S proteasome (Flick et al., 2006). However, it is still unclear how Lys48-linked ubiquitination inactivates the transcription activity of Met4, which seems independent of Met4 degradation by the 26S proteasome.

1.3.3. Lys63-linked Ub chain

The non-proteolytic function of ubiquitination was initially revealed by the study of the Lys63 residue of yeast Ub. The Ub-K63R mutation caused a defect in DNA repair in yeast cells, but without any effect on proteolysis (Spence et al., 1995). It is now known that the Lys63-linked polyubiquitination also has important functions in the immune response, protein trafficking, and ribosomal protein synthesis in addition to DNA repair (Chen and Sun, 2009; Hicke and Dunn, 2003; Spence et al., 2000).

In the DNA damage response, the Lys63-linked ubiquitination of PCNA plays a key role in the error-free mode of DNA lesion bypass (Ulrich and Walden, 2010). PCNA encircles DNA and serves as a platform to recruit proteins involved in DNA replication and DNA repair. Different modifications of PCNA have important roles in these processes. Monoubiquitination at the Lys164 residue of PCNA enables the recruitment of a specialized polymerase to bypass the damage site. Further, the same lysine site could be modified by the attachment of a Lys63-linked Ub chain, resulting in an error-free mode of DNA damage lesion bypass (Ulrich and Walden, 2010). The E2 Ubc13 in yeast, together with the E2 variant Mms2, is the only E2 responsible for the Lys63-linked Ub chain assembly.

The role of Lys63-linked ubiquitination in the immune response was uncovered from

studying the mammalian NF-κB signaling pathway, in which the transcription factor NF-κB controls the expression of a large number of genes involved in immunity, inflammation, and cell survival (Chen et al., 1995). NF-κB is normally maintained in the cytoplasm through binding to its inhibitory protein IκB. Upon stimulation of cells with different agents, such as microbial pathogens, IκB is phosphorylated by its upstream kinase IKK and then polyubiquitinated with the Lys48-linked Ub chain by the E3 complex $SCF^{\beta TrCP}$ resulting in IκB degradation and the release of NF-κB, which then enters the nucleus. The Lys63-linked ubiquitination is connected to this pathway through an E3, TRAF6 (TNF Receptor Associated Factor 6). The E2 complex UBE2S-UEV along with TRAF6 catalyzes Lys63-linked polyubiquitination of TRAF6 itself. The Lys63-linked Ub chain on TRAF6 serves as a protein-binding platform and recruit a kinase complex to activate IKK, which phosphorylates IκB (Chen and Sun, 2009).

The non-proteolytic function of Lys63-linked polyubiquitination was also found in endocytosis, initially in yeast. The monoubiquitination of plasma membrane proteins and receptors serves as a signal to trigger endocytic internalization, and blocking of Lys63-linked polyubiquitination reduces the rate of permease undergoing endocytosis (Galan and Haguenauer-Tsapis, 1997). However, the details of this process need further investigation since some ubiquitination-defective receptor proteins still undergo internalization from the cell surface (Huang et al., 2007b; Martins et al., 2015).

Although the Lys63-linked Ub chain has been shown to have important non-proteolytic roles, recent evidence shows that it can also serve as a proteolytic signal for

proteasome-dependent degradation. Tau protein, a microtubule-associated protein in human cells plays a critical role in the nervous system and defects in this protein are associated with Alzheimer's and Parkinson's diseases (Mandelkow and Mandelkow, 2012). Degradation of Tau was found to be through the 26S proteasome and dependent on either the Lys63-linked Ub chain or a Ub-binding protein p62. p62 acts as an autophagy cargo protein targeting proteins for autophagy and preferentially recognizes the Lys63-linked Ub chain. Thus, ubiquitinated Tau with a Lys63-linked Ub chain can be recognized by p62 leading to its degradation through the 26S proteasome (Babu et al., 2005). Recently, a study on the degradation of proapoptotic regulator TXNIP (Thioredoxin Interacting Protein) revealed that the Lys63-linked Ub chain acted as a "seed" for the Lys48/Lys63 branched Ub chains and triggered proteasomal degradation (Ohtake et al., 2018).

1.3.4. Lys11-linked Ub chain

The Lys11-linkage was first reported from the analysis on the specificity of the human E2 UBE2S and yeast E2 Ubc2 *in vitro* (Baboshina and Haas, 1996). Recombinant UBE2S catalyzes Ub chain formation exclusively through the Lys11 residue of Ub. Recent work revealed that the Lys11-linked Ub chain also acts as a proteasomal degradation signal in cell cycle regulation (Wickliffe et al., 2011b). When the proteasome was inhibited, the abundance of the Lys11-linked Ub chain increased (Kim et al., 2011). Also, the abundance of the Lys11-linked, but not the Lys48-linked Ub chain increased when the APC/C complex was inactivated (Matsumoto et al., 2010). Conversely, the level of the Lys11-linkage decreased when cells exited the cell cycle during differentiation (Dammer et al., 2011).

It has been shown in mammalian cells that the large E3 complex APC/C and two E2s, UBE2C and UBE2S are required for the sequential steps of Lys11-linked Ub chain assembly (Figure 1.6). The APC/C complex recognizes substrates containing the degron sequences, 9-residue D-box (R-X_2-L-X_2-I/V-X-N) or KEN-box (K-E-N-X_3-N/D) (Sivakumar and Gorbsky, 2015). At the chain initiation, the E2 UBE2C transfers the first Ub to substrates by binding to the RING domain of APC11 and also catalyzes the formation of a short Lys11-linked Ub chain (Brown et al., 2016). Following the initiation, Lys11-linked Ub chain is extended by another E2 UBE2S. UBE2S interacts with the APC/C co-activators CDC20 and CDH1, as well as certain subunits of APC/C (Brown et al., 2016). The extension of the Lys11-linked Ub chain seems to be tightly controlled during the cell cycle. The expression of UBE2S is cell cycle regulated. Interestingly, UBE2S binds to CDC20 at the early stages of mitosis and CDH1 at the later stages of mitosis and G1 (Williamson et al., 2009). These findings indicate important roles of Lys11-linked ubiquitination in cell cycle regulation.

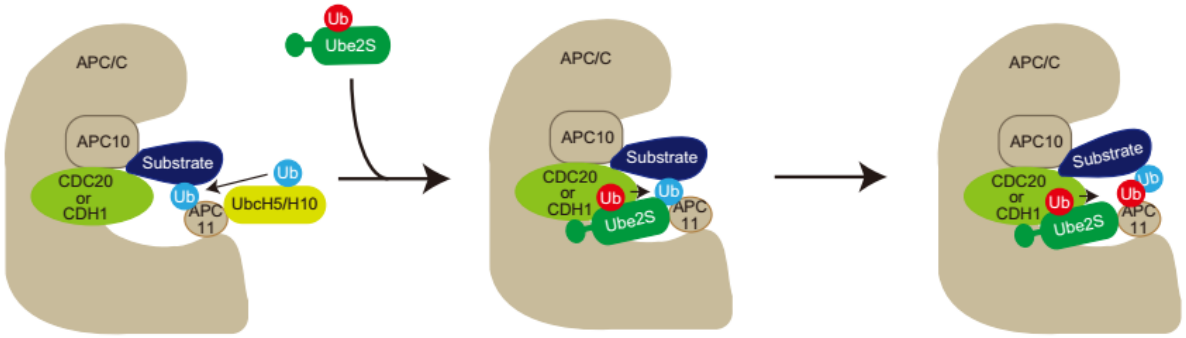

Figure 1.6 Sequential K11-linked Ub chain assembly by APC/C complex with two E2s: UBE2C and UBE2S. At the initial step, UBE2C (UbcH5/H10) is recruited by the RING E3 ligase APC11 to APC/C complex together with its co-activator CDC20 or CDH1 binding to the subunit APC10, to start the ubiquitination of substrate. Then, UBE2S is recruited to the APC/C complex and stabilized, to facilitate the Ub chain elongation exclusively through the Lys11 linkage. The figure is from (Iwai and Tanaka, 2014) and used with permission.

The Lys11-linkage was also identified in yeast (Xu et al., 2009b). The yeast mutant which has a Ub-K11R mutation is hypersensitive to the endoplasmatic reticulum (ER) stress inducer DTT and tunicamycin, indicating that the Lys11-linked Ub chain is important for the ERAD (ER-associated degradation) pathway. It is unclear whether in higher eukaryotes the Lys11-linked Ub chain is also involved in the ERAD pathway. The other difference between yeast and humans is that the human UBE2S does not appear to have a yeast homolog.

Most recently, Lys11-linked ubiquitination was also implicated in the DNA damage response (Paul and Wang, 2017). Following laser-induced DNA damage in human cells, signals of Lys11-linked ubiquitination accumulated at the DNA damage sites in an ATM (ataxia-telangiectasia mutated) dependent manner. The E2 UBE2S could interact with RING-type E3 RNF8 to regulate the Lys11-linked Ub chain assembly. Additionally, the histone H2A/H2AX were found to be modified by the Lys11-linked Ub chains. Interestingly, the

APC/C complex was not required in the Lys11-linked Ub chain assembly on the damaged chromatin (Paul and Wang, 2017). This finding suggests a possible new mechanism for the Lys11-linked Ub assembly.

1.4. Ubiquitination in plants and particularly in Arabidopsis

Currently, *Arabidopsis thaliana* is the most widely used model for plant molecular biology and genetics studies. It has a number of advantages for molecular studies of plants, including a small and completely sequenced genome, a rapid life cycle, ease of transformation with *Agrobacterium tumefaciens*, and a large number of T-DNA insertion mutant lines and genomic resources available. Bioinformatic analysis showed that about 5% of the Arabidopsis genome encodes proteins involved in ubiquitination (Kraft et al., 2005), suggesting wide-spread roles of protein ubiquitination in plants. The study of ubiquitination in Arabidopsis started from the characterization of genes encoding Ub (Callis et al., 1990). Arabidopsis Ub is encoded by multiple genes belonging to two different groups: homomeric and heteromeric Ub genes (Callis et al., 1990). Homomeric Ub genes, also called polyUb genes encode multimers of Ub as a repeated head-to-tail structure within a protein. The second group of genes encode a Ub which is followed by a different protein, either a small ribosomal protein or Ub-like protein called RUB (Related to Ub). The phenomenon of co-synthesis of Ub and the ribosomal protein is universally existent in animals, yeast, and plants (Callis, 2014a). Studies of the yeast *UBI3* suggested that the Ub co-expressed with the ribosomal protein serves as a chaperone to facilitate the pre-rRNA processing and ribosome assembly (Finley et al., 1989). There is only very limited knowledge about the specific role of

each Ub gene due to the functional redundancy of these genes. Presumably, the high copy number of Ub genes provide a sufficient source of Ub for many different cellular processes.

1.4.1. Biological functions of E1s in Arabidopsis

There are two E1 genes in the Arabidopsis genome: *UBA1* (*Ub Activation 1*) and *UBA2*. The two genes share a high degree of identity in nucleotide sequences. Both the UBA1 and UBA2 proteins can activate Ub transfer to several E2s with similar efficiencies *in vitro* (Hatfield et al., 1997), although evidence suggests that the two E1s may have different biological functions in plants. A mutant allele of *UBA1* was identified from a suppressor screen in a mutant, called *snc1 npr1*, involved in plant pathogen resistance (Goritschnig et al., 2007). *NPR1* (*Nonexpression of PR genes 1*) encodes a transcription coactivator which is important for activating a large set of defense-related genes (Kinkema et al., 2000), while *SNC1 (Suppressor of npr1-1 Constitutive 1)* encodes a TIR-NB-LRR R-protein (Toll Interleukin1 Receptor-Nucleotide Binding-Leu-Rich Repeat Resistance protein) involved in the salicylic acid (SA)-dependent defense response (Li et al., 2001). The gain-of-function mutant *snc1* plants constitutively expressing *PR* (*Pathogenesis-Related*) genes are pathogen resistant. In the screen for the suppressors of *snc1 npr1* double mutant, the *mos5* (*modifier of snc1*) mutant was identified to be a *UBA1* allele with a point mutation and a deletion at the C-terminus of UBA1. These mutations suppress both the phenotypes of the *snc1 npr1* mutant plants and the induction of *PR* genes by *SNC1*. The *mos5* mutant plants are dwarf and exhibit enhanced susceptibility to some pathogens (Goritschnig et al., 2007). However, it still unclear whether the *mos5* is a complete or partial loss-of-function allele of *UBA1*. On the other hand,

the *uba2* mutant has been characterized and shows no obvious phenotypes, indicating UBA1 may be more important in plants. Further, the double Arabidopsis mutant *mos5 uba2* could not be obtained, suggesting the plants are not viable when both the *UBA* genes were inactivated (Goritschnig et al., 2007), consistent with the notion that ubiquitination is essential for plants.

1.4.2. Biological functions of E2s in Arabidopsis

Arabidopsis has 37 Ub E2 genes referred to as *UBC*s, which could be divided into 16 subgroups (Kraft et al., 2005). *In vitro* results have shown that most of the recombinant E2 proteins possess the classical E2 activity of forming the E2-Ub conjugate through a thioester-linkage or the ability to catalyze the formation of a Ub chain (Kraft et al., 2005; Zhao et al., 2013). However, very limited information is available on the specific ubiquitination reactions which each of the E2s is involved in. Furthermore, the biological functions for many E2s remain largely unknown, although several of them have been studied.

Arabidopsis UBC1 and UBC2, belonging to the subfamily III, are homologs of the yeast Rad6. The yeast Rad6 is known to play a critical role in the PCNA ubiquitination for DNA repair and the histone monoubiquitination for transcriptional activation (Hoege et al., 2002; Kao et al., 2004). Arabidopsis UBC1 and UBC2, together with two closely related RING-type E3s called HUB1 (Histone Monoubiquitination 1) and HUB2, have been shown to be involved in histone 2B monoubiquitination and regulation of flowering time (Cao et al., 2008; Gu et al., 2009; Xu et al., 2009a). However, UBC3, the other member of the subfamily III, is not redundant with UBC1 and UBC2, since only the *ubc1 ubc2* double mutant, not the

ubc1 ubc3 or ubc2 ubc3 double mutant, show the early flowering phenotype (Cao et al., 2008).

Arabidopsis UBC18, one of the four-member subfamily VII, was recently reported to regulate abiotic stress response by promoting the ERF1 (Ethylene Response Factor 1) ubiquitination (Cheng et al., 2017). ERF1 has been identified as a downstream component of the ethylene (ET) signaling pathway. Constitutive expression of *ERF1* in Arabidopsis resulted in increased resistance to the necrotrophic pathogens such as *Botrytis cinerea* (Berrocal-Lobo et al., 2002). Overexpression of *UBC18* increased the ERF1 ubiquitination, which led to a decrease in the protein abundance of ERF1 and a reduction in the plant stress response. Conversely, down-regulation of *UBC18* resulted in decreased ERF1 ubiquitination, leading an increased level of ERF1 and enhanced stress response of mutant plants (Cheng et al., 2017). However, it is still not clear whether the other three members (UBC15, UBC16, and UBC17) have a similar function to UBC18.

UBC21, the sole member of the subfamily IX, was identified initially as PEX4 (peroxin 4) through screening for mutants defective in peroximal processes (Zolman et al., 2005). It is tethered to the peroxisome membrane through a peroxisomal protein PEX22 and suggested to function in the ubiquitination of the peroxisome matrix protein receptor, PEX5. In yeast, Pex5 can be monoubiquitinated for translocation and polyubiquitinated mainly through the K48-linked Ub chain for degradation by a complex consisted of three E3 ligases, Pex2, Pex10 and Pex12 (Platta et al., 2004). Studies of the Arabidopsis homologs to these E3 ligases indicate the existence of a similar mechanism in plants (Hu et al., 2012).

UBC24, one of the four members in the subfamily IX, functions in organic phosphate (Pi) signaling and was originally identified as PHO2 (Phosphate Overaccumulator 2). The *pho2*/*ubc24* mutant plants overaccumulate Pi in leaves and display Pi toxic symptoms as chlorosis and necrosis in Pi-rich soil (Aung et al., 2006; Bari et al., 2006). More recent results have shown that UBC24/PHO2 works with an E3 named NLA (Nitrogen Limitation Adaptation) in polyubiquitination, with a Pi transporter PT2 as a downstream target leading to its degradation via the 26S proteasome (Lin et al., 2013; Park et al., 2014).

UBC32, a member of the subfamily XIV, was found to be a component of the ERAD complex, and it is involved in the brassinosteroid (BR)-mediated growth promotion (Cui et al., 2012). UBC32 has been shown to be involved in the polyubiquitination and degradation of a protein, which is an ERAD substrate and encoded by a barley powdery mildew resistance gene (Cui et al., 2012). In addition, AtOS9, a homolog of the yeast ER luminal lectin Yos9 and a component of the transmembrane E3 complex, is also modulated by UBC32 (Chen et al., 2017).

UBC35 and UBC36, two members of the subfamily XV, are closely related to the Ubc13 proteins of non-plant species and they could complement the yeast *ubc13* mutant for spontaneous mutagenesis and sensitivity to DNA damaging agents (Wen et al., 2006) Accordingly, these two E2s are also referred to as UBC13A and UBC13B (Wen et al., 2006). In yeast and humans, Ubc13 and its homologs are the only known E2s responsible for catalyzing K63-linked ubiquitination (Andersen et al., 2008; Chen and Sun, 2009). Arabidopsis UBC13A has been shown to catalyze K63-linked ubiquitination *in vitro* (Wen et

al., 2006). The *ubc13* double mutant of Arabidopsis displays strong phenotypes including shortened primary roots, reduced number of lateral roots, and very few root hairs (Li and Schmidt, 2010; Wen et al., 2014). Further, in yeast and humans, Ubc13 proteins require a partner protein, Ub-conjugating enzyme variant (UEV), which is a UBC domain-containing protein, but lacks the catalytic cysteine. Four Arabidopsis *UEV* genes have been identified with *UEV1D* implicated in DNA damage response (Wen et al., 2008). Results from these studies indicate that UBC13A/B (UBC35/36) function in different processes and likely catalyze K63-linked ubiquitination in plants, although *in vivo* evidence for K63-linked ubiquitination remains to be obtained.

1.4.3. Biological functions of E3s in Arabidopsis

The Arabidopsis genome has over 1000 genes encoding E3 ligases (Stone et al., 2005), which is almost twice as many as the number of E3s in the human genome, indicating expanding roles of E3 ligases in plants. There are mainly three classes of E3 ligases: HECT, RING, and U-box, depending on the feature domain they carry. The large number of E3 ligases makes it possible to regulate specifically a large number of substrates required for plant developmental processes and responses to environmental changes. It is not possible to cover all the E3s here. Instead, the major types and some specific examples of Arabidopsis E3s will be reviewed.

There are 7 HECT-type E3s identified in Arabidopsis. The number of this type of E3s varies among other species, with 3 HECT E3s in yeast and 30 HECT E3s in humans. The 7 Arabidopsis HECT E3s can be grouped into four UPL (Ub-Protein Ligase) subfamilies:

UPL1/2, UPL3/4, UPL5, and UPL6/7 (Downes et al., 2003). In an *in vitro* assay, the Arabidopsis UPL1 could conjugate Ub along with a specific E2 UBC8 (Bates and Vierstra, 1999). However, the biological function of either UPL1 or UPL2 is not known. A mutant allele of *UPL3, kaktus*, was reported to have an increased number of trichome branches and hypersensitivity to gibberellic-acid 3 (GA3) (Downes et al., 2003; El Refy et al., 2003). However, inactivation of *UPL4*, which is in the same subfamily as *UPL3*, did not result in such phenotypes. UPL5 was found to be involved in leaf senescence, with a transcription factor WRKY53 as its potential target for degradation (Miao and Zentgraf, 2010). Overexpression of *WRKY53* in enhanced the senescence phenotype of the *upl5* mutant compared to the expression in WT background. Despite these studies, our understanding on the functions of the HECT-type E3s remains rather limited.

There are 469 Arabidopsis genes encoding potential RING-type E3 ligases, defined by a typical or variant RING domain (Stone et al., 2005). In comparison, the human and yeast genomes have about 300 and 47 RING-type genes respectively (Finley et al., 2012; Li et al., 2008). A typical RING domain forms a globular octet structure with four pairs of zinc-binding Cys/Cys or Cys/His residues in a cross brace (Freemont, 1993). The space between the two Cys/Cys or Cys/His residues in a pair is strictly conserved. A variant of RING domain has some variability on the Cys and His residues as well as the length of the spacer. While some RING-type E3s are small proteins carrying the RING domain only, other RING-type E3s have additional protein-protein interacting motifs (Stone et al., 2005). The vast majority of Arabidopsis RING-type E3s have not been characterized regarding the specific

reactions they catalyze and the E2-E3 interaction specificity.

The RING-type E3s can be grouped in two subtypes: monomeric RING-type E3s, which function as single proteins; and multimeric RING-type E3s, which needs additional proteins to function and recognize the substrates.

A subset of monomeric RING-type E3s have been found to target transcription factors involved in plant stress responses. These E3s includes DRIP1 (DREB2A-Interacting Protein 1)/DRIP2, and RGLG1 (RING domain Ligase 1)/RGLG2 (Cheng et al., 2012; Qin et al., 2008). DREB2A (Dehydration-Responsive Element-Binding Protein 2A) is a transcription factor which controls the expression of many drought and salt stress-inducible genes (Sakuma et al., 2006). The RING-type E3 DRIP1 or DRIP2 interacts with DREB2A and facilitates the ubiquitination of DREB2A *in vitro*. Also, DREB2A protein becomes stable in *drip1 drip2* double mutant plants and overexpression of *DREB2A* enhances the drought tolerance in double mutant plants (Qin et al., 2008). Similarly, another group E3s RGLG1 and RGLG2 carrying a RING domain on their C-terminus, targeting the transcription Factor ERF53 (Ethylene Response Factor 53) for degradation when plants are under water and salt stress. Additionally, drought tolerance is enhanced in *rglg1 rglg2* double mutants when overexpressing *ERF53* (Cheng et al., 2012). These E3s function as negative regulators of transcription factors which respond to dehydration (or the stress condition). In normal conditions, these E3s target the transcription factors for degradation and keep them in a low level. Under the stress condition, the E3 activity is reduced resulting in an increased level of those transcription factors and increased stress tolerance of the plants.

The multimeric RING-type E3s are well characterized as Cullin-RING E3 ligases (CRLs). A typical CRL contains three to five subunits: a Cullin protein (CUL) as the scaffold to bring subunits together; a RING domain-containing protein RBX1 (RING box 1) responsible for E2 binding; a substrate-recognition protein; and an adaptor protein linking CUL, and a substrate-recognition protein (Hotton and Callis, 2008). The adaptor protein may or may not be needed. Arabidopsis has six cullin-like proteins: CUL1, CUL1b, CUL3a, CUL3b, CUL4, and APC2. They all contain a conserved cullin region around 200 amino acids, with a protein size varying from 85 to 98 kD (Callis, 2014a). There are four subtypes of cullin-based E3s in plants, and all have the same RBX1 protein encoded by two genes (*RBX1a* and *RBX1b*). Only *RBX1a* is significantly expressed (Gray et al., 2002; Lechner et al., 2002). It is an essential gene, and down-regulation of *RBX1a* causes dwarf and poor fertility phenotypes of the plants (Gray et al., 2002; Lechner et al., 2002).

The best known CRL subtype is referred to as an SCF^X for SKP-CUL1-F-box protein. The superscripted X stands for an F-box protein, which functions as a recognition subunit and binds to the CUL1-interacting adaptor protein SKP (S-phase Kinase-associated Protein). For the other CUL-based CRLs, different adaptor and recognition proteins are utilized (Hotton and Callis, 2008). Arabidopsis has only two *CUL1* and two *RBX1* genes, but many more *SKP* and *F-box* genes (about 21 *SKP* and 694 *F-box* genes). The large numbers imply numerous possible combinations of SKP and F-box proteins, which may be needed for diverse processes and functions (Choi et al., 2014).

Some of the best examples of CRLs are found in plant hormone signaling (Hua and

Vierstra, 2011). In some cases, the F-box proteins function as hormone receptors. Auxin is an important plant hormone involved in almost every aspect of plant growth and development. TIR1 (Transport Inhibitor Response 1) is an F-box protein as part of an SCF^{TIR1} E3 complex in auxin signal transduction (Figure 1.7) (Gray et al., 2001). One main target of the SCF^{TIR1} E3 complex is a family of proteins referred to as Aux/IAA proteins which functions as the negative regulators of the transcription factors called ARFs (Auxin Response Factors). Auxin binds to a pocket of the TIR1 protein, and the binding facilitates the interaction between the SCF^{TIR1} complex and substrate Aux/IAA proteins, leading to subsequent ubiquitination and degradation of Aux/IAA proteins (Tan et al., 2007). According to the currently accepted concept, the degradation of Aux/IAA proteins releases ARFs which then can function to activate downstream genes required for auxin response. A similar mechanism has also been found in the signaling pathway by another plant hormone jasmonic acid (JA). COI1 is an F-box protein and a subunit of the CRL complex SCF^{COI1}, and acts as a receptor of JA (Sheard et al., 2010).

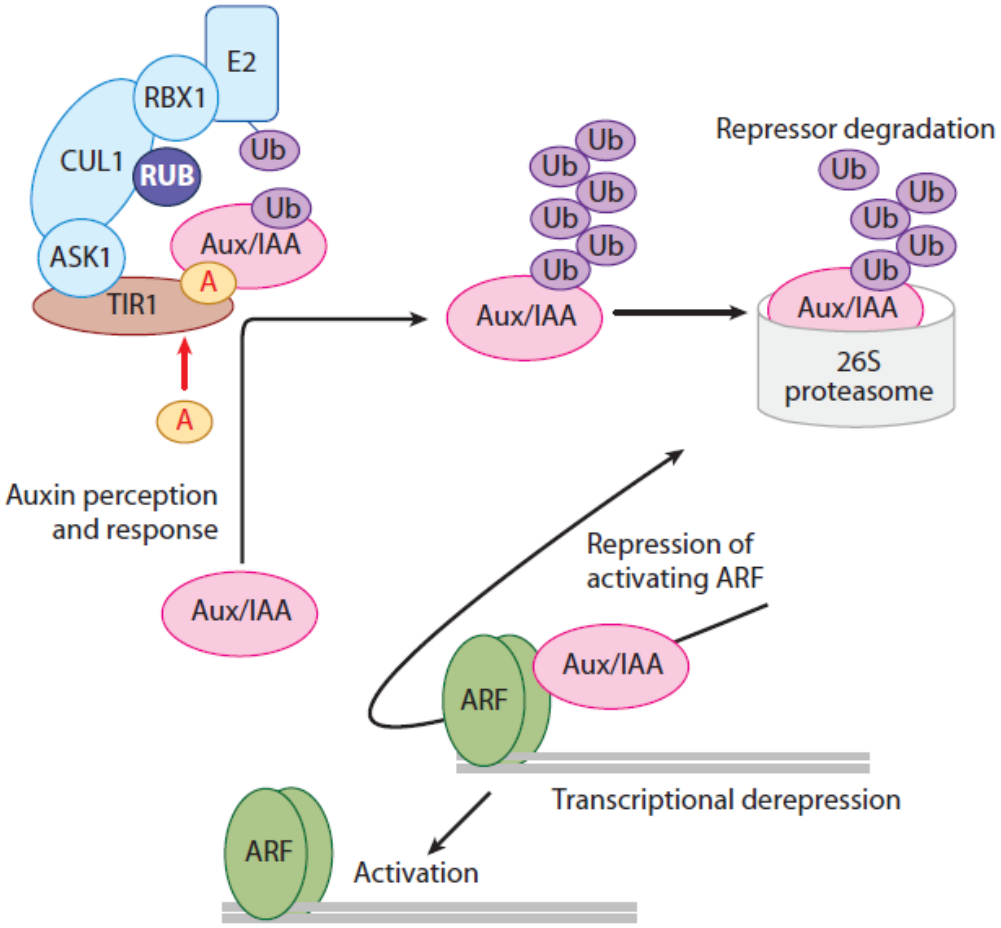

Figure 1.7 Auxin signaling pathway mediated by ubiquitination. The auxin response factors (ARFs) are a group of transcription factors which control the expression of many genes in response to auxin. The activity of ARFs is repressed by Aux/IAA proteins. The binding of auxin (A) to its receptor TIR1 in a SCF^{TIR} E3 complex facilitates the binding of TIR1 to Aux/IAA proteins. After TIR1 binds to Aux/IAA proteins, the Aux/IAA proteins become ubiquitinated and subsequently degraded by the 26S proteasome. The degradation of Aux/IAA proteins thus frees ARF proteins to activate the transcription of many auxin-responsive genes. The SCF^{TIR1} complex consists of: a cullin protein, CUL1; RING E3, RBX1; an adaptor protein, Arabidopsis SKP1 (ASK1), and an F-box protein, TIR1. The RUB is a modifier of SCF^{TIR} complex. The figure is from (Mockaitis and Estelle, 2008) and used with permission.

There are 64 Arabidopsis genes encoding U-box-type E3s, and the number is much higher than those for other eukaryotic species (Yee and Goring, 2009). Only 2 and 21 U-box genes are found in yeast and humans, respectively (Cyr et al., 2002; Li et al., 2008). The U-box E3 proteins (PUBs) are so named due to a conserved U-box domain. The 64 Arabidopsis PUBs can be further grouped into 13 subfamilies, depending on the presence and location of additional domains, including the ARM (Armadillo) repeats, Ser/Thr kinase domain, WD40 repeats, TPR (Tetratricopeptide) domain, and peptidyl-prolyl isomerase (Wiborg et al., 2008; Yee and Goring, 2009). The ARM repeat domain is the most common one, which 41 out of 64 Arabidopsis PUBs carry and is responsible for the interaction with substrates (Jung et al., 2015). Recent studies of Arabidopsis PUBs have uncovered their biological functions in different aspects of plant development and also in response to biotic and abiotic stresses (Trujillo, 2018). CHIP (Carboxy terminus of HSP70-Interacting Protein) is one of the three PUBs which has a counterpart in humans (Yan et al., 2003). CHIP showed E3 activity *in vitro* and its transcript level was up-regulated in response to heat treatment (Yan et al., 2003). The plants overexpressing Arabidopsis *CHIP* were more sensitive to the heat treatment. CHIP interacts and ubiquitinates two substrates, ClpP4 and FtsH1, which belong to two chloroplast protease complexes, Clp (Caseinolytic Protease) and FtsH (Filamentation temperature sensitive H), respectively. The plants overexpressing *CHIP* were found to have reduced levels of ClpP4 and FtsH1 (Shen et al., 2007a; Shen et al., 2007b).

1.4.4. Biological functions of specific Lys-linked ubiquitination in Arabidopsis

In Arabidopsis, the abundance of specific Lys-linked Ub chains has been found in the

following order: Lys48-, Lys63- and Lys11-linked Ub chains, followed by Lys33-, Lys6-, and Lys29-linked Ub chains (Kim et al., 2013b; Maor et al., 2007). The Lys48-linked Ub chain is well known for targeting substrate proteins for degradation, thus controlling their levels precisely and timely. The non-proteolytic functions of ubiquitination are much less understood. Recent results have started to show the possible biological functions of Lys63-linked ubiquitination in plants.

The Lys63-linked ubiquitination in plants was first implemented in DNA damage response. The yeast E2 Ubc13 has been well studied as a specific E2 for Lys63-linked ubiquitination and mediates DNA damage response (Hofmann and Pickart, 1999). The Arabidopsis homologs, UBC13A and UBC13B (also called UBC35 and UBC36) are able to complement the yeast *ubc13* mutant which is sensitive to DNA damage treatment, indicating a conserved function of UBC13 in plants (Wen et al., 2006). Similar functional complementation was observed for Arabidopsis UEV1A-D, homologs of the yeast E2 variant UEV1 (Wen et al., 2008). The Arabidopsis UBC13-UEV pair could catalyze the Lys63-linked Ub chain formation *in vitro*. Further, the *uev1d* mutant showed hypersensitivity to the DNA damage reagent MMS (Methyl Methanesulfonate) during seed germination. Additionally, PCNA in Arabidopsis could be ubiquitinated by UBC13-UEV and the E3 RAD5a, although the Ub linkage specificity was not experimentally determined (Strzalka et al., 2013). Collectively, these results suggest a conserved function of Lys63-linked ubiquitination in DNA damage response in yeast and plants

The role of Lys63-linked ubiquitination in hormone signaling has also been reported.

The double mutant (*rglg1 rglg2*) of two RING E3s, RGLG1 and RGLG2, showed a reduced apical dominance and an altered phyllotaxy, which was believed to be regulated by auxin transport (Yin et al., 2007). Both RGLG1 and RGLG2 could interact with the Arabidopsis UBC13 and catalyze the Lys63-linked Ub chain *in vitro*. The double mutant also showed a decreased response to exogenous auxin and a reduced level of the auxin efflux transporter PIN1 (Yin et al., 2007). More recently, an auxin efflux transporter PIN2, which functions in gravity response, was found to be modified through Lys63-linked ubiquitination in an RGLG1/2-dependent manner (Leitner et al., 2012). These results indicate that Lys63-linked ubiquitination plays an important role in auxin response.

Another piece of evidence linking Lys63-linked ubiquitination to auxin signaling came from the studies of the *ubc13a ubc13b* double mutant in Arabidopsis. The seedlings of *ubc13* double mutant displayed strong phenotypes including shortened primary roots, reduced number of lateral roots, and very few root hairs. In addition, the double mutant was insensitive to auxin treatment, had reduced auxin response and increased IAA17 activity in the form of IAA17-GUS reporter fusion (Wen et al., 2014). Based on these results, it was proposed that UBC13 is involved in the degradation of Aux/IAA proteins, and in the *ubc13* double mutant Aux/IAA protein levels are increased resulting in the observed root phenotypes (Wen et al., 2014).

Lys63-linked ubiquitination is also implicated in the signaling of the growth-promoting hormone brassinosteroid (BR) since it was observed that the BR receptor BRI could be modified by the Lys63-linked Ub chain (Martins et al., 2015). Expression of a

ubiquitination-defective BRI1 variant resulted in BR hypersensitivity. It is not known whether UBC13 is directly involved in this regulation.

Recently, another study in rice suggests that Lys63-linked ubiquitination and Lys48-linked ubiquitination coordinately regulate plant architecture (Wang et al., 2017). The rice transcription factor OsIPA1 (Ideal Plant Architecture) has a major role in affecting rice architecture. One of its interacting proteins named OsIPI1 is a RING-type E3 ligase and can ubiquitinate OsIPA1. Interestingly, the results suggest that OsIPI1 can ubiquitinate OsIPA1 differently, promoting Lys48-linked ubiquitination and the degradation of OsIPA1 in panicles, while promoting Lys63-linked ubiquitination and the stabilization of OsIPA1 in shoot apexes (Wang et al., 2017).

1.5. Objectives of this study

Therefore, there is a great need to understand the functions of E2s in plants. Our main interests are on the plant E2s that can catalyze other forms of Ub chains instead of the typical Lys48-lined Ub chain. My thesis has two main parts. The first part is to further study the functions of Arabidopsis UBC13, particularly in the identification and characterization of E3 ligases interacting with UBC13. The second part is to identify and study the function of an Arabidopsis E2 that can catalyze Lys11-linked ubiquitination. With time, the work in the second part became more interesting and important, forming the central part of this thesis.

The specific objectives pertaining to Part I are:

(1) To identify E3 ligases that interact with Arabidopsis UBC13A

(2) To study the functions of UBC13-interacting E3 ligases

(3) To investigate how UBC13A/B functions in auxin signaling pathway

The specific objectives pertaining to Part II are:

(1) To identifying and characterize an Arabidopsis E2 capable of catalyzing Lys11-linked ubiquitination

(2) To determine the functions of UBC22 in reproductive and vegetative plant development

(3) To analyze the regulation of UBC22 expression patterns and protein stability

2. CHAPTER TWO - MATERIALS AND METHODS

2.1. Plant materials and assays

2.1.1. Plant materials and growth

Arabidopsis thaliana ecotype "Columbia" and its mutant derivatives were used in this study. The single T-DNA insertion mutant lines obtained from the Arabidopsis Biological Resources Center (ABRC) or Nottingham Arabidopsis Stock Centre (NASC) are listed in Table 2.1. To generate a double mutant, homozygous single mutant plants were obtained and crossed, and homozygous double mutants were identified in the F2 population by genomic PCR analysis. Higher order mutants were created by crossing lower order mutants, e.g. crossing a single and double mutant to create a triple mutant. The plants were grown in pots and placed in a growth chamber or a growth room (20°C constant, 16/8 h day/night photoperiod with a day light fluence rate of 90 - 120 μm/m^2/min). Genomic DNA was isolated and PCR performed as described below.

Table 2.1 List of Arabidopsis T-DNA insertion lines

Gene name	AGI code	T-DNA
UBC22	*AT5G05080*	SALK_ 061679 GK_642C08
UMI-A	*AT5G15790*	SALK_ 061679
UMI-B	*AT5G15790*	SALK_ 013618
UMI-C	*AT3G02290*	GK_ 262E04
UMI-D	*AT4G23450*	SALK_ 110094
UMI-E	*AT5G41350*	SALK_ 104783
UMI-F	*AT4G00335*	GK_ 843C09

2.1.2. Plant transformation

Agrobacterium tumefaciens cells carrying a construct based on either the pBI121 (Clontech) or the pCambia1300 (http://www.cambia.org/daisy/cambia/585) plant vector were used to transform Arabidopsis plants. Arabidopsis plants were grown in a growth chamber with 9 plants per pot. *A. tumefaciens* cells containing a construct of interest were grown on the 2 x YT agar plate (1.6% peptone, 0.5% yeast extract, 0.5% NaCl, 1.5% Agar and adjust pH 7.0) for three days. Then, cells were harvested and resuspended in 300 mL of 1/2-strength Murashige and Skoog (MS) medium plus 5% sucrose. Before infiltration, the surfactant Silwet-77 was added into the suspension to a final concentration of 0.02%. The inflorescence of 5 to 6 week-old plants was submerged into the suspension and then infiltrated under a vacuum of 600-700 mm Hg for 2 min. Infiltrated plants were put back into the growth chamber for setting seeds (T1). T1 seeds were screened on the plates of 1/2 MS medium (2.15 g/L MS salts (Sigma), 1% sucrose, 0.7% agar, pH 5.7) containing proper selection antibiotics (50 μg/mL kanamycin for pBI121-based constructs and 40 μg/mL hygromycin for pCambia1300-based constructs) and 300 μg/mL timentin. The kanamycin-resistant or hygromycin-resistant seedlings were selected and transferred to soil for further characterization and seed production.

2.1.3. Root growth and seed germination assays

Arabidopsis seeds were sterilized and stored at 4 °C for two days before being plated on 1/2 MS agar plates. For the root growth assay, the medium was supplemented with a given concentration of the test reagents, such as naphthaleneacetic acid (NAA, a synthetic auxin),

kinetin (KN, one of the cytokinins), methyl jasmonate (MeJA, a derivate of jasmonic acid), salicylic acid (SA), abscisic acid (ABA), 1-aminocyclopropane-1-carboxylic acid (ACC, a precursor of ethylene), mannitol (as an osmolyte), or N,N′ -dimethyl-4,4′ -bipyridinium dichloride (Paraquat, to produce oxidative stress), etc. Wild-type (WT) seedlings were grown side by side with mutant seedlings on the same plate, and the plates were placed vertically in the growth chamber. After 7 or 9 days, the plates were photographed. The primary root length of each seedling was measured using NIH ImageJ Software (version 1.42; https://imagej.nih.gov/ij/) and expressed as the percentage of the average length of the control WT roots in the same experiment.

For the seed germination assay in response to ABA, the 1/2 MS agar plate was supplemented with different concentrations of ABA analog, PBI425 (kindly provided by Dr. Adrian Cutler, National Research Council Saskatoon), which is more stable than ABA (Cutler et al., 2000). WT seeds were grown side by side with mutant seeds on the same plate, and then the plates were incubated horizontally in a growth chamber. After 7 days, germinated seeds were counted, and the percentage of germinated seeds was obtained. Also, the percentage of seedlings with green cotyledons was determined if needed.

2.1.4. Treatment of plants with *Botrytis cinerea*

One strain of *Botrytis cinerea* (kindly provided by Dr. Yangdou Wei, Dept. of Biology, Univ. of Saskatchewan) was grown on potato dextrose broth (PDB) agar plate at 22 °C for 7 days. Conidial spores were collected from plates and suspended in PDB medium to 5 x 10^5 /mL conidial spores. Leaves (third pair) were detached from 4 to 6 week-old *Arabidopsis*

plants and maintained on wet filter papers in large Petri dishes. For infection, 5 µL of the spore suspension was applied on each of the leaves. The Petri dishes containing inoculated leaves were wrapped with Parafilm and placed on the lab bench. To evaluate *B. cinerea* infection, the diameters of the lesions were measured after 3 days of the inoculation. For visualizing *B. cinerea* hyphae growth in Arabidopsis leaves, 1 cm^2 of infected leaf tissue was stained with trypan blue dye solution (0.4% (w/v) trypan blue) in a microcentrifuge tube and then observed under a microscope.

2.2. Microscopic and histochemical staining techniques

2.2.1. Microscopic analysis

For analyzing ovule or female gametophyte development, pistils of flowers or flower buds were removed and cuts were made on both sides of the pistil replum using a scalpel to expose ovules. The samples were fixed in a FAA solution (formaldehyde : acetic acid : ethanol : water (1 : 2 : 10 : 7)) for 1 hour, washed in 10-20% ethanol three times each for 5-10 min, and transferred to water. The ovules were detached, mounted in a clearing solution (chloral hydrate: water: glycerol (8 : 2 : 1)) and observed under a Leica DM2500 microscope equipped with differential interference contrast (DIC) optics. Photographs were taken using a Leica DFC450C digital microscope camera. For confocal microscopic analysis, the ovules were detached, mounted in a mounting solution (20 mM Tris-HCl pH 8.0, 0.5% (w/v) N-propyl gallate, 50% (v/v) glycerol) and analyzed using a ZEISS LSM 510 Confor2 microscope.

For aniline blue staining, the pistils were collected and cuts made along the carpel

using a scalpel, and then fixed in FAA solution overnight. The samples were then washed in 25%, 15% ethanol, and water sequentially for 10 min each. After washing, the pistils were placed in a 0.1% aniline blue solution in a microcentrifuge tube and vacuumed infiltrated for 1 min. After 4-h incubation in the dark, they were washed twice with PBS (Phosphate Buffered Saline, 137 mM NaCl, 2.7 mM KCl, 10 mM Na_2HPO_4, 1.8 mM KH_2PO_4, pH 7.4) for 20 min each. Ovules were then picked up and mounted on a glass slide. Fluorescence was observed under a Leica DM2500 microscope using the following filter set: excitation filter: LP 340-380 nm; dichromatic mirror: 400 nm; and emission filter: LP 425 nm.

2.2.2. Histochemical analysis of GUS reporter expression

Histochemical GUS staining was performed as described (Jefferson, 1987) with minor modifications. Seedlings and flowers were vacuum-infiltrated for 1 min in the GUS staining solution (50 mM PO_4^{3-} pH 7.0, 2 mM $K_3(Fe(CN)_6)$, 2 mM $K_4(Fe(CN)_6)$, 10 mM Na_2EDTA pH 8.0, 0.08% Triton X-100, 0.5 mg/ml X-gluc) and incubated at 37°C for overnight. The pistils were first fixed in 3.7% formaldehyde in the GUS staining buffer without X-gluc for 15 min and washed with GUS staining buffer without X-gluc for 5-10 min. They were then incubated in the GUS staining solution at 37°C for 2-24 hours (depending on the materials). After washing with 10-25% ethanol for 5-10 min by 3 times, ovules were mounted in the clearing solution (see the above) and examined under the microscope equipped with DIC optics.

2.3. Molecular biology techniques

2.3.1. Isolation of Arabidopsis genomic DNA and RNA, and cDNA synthesis

Genomic DNA was prepared using a method (Edwards et al., 1991) with modifications. A disc of Arabidopsis leaf was pinched out by the lid of a sterile microcentrifuge tube. Then, 400 µL of extraction buffer (200 mM Tris-HCl pH 7.5, 250 mM NaCl, 25 mM EDTA, 0.5% (w/v) SDS) was added and tissue was ground with a disposable plastic grinder until the entire tissue was ground. The tube was centrifuged at 14,000 x g for 5 minutes. The supernatant of 400 µL was transferred to a fresh 1.5 mL microcentrifuge tube containing 400 µL isopropanol, and mixed by inversions. The tube was left at room temperature for 10 min, followed by centrifugation at 14,000 x g for 10 min. The supernatant was discarded, and the pellet was dried for about 10 min at room temperature. The pellet was then dissolved in 100 µL water. For a 20 µL polymerase chain reaction (PCR) reaction, 1 µL of DNA sample was used.

Total RNA from desired tissues of Arabidopsis was isolated using TRIzol reagent (Invitrogen). Arabidopsis tissue (100 mg) was ground in liquid nitrogen and about 80 mg of powder was transferred into 800 µL of TRIzol reagent in a 1.5 mL microcentrifuge tube. The mixture in the tube was shaken vigorously by hand and left on ice for 20 min. After centrifuge at 14, 000 x g for 10 min at 4 °C, the supernatant was transferred into a new tube and 200 µL of chloroform was added followed by hand-shaking for a few seconds. The samples were left at room temperature for 5 min before being centrifuged at 14, 000 x g for 10 min at 4 °C. The aqueous phase on the top (250 µL) was then transferred into a new tube and 250 µL isopropanol was added, followed by mixing with hand shaking. The sample was incubated at room temperature for 15 min and centrifuged at 14, 000 x g for 15 min at 4 °C.

The supernatant was discarded, and the pellet was washed with 1 mL 70% ice-cold ethanol. After centrifugation at 7, 500 x g for 5 min at 4 °C, the pellet was air dried for 5-10 min. The RNA samples were stored at -80 °C for further uses.

The synthesis of the first-strand cDNA was performed with the ThermoScript RT-PCR kit (Invitrogen) according to the manufacturer's instructions. Typically, for each sample, 1 µg of total RNA was reverse-transcribed in a 10 µL cDNA synthesis reaction. The cDNA mixture was diluted 3 times with sterile H_2O, and 1 µL was used in a 20 µL PCR reaction.

2.3.2. Polymerase chain reaction (PCR) and real-time quantitative PCR (qPCR)

PCR was used to amplify DNA fragments for the purposes of cloning and other analyses. PCR reaction mixtures were created using the recipe guidelines in the instruction manual for the Taq DNA polymerase (Invitrogen). A T100 programmable thermal controller (Bio-Rad) was used as the thermocycler to carry out various amplifications. As a program guideline, a denaturing temperature of 94 °C for one minute was followed by an annealing temperature for 1 min, and primer extension was carried out at 72 °C for 1 min per kilobase of DNA to be amplified. These three steps were usually repeated for a total of 30 cycles. The annealing temperature, extension time, and total cycles may vary depending on primers and DNA fragments to be amplified. qPCRs were performed using Green-2-Go 2X qPCR Mastermix (BioBasic) on a CFX48 Real-Time PCR System (Bio-Rad), following the manufacturer's instructions. Each sample had at least three biological replicates. Data were analyzed with the CFX software (Bio-Rad).

Table 2.2 List of primers used for genotyping and real-time qPCR in this study

Primer	Purpose	Primer sequences
HW669	*AT5G38895*, forward	CAGTGTCGAGAATGGGTGCTTTCT
HW670	*AT5G38895*, reverse	CAGTGCGGCCGCCTAAGAAGTTTC
HW727	*AT5G15790*, forward	CAGTGTCGACAATGGGCTGTGTTT
HW728	*AT5G15790*, reverse	CAGTGCGGCCGCTTACGGTGTTTC
HW627	*AT3G02290* , forward	ACTGGGATCCAGCCAAGACCTCTGC
HW628	*AT3G02290* , reverse	ACTGGTCGACGTTCGAATTGCAT
HW729	*AT4G23450* , forward	CAGTGTCGACAATGGGTTGCTGCT
HW730	*AT4G23450* , reverse	CAGTGCGGCCGCTTATGATTCAGT
HW671	*AT5G41350*, forward	CAGTGTCGACAATGGGAGGTTGCT
HW672	*AT5G41350*, reverse	CAGTGCGGCCGCCTAGTCAAGAGT
SW16	*AT4G00335*, forward	CTTCTCACTTTTCTTCACC
HW732	*AT4G00335*, reverse	CAGTGCGGCCGCCTAGTTCAAGCG
HW1089	*UBC22*, forward	CAGTGTCGACAATGGCTAGTAATGAGAATCTACC
HW1090	*UBC22*, reverse	CAGTGCGGCCGCTCATAGTCTCTTCAAGCTTT
HW659	LB primer, for GK Line	ATATTGACCATCATACTCATTGC
HW1330	LB primer, for SALK line	TGGTTCACGTAGTGGGCCATCG
HW471	*AT4G33380*, forward	ATGAGAAGCTGGAGGAAGC
HW1470	*AT4G33380*, reverse	TCCTCAGGCTCTTCCTCTC
HW1471	*PR-1*, forward	TCTTCCCTCGAAAGCTCAAG
HW1472	*PR-1*, reverse	CGCTACCCCAGGCTAAGTTT
HW1473	*PR-2*, forward	ACAAGCAATGCAGAACATCG
HW1474	*PR-2*, reverse	AGATTCACGAGCAAGGGAGA
HW1475	*PDF1.2*, forward	CACCCTTATCTTCGCTGCTC
HW1476	*PDF1.2*, reverse	TGCTGGGAAGACATAGTTGC
HW1477	*PR-4*, forward	CGAACTTGTCCCGGTAACAT
HW1478	*PR-4*, reverse	AGCACTCACGGCTCTCAAAT
HW1479	*VSP2*, forward	ACCGTTGGAAGTTGTGGAAG
HW1480	*VSP2*, reverse	CCAAATCAGCCCATTGATCT
HW1481	*LOX2*, forward	GGATACATAACGGCCCAAGA
HW1482	*LOX2*, reverse	AGGCATCTCAAACTCGCACT
HW1483	*ORA59*, forward	AAGAGTGTGGCTTGGGACAT
HW1484	*ORA59*, reverse	GGACGGTTTCTCATGGAGTG

HW1485	*MYC2*, forward	ACCGACGACAACGCTTCTAT
HW1486	*MYC2*, reverse	CCAACCTTCGTGTGTTCCTT
HW1493	*ERF1*, forward	CCTTCCGATCAAATCCGTAA
HW1494	*ERF1*, reverse	ACCCTCTCATCGAGAAAGCA
HW1495	*ERF6*, forward	CGATTCCTTCACGTTCCAAT
HW1496	*ERF6*, reverse	GCCTCATCCTCACTCCTCTG
HW1497	*ERF96*, forward	GAGACGACCTTGGGGAAAAT
HW1498	*ERF96*, reverse	CGGTGGAAGAAGAGACACCA
HW1499	*ERF104*, forward	ACCAACCAATCCCCTAAACC
HW1500	*ERF104*, reverse	GTCCCAAGCCAGATCCTACA

2.3.3. Preparation of competent cells

For preparing *E. coli* (strain DH10B) competent cells, one liter of cell culture in LB (Lennox broth) was incubated at 37 °C until the optical density (OD) at 600 nm (OD_{600}) reached about 0.4. The culture was centrifuged at 4,000 x g for 10 min in a Beckman JA10.5 rotor, and the pellet was resuspended in 500 mL of ice-cold sterile 10% glycerol. The centrifugation was repeated 4 times, with each pellet resuspended in a reduced volume of ice-cold 10% glycerol. After the last centrifugation, the pellet was resuspended in 500 μL of 10% glycerol. The cells were aliquoted into 1.5 mL microcentrifuge tubes to a volume of 20 μL and were quickly placed in a -80 °C freezer for storage.

E. coli (strain BL21 (DE3) chemically competent cells were prepared similarly. One liter of cell culture was incubated at 37 °C until the OD_{600} reached 0.4. The culture was centrifuged at 4,000 x g for 10 min in a Beckman JA10.5 rotor, and the pellet was resuspended in 500 mL of ice-cold 0.1 M $CaCl_2$ solution. The centrifugation was repeated 4 times, with each pellet resuspended in a reduced volume of 0.1 M $CaCl_2$ solution. The last

pellet was resuspended in 500 μL of 0.1 M $CaCl_2$ in 10% glycerol. The cells were aliquoted into 1.5 mL microcentrifuge tubes to a volume of 20 μL and stored in a -80°C freezer.

2.3.4. Bacterial transformation

E. coli competent cells (DH10B) were transformed by electroporation. The plasmid DNA or diluted ligation mixture (1 μL) was added to one side wall of an electroporation cuvette (1 mm gap, Bio-Rad) and competent E. coli cells (20 μL) added. Following gentle mixing, the cells were electroporated using Electroporator 2510 (Eppendorf) with a voltage of 1.80 kV (for cuvettes with a 1 mm gap). Immediately after electroporation, a volume of 180 μL of SOC medium (2% w/v tryptone, 0.5% w/v yeast extract, 10 mM NaCl, 20 mM glucose) was added to the cuvette. The cells were transferred to a 1.5 mL microcentrifuge tube. After incubation at 37 °C for 1 hour, the cells were spread on LB (Lennox broth) agar plates containing proper antibiotics. These plates were incubated at 37 °C overnight for single colonies to grow.

E. coli competent cells (BL21 (DE3)) were transformed using a heat-pulse method. The plasmid DNA was added to competent cells in a microcentrifuge tube and incubated on ice for 20 min. For heat-pulse treatment, the tube was incubated in a 42 °C water bath for 45 seconds, and then on ice for 2 min. A total volume of 180 μL of SOC medium was added into the mixture. After incubation at 37 °C for 1 hour, the cells were spread on LB agar plates containing proper antibiotics.

2.3.5. Construct preparation

Plasmid construct preparations followed the general molecular cloning protocols

(Sambrook and Russell, 2001). Restriction enzymes were from Fisher Scientific (formerly Invitrogen; www.fishersci.ca) or New England BioLabs (https://www.neb.ca/). T4 DNA ligase was from Invitrogen. Enzymes were used with buffers supplied. Plasmid DNA isolation kits were from Promega (www.promega.ca) and BioBasic (www.biobasic.com). PCR DNA purification and DNA gel extraction kits were from BioBasic. Kits were used according to manufacturers' instructions.

In general, for cloning a DNA fragment into a vector, the DNA fragment was amplified from either cDNA or genomic DNA by PCR using the *Pfu* DNA polymerase with forward and reverse primers, each of which incorporates a restriction site at the 5'-end plus 3-4 extra nucleotides. The amplified DNA fragment was digested with two enzymes, one for each of the two ends, in a proper enzyme buffer at 37 ^{o}C. The vector with desirable restriction sites was digested with the same enzymes. In some cases, the insert DNA was from a previously prepared construct and released by the enzyme digest. The digested vector and insert DNA fragments were subjected to electrophoresis in agarose gels (normally 1%). The DNA bands were excised and purified using a DNA gel extraction kit. The purified digested insert and vector DNAs were added into a ligation reaction (usually 10 uL in volume) containing the ligase buffer and T4 DNA ligase. The ligation mixture was incubated at room temperature overnight. Following the incubation, the ligation mixture was diluted 1:3 with H_2O and 1 μL was used to transform *E. coli* competent cells. The colonies were screened by PCR with primers specific for the insert. Plasmid DNA was isolated from the cell cultures grown up from positive colonies and sequences were further verified by DNA sequencing.

For protein expression in Arabidopsis, *UBC22* coding sequence or other target genes were cloned into the plant expression vector modified from pBI121 (Clontech) or pCambia1300 (http://www.cambia.org/daisy/cambia/585.html) behind the CaMV (cauliflower mosaic virus) 35S promoter. The plant vectors were modified to have an HA (influenza hemaglutinin) tag (Li et al., 2016a) or yellow fluorescence protein (YFP), and used to express HA-tagged or YFP-fused target proteins e.g. UBC22. For complementation of *ubc22* mutants, a 3.2 kb promoter region (-3219 to -18 positions upstream of ATG) of *UBC22* was cloned as a HindIII-BamHI fragment to replace the 35S promoter.

For yeast two-hybrid analysis, E2-encoding genes were cloned into the GAL4 DNA-binding domain (GAL4-BD) vector (pGBT9, Clontech), while E3-encoding genes were cloned into the GAL4 DNA activation domain (GAL4-AD) vector (pGAD424, Clontech).

For protein expression in *E.coli*, the full-length coding region of *UBC22* was cloned into the expression vector pET28c (Novagen) downstream of the T7 promoter. For protein expression in yeast, the full-length *UBC22* and truncated *UBC22* fragments were cloned into the yeast expression vector modified from pYES2 (Stratagene) and containing a green fluorescence protein (YFP) for protein fusion (Li et al., 2016a).

UBC22-CRISPR (Clustered Regularly Interspaced Short Palindromic Repeats)/Cas9 construct was prepared using the vector system as described (Ma et al., 2015). Two target sequences were selected within *UBC22*, and each region as a sgRNA (sequence-specific single guide RNA) fragment was cloned into an intermediate vector *pYLsgRNA* to form a sgRNA expression cassette. Two sgRNA expression cassettes were released from the

intermediate vectors by enzyme digestion and ligated into one *pYLCRISPR/Cas9* binary vector (Ma et al., 2015). The construct was used to transform WT Arabidopsis plants.

2.3.6. Protein extraction

Plant materials such as seedlings were homogenized with a plastic pestle in a 1.5 mL tube containing protein extraction buffer (50 mM Tris-HCl pH8.0, 200 mM NaCl, 10 mM DTT (dithiothreitol), 1% (v/v) Triton X-100, Sigma protease inhibitor cocktail (Sigma # P9599)). Cell extracts were centrifuged at 14,000 x g for 10 min at 4 ºC. The supernatant was transferred into a fresh tube and centrifuged again for 5 min. The protein sample was stored at -80 ºC for further analysis. Bradford protein assay was used to determine total protein concentration (Bradford, 1976).

2.3.7. Recombinant protein expression and purification

E. coli BL21 (DE3) cells transformed with the desired construct as described above were grown overnight at 37 °C in 1 mL LB medium with 50 μg/mL kanamycin. In the next day, the 1 mL starter culture of cells was used to inoculate 50 mL LB medium containing 50 μg/mL kanamycin. Cells were allowed to grow to an OD_{600} of 1.0 and then induced with the final concentration of 0.2 mM isopropyl-β-D-thiogalactopyranoside (IPTG) for 4 h. The induced cells were harvested by centrifugation at 4,000 x g for 5 min in a Beckman JA10.5 rotor.

His-tagged recombinant proteins were purified using Ni-NTA Spin columns (Qiagen Ni-NTA Spin Kit) following the manufacturer's instructions with minor modifications. Cells harvested from a 70 mL culture were resuspended in 630 μL buffer NPI-10 (50 mM

NaH_2PO_4, 300 mM NaCl, 10 mM imidazole, pH 8.0). A volume of 70 µL lysozyme (10 mg/mL, ThermoFisher Scientific) and 3 units (for each mL of culture) of nuclease (Benzonase, ThermoFisher Scientific) were added into the cell suspension. After incubation on ice for 20 min, the cell lysate was centrifuged at 12,000 x g for 20 min at 4 °C and the supernatant (cleared lysate) was saved. The Ni-NTA spin column was equilibrated with 600 µL buffer NPI-10 (50 mM NaH_2PO_4, 300 mM NaCl, 10 mM imidazole and adjust pH 8.0) and centrifuged for 2 min at 890 x g. After the cleared lysate of 700 µL was loaded onto the pre-equilibrated Ni-NTA spin column, the column was centrifuged for 5 min at 270 x g (approx. 1500 rpm). The Ni-NTA spin column was then washed twice, each with 600 µL wash buffer NPI-20 (50 mM NaH_2PO_4, 300 mM NaCl, 20 mM imidazole and pH 8.0). Finally, the His-tagged recombinant protein was eluted from the column with 300 µL elution buffer NPI-500 (50 mM NaH_2PO_4, 300 mM NaCl, 500 mM imidazole and adjust pH 8.0) and stored at -80 °C for future use.

2.3.8. Sodium dodecyl sulfate-polyacrylamide gel electrophoresis (SDS-PAGE)

SDS-PAGE was performed using the Mini-Protean 3 gel apparatus (Bio-Rad). In general, protein samples in microcentrifuge tubes were added with a 4X protein sample buffer (200 mM Tris-HCl pH 6.8, 8% (w/v) SDS, 40% (v/v) glycerol, and 400 mM DTT) and then heated at 95 ^{o}C for 5 minutes. After cooling briefly one ice, protein samples were centrifuged briefly and loaded onto the gel. Usually 12% discontinuous (5% stacking and 12% separating) Tris-glycine polyacrylamide (37:1 acrylamide:bisacrylamide) gels were used. Following electrophoresis, the gels were stained with Coomassie Brilliant Blue staining

solution (0.025% (w/v) Coomassie Brilliant Blue R250, 40% (v/v) methanol, and 7% (v/v) acetic acid) for about 45 min, followed by incubation in a destaining solution (40% (v/v) methanol and 10% (v/v) acetic acid) until protein bands could be visualized.

2.3.9. Western blotting

Following SDS-PAGE, the resolving gel was equilibrated for 5 min in the transfer buffer (25 mM Tris base, 192 mM glycine, and 20% (v/v) methanol) along with an equal-sized piece of polyvinylidene difluoride (PVDF) membrane and 2 sheets of filter papers. These components were assembled as a "sandwich" cassette in the order of (cathode to anode) filter paper, PVDF membrane, gel, and filter paper. For transferring proteins to the membrane, the cassette was placed in a Mini Trans-Blot electrophoretic transfer tank (Bio-Rad) with 700 mL transfer buffer, and the transferring was performed at a constant voltage of 100 V for 60 min. Following the transfer, the membrane was washed with 1X PBS and then incubated in a blocking solution (5% (w/v) skim milk in 1X PBS) at room temperature for 1 h. The membrane was incubated with the primary antibody in the blocking solution with 0.1% (v/v) Tween-20 (PBST) at 4 °C for overnight. The monoclonal antibodies against GFP (sc-9996) and HA-tag (sc-7392) protein were from Santa Cruz Biotechnology. After the incubation, the membrane was washed with 1X PBST three times for 10 min each and then incubated with the secondary antibody conjugated with horseradish peroxidise (e.g., Bio-Rad goat anti-mouse IgG horseradish peroxidase conjugate, #170-6516) in the blocking solution for 1 h. After the incubation, the membrane was washed with 1 x PBST three times for 10 min each. After the washing, ECL Prime or ECL Plus reagent (GE Health) was applied to the

membrane according to the manufacturer's instructions. The membrane was placed into GeneSys imaging system (Syngene) for visualization of the protein to be detected.

2.3.10. *In vitro* Ub dimer assay

In vitro Ub conjugation reactions were performed using the purified His-tagged UBC22. The Ub thioester/conjugation initiation reagents were purchased from Boston Biochem (K-995). Unless noted otherwise, the reaction mixture contained 5 μM purified His-UBC22 and 62.5 μM Ub in the supplied reaction buffer, while concentrations of other components followed the manufacturer's instructions. The K11R, K48R and K63R mutant Ub proteins were purchased from Boston Biochem (UM-K11R, UM-K48R, and UM-K63R). The conjugation reactions were performed at 30 °C for 4 hours. Samples were added with 4X non-reducing loading buffer (200 mM Tris-HCl pH 6.8, 8% SDS, 0.2% (w/v) bromophenol blue, and 40% (v/v) glycerol) and heated at 95 °C for 5 min, then subjected to SDS-PAGE (15% gel). Ub protein bands were detected by western blotting using a monoclonal mouse anti-Ub antibody (P4D1, Cell Signaling Technology) and a horseradish peroxidase-conjugated goal anti-mouse antibody (Bio-Rad). The signal was visualized with ECL Prime reagent (GE Health) according to the manufacturer's instructions.

2.3.11. Yeast transformation

Yeast transformation utilized a modified dimethyl sulfoxide (DMSO)-enhanced method (Hill et al., 1991). A 1 mL culture of yeast cells grown overnight at 30°C in the yeast peptone dextrose (YPD) medium (1% (w/v) yeast extract, 2% (w/v) peptone, and 2% (w/v) glucose) was sub-cultured into 3 mL of fresh YPD. After culturing at 30 °C for about 6 hours

with shaking at 200 rpm, the cells were harvested by centrifugation, washed with 400 μL LiOAc solution (0.1 M lithium acetate, 10 mM Tris-HCl pH 8.0, 1 mM EDTA), and resuspended in 100 μL of the same solution. Then, the cell suspension was added with 5 μL denatured carrier DNA (single-stranded salmon sperm DNA) and 0.1 μg plasmid DNA, and mixed well. After incubation at room temperature for 5 min, 280 μL of the plating solution (50% (v/v) polyethylene glycol 4000 in LiOAc solution) was added and mixed by inverting 4-6 times. The transformation mixture was then incubated overnight at room temperature. In the next day, 40 μL of DMSO was added, and the mixture was treated with a 5-min heat shock in a water bath at 42 °C. The yeast cells were then washed with sterile ddH_2O, resuspended in 100 μL of ddH_2O and plated on synthetic defined (SD) agar plates lacking a specific amino acid(s) (e.g. Ura) for selection. The plates were incubated at 30°C for 3 days for the colonies to grow.

2.3.12. Yeast two-hybrid analysis

The yeast two-hybrid strain PJ69-4A was co-transformed with different combinations of GAL4-BD and GAL4-AD constructs (James et al., 1996). The co-transformed colonies were initially selected on SD-Leu-Trp plates. For each transformation, at least three independent colonies were grown on SD-Leu-Trp plates and then plated onto either SD-Leu-Trp-His plates or SD-Leu-Trp-His plates containing various concentrations of 1,2,4-amino triazole (3-AT) to test the activation of the P_{GAL1}-*HIS3* reporter gene, or SD-Ade plates to test the activation of the P_{GAL1}-*ADE* reporter gene. Plates were incubated for 3 days at 30 °C for the colonies to grow.

2.3.13. Protein expression in yeast

pYES2-based constructs were used to transform MaV203 cells (Life Technologies), and the protein expression in the transformant cells can be induced by galactose. Single colonies selected from SD-Ura plates were used to inoculate into culture tubes each with 3 mL of SD-Ura medium. The cultures were incubated at 30 ºC in a shaking incubator (250 rpm) overnight to reach an OD_{600} value of 1.0. The cells were harvested by centrifugation at 800 x g for 5 min at room temperature, and the supernatant was decanted. Cells were then washed with 2 mL sterile water and resuspended in 3 mL of YPD-galactose (1% (w/v) yeast extract, 2% (w/v) peptone, 1% (w/v) galactose, and pH 6.5) medium to induce protein expression. The culture was incubated with shaking at 30 ºC for 4 h. Subsequently, 1 mL of culture was transferred to a 1.5 mL microcentrifuge tube and centrifuged at 15,000 x g for 15 seconds. The cell pellet was resuspended in 50 µL of ice-cold protein extraction buffer (Yeastbuster Protein Extraction Reagent (Novagen) with 1X tris(hydroxypropyl)phosphine (THP) solution and 2X protease inhibitor cocktail (Roche). Two 0.5 mm glass beads were added to the mixture, which was then incubated at 25ºC with gentle shaking for 20 min. After centrifugation at 16,000 x g at 4ºC for 20 min, the supernatant containing induced protein was transferred to a fresh tube and stored at -80 ºC for further analysis.

2.3.14. RNA-seq preparation and analysis

Purified total RNA was precipitated and resuspended in RNase-free water to a final concentration of 100 ng/µL. Fifteen cDNA libraries were constructed using the TruSeq RNA Sample Preparation Kit v2 (Illumina) using RNAs from Type I, Type II, Type III, Type IV

ubc22 mutant and also WT plants, with three biological replicates for each type. Paired-end sequencing was conducted on the Illumina HiSeq2500 (Illumina), generating 101-nucleotide reads, at the National Research Council, ACRD-Saskatoon, Canada. Sequencing adapters were removed, and low-quality reads were trimmed using Trimmomatic with default settings (Bolger et al., 2014). The filtered reads were mapped to TAIR10 genome sequence using STAR software program (Dobin et al., 2013). Transcripts were identified using StringTie (Pertea et al., 2015) and followed by Cuffmerge tool (Trapnell et al., 2012). HTseq-count (Anders et al., 2015) was employed to count the reads spreading at the exonic regions of each gene. Differential expression analysis was performed with DEseq2 between mutants and WT (Love et al., 2014). Normalized counts from DESeq2 were expressed as gene expression levels. Genes with less than 10 reads across all samples were excluded to eliminate the extremely low expressed transcripts. Functional annotations of genes were obtained from the Bio-Array Resource for Arabidopsis Functional Genomics database (BAR) (http://bar.utoronto.ca/) using the AGI numbers. Hierarchical clustering was performed to identify the expression patterns of differentially expressed genes. Gene Ontology (GO) enrichment was analyzed using ClusterProfiler (Yu et al., 2012).

3. CHAPTER THREE - STUDIES OF MECHANISMS UNDERLYING THE PLANT GROWTH PHENOTYPES OF *ubc13* DOUBLE MUTANT

3.1. Introduction

The auxin insensitivity shown by the *ubc13* double mutant resembles the auxin resistant phenotypes of Aux/IAA protein-stabilizing mutants and loss-of-function ARF mutants. It is known that some Aux/IAAs and ARFs are important for root and root hair development. For instance, IAA12/BODENLOS and its interacting ARF5/MP have been well studied for their function in the development of the embryonic root in Arabidopsis (Hamann et al., 2002; Hardtke and Berleth, 1998). For lateral root development, IAA14 and its partners ARF7 and ARF9 are critical (Fukaki et al., 2002; Okushima et al., 2007). In the IAA14-stabilizing mutant or *arf7 arf9* double mutant, the lateral root formation is completely inhibited. Similarly, root hair density is reduced in some Aux/IAA protein-stabilizing mutants (Ishida et al., 2008) and in particular, the stabilization of IAA17 (AXR3) completely blocks the initiation and elongation of root hairs (Knox et al., 2003). It has been proposed that increased Aux/IAA protein levels may be the underlying reason for the strong root phenotypes in the *ubc13* double mutant. Indeed, the level and activity of IAA17-GUS fusion protein were higher in the *ubc13* double mutant than in the WT (Wen et al., 2014).

It is difficult to fully understand the functions of UBC13 without knowing which E3s it interacts, and very little is known about the E3s involved in UBC13-mediated ubiquitination. As reviewed earlier, only one pair of E3s, RGLG1 and RGLG2, have been shown to interact with UBC13 and catalyze the formation of the K63-linked Ub chains *in*

vitro (Yin et al., 2007). However, the *rglg1 rglg2* double mutant has reduced apical dominance and altered phyllotaxy which have little overlap with the phenotypes displayed by the *ubc13* double mutant. Interestingly, it has been reported that K63-linked polyubiquitination of the auxin transporter PIN2 is affected in the *rglg1 rglg2* double mutant suggesting an important role of RGLGs in the auxin signaling pathway (Leitner et al., 2012). Therefore, identification and characterization of E3s that interact with UBC13 could let us gain further insight into the specific components functioning in the UBC13-mediated pathway.

3.2. Results

3.2.1. Studies of UBC13-Interacting E3s

3.2.1.1. Identification of UBC13-Interacting E3s

One important aspect of understanding the UBC13-mediated pathway is to identify E3s that interact with UBC13. In the Arabidopsis genome, there are over 1,000 genes that are predicted to encode E3 ligases, and close to 40 genes for E2s (Kraft et al., 2005; Stone et al., 2005). It is reasonable to assume that a small subset of E3s can interact with UBC13.

One way to identify E3 ligases that can interact with UBC13 is the yeast two-hybrid method. We took some rationalized approaches to identify E3s that could interact with UBC13 in Arabidopsis. In one approach, we used the sequences of yeast and human E3s that have been shown to interact or possibly interact with yeast and human UBC13 proteins to search for the related Arabidopsis protein sequences. Also, the putative E3 proteins in the Arabidopsis genome have been classified based on protein sequence similarity (Kraft et al.,

2005). Some RING-type E3s were shown to be able to catalyze *in vitro* protein ubiquitination with UBC13. Since the RING domain in E3s is responsible for the interaction with an E2 such as UBC13, the fragments of different E3s containing the RING domain were cloned and analyzed for the interaction with UBC13 in the yeast two-hybrid assay. An initial survey was conducted by Dr. Rui Wen. From about twenty E3s surveyed, four were found to interact with UBC13. Those E3s belong to several different subclasses (Kraft et al., 2005). Further, similar analysis was performed on E3s that are neighboring subclasses of E3s which have shown to interact with UBC13. As a result, three additional groups of E3s were found to interact with Arabidopsis UBC13 by the yeast two-hybrid assay. Among them, one group consisting of six members was tentatively named UMI (UBC13-Interacting E3s) (Figure 3.1 and Table 3.1).

The six members of the UMI family and other closely related E3s were analyzed regarding the specificity of interactions with different E2s. Several representative E2s from different E2 subgroups (UBC3, 7, 8, 30 and 34), were chosen for the analysis. For example, UBC3, from the UBC group III, is closely related to yeast Ubc2/Rad6 and human UBE2A/2B. UBC8 and UBC30 are from the largest subgroup VI, which are similar to yeast Ubc4/5 and human UBE2D1 to 4. The E2s, belonging to this subgroup, are the most generic E2s which can work with many different RING E3s to promote polyubiquitin chain assembly *in vitro* (Kraft et al., 2005). Among them, UBC8 is active with the most number of E3s and UBC30 is active with the least number of E3s based on the results of (Kraft et al., 2005). Our yeast two-hybrid results showed that the six UMI E3s could interact with UBC13A, and the majority of them could also interact with UBC8 and/or UBC30. However, their interactions with UBC13

were stronger than the interactions with UBC8 and UBC30 based on cell growth in the yeast two-hybrid assay (Figure 3.1), suggesting possibly a preferential binding to UBC13A.

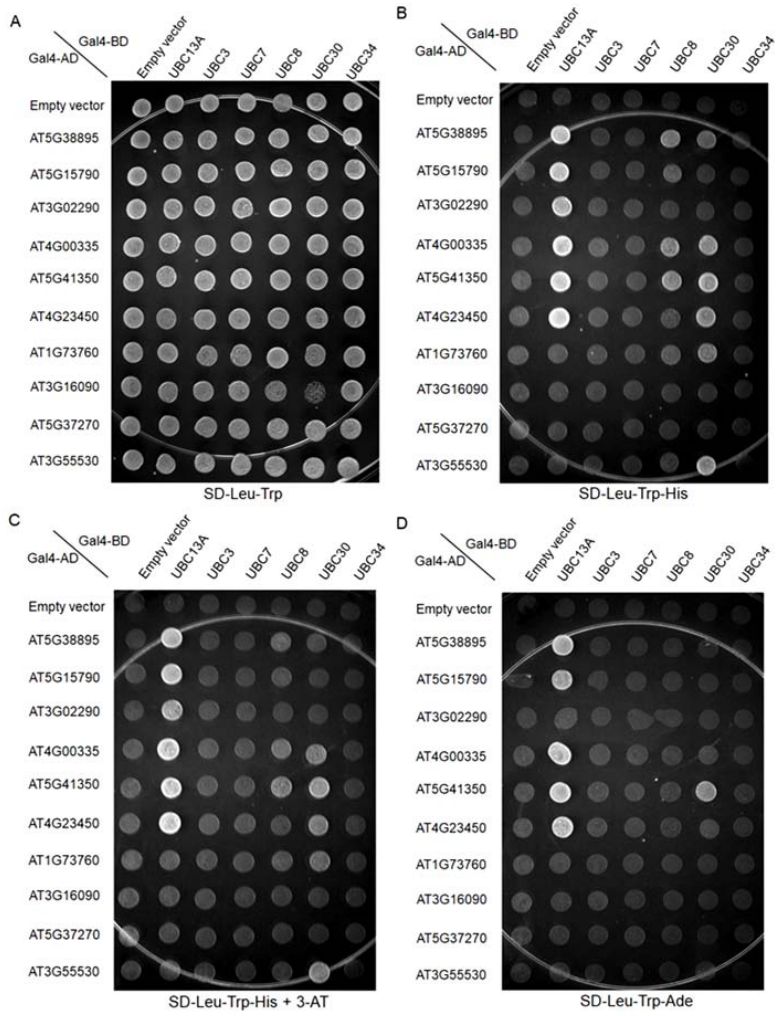

Figure 3.1 Analysis of interactions between E2s and E3s in a yeast two-hybrid assay. The E3 genes were cloned into the GAL4 DNA activation domain (GAL4-AD) vector (from pGAD424), and the E2s were cloned into the GAL4 DNA-binding domain (GAL4-BD) vector (from pGBT9). One GAL-AD construct and one GAL-BD construct were used to co-transform the yeast strain PJ69-4A. The E2s and E3s are indicated on the top and the left side of the image. The full-length coding regions of the E2s and E3s were used, except for *AT3G02290* for which the RING domain was used in this experiment. The transformants were grown on different SD medium plates. (A) SD medium plate lacking leucine and tryptophan (SD-Leu-Trp); (B) SD medium plate lacking leucine, tryptophan, and histidine (SD-Leu-Trp-His); (C) SD medium plate lacking leucine, tryptophan, and histidine, but supplemented with 1.5 mM 3-Amino-1,2,4-triazole (3-AT) (SD-Leu-Trp-His + 3-AT); (D) SD medium plate lacking leucine, tryptophan, and adenine (SD-Leu-Trp-Ade).

Table 3.1 Summary of interactions between E2s and E3s in a yeast two-hybrid assay.

E2 / E3	UBC13A	UBC3	UBC 7	UBC 8	UBC 30	UBC 34
	AT1G78870	AT5G62540	AT5G59300	AT5G41700	AT5G56150	AT1G17280
AT5G38895	+++	-	-	++	+	-
AT5G15790	+++	-	-	+	-	-
AT3G02290	+++	-	-	+	-	-
AT4G00335	+++	-	-	++	++	-
AT5G41350	+++	-	-	++	+++	-
AT4G23450	+++	-	-	-	++	-
AT1G73760	-	-	-	-	++	-
AT3G16090	-	-	-	-	-	-
AT5G37270	-	-	-	-	-	-
AT3G55530	-	-	-	-	++	-

The E3s were cloned into the GAL4 DNA activation domain (GAL4-AD) vector (from pGAD424), and the E2s were cloned into the GAL4 DNA-binding domain (GAL4-BD) vector (from pGBT9). The full-length coding regions were used for all genes. One GAL4-AD construct and one GAL4-BD construct were used to co-transform the yeast strain PJ69-4A and transformants were grown on different selection plates for evaluation (Figure 3.1). "-" means no cell growth on SD-Leu-Trp-His plates, indicating no interaction between the pair of E2 and E3. "+" means cell growth on plates of SD-Leu-Trp-His, suggesting an interaction between the E2-E3 pair. "++" means cell growth on plates of SD-Leu-Trp-His + 1.5 mM 3-AT, suggesting a stronger interaction between the E2-E3 pair. "+++" means cell growth on plates of SD-Leu-Trp-Ade, suggesting an even stronger interaction between the E2-E3 pair.

3.2.1.2. Sequence analysis of UMI E3s

Sequence analysis revealed six closely related members in this clade of E3s, which we refer to as the UMIs: *AT5G38895 (UMI-A), AT5G15790 (UMI-B), AT3G02290 (UMI-C), AT4G23450 (UMI-D), AT5G41350 (UMI-E)* and *AT4G00335 (UMI-F)*. These six E3s can be further grouped into two subgroups (Figure 3.2). The six *UMI* genes encode relatively small proteins of about 150-230 amino acids. They share a highly conserved RING finger domain of about 40 amino acids, which is close to the C-terminus (Figure 3.3). However, the two subgroups have distinct N-terminal extensions, with the UMI-ABC subgroup having a shorter N-terminal extension than the other subgroup. It is interesting to observe that the full-length UMI-C had a stronger interaction with UBC13 than the truncated UMI-C lacking the N-terminal extension suggesting that the N-terminal extension may enhance the E2-E3 interaction (Figure 3.1). It remains to be determined whether this is true for the other UMI members.

RHF1a (RING-H2 group F 1a) and RHF2a are a pair of closely related E3s. Down-regulation of *RHF1a* and *RHF2a* has been reported to affect several aspects of plant growth and development (Liu et al., 2008). RHF1a/2a proteins share a conserved RING finger domain with UMIs, but the protein size is much larger with about 370 amino acids.

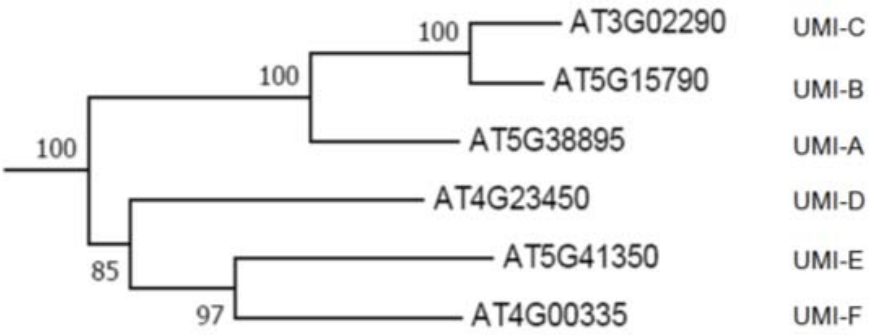

Figure 3.2 Phylogenetic analysis of Arabidopsis UMI E3s. Protein sequences of 6 related genes in this family (clade) were aligned using the program ClustalX2 with default parameters, and the tree was derived from the program MEGA4. The six members can be divided further into two subgroups, and each member is assigned with a letter to differentiate.

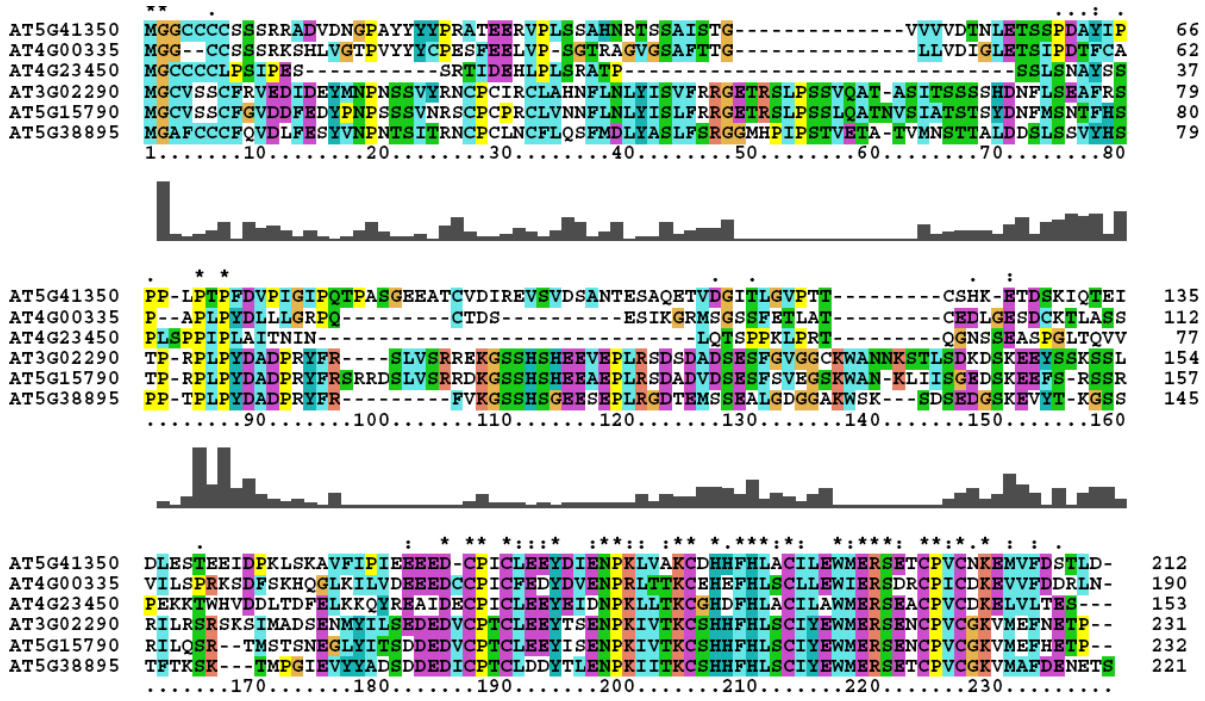

Figure 3.3 Amino acid sequence analysis of UMI family proteins. Amino acid sequences of 6 members in this family were aligned using the program ClustalX2 with default settings.

The UMI family of E3s and RHF1a/2a are clustered into the RING-H2 subtype of E3 (Stone et al., 2005). In this subtype of E3, the RING domain has a unique pattern with two His residues at the metal-ligand positions 4 and 5. The RING-H2 subtype of Arabidopsis has the most members with 241 RING-type E3s (Stone et al., 2005). Since the RING domain is responsible for the interaction with an E2, the interaction between UMIs and UBC13A might be determined by the RING domain sequence of UMIs. Sequence analysis showed that a few unique residues are shared in the RING domains of UMI family and RHF1a/2a (Figure 3.4). For example, the Pro residue between metal-ligand positions 2 (Cys) and 3 (Cys), and the Ser residue between metal-ligand positions 6 (Cys) and 7 (Cys) are only present in the UMI E3s and RHF1a/2a, but absent in the E3s which did not show an interaction with UBC13A. It would be interesting to determine experimentally whether these two residues play an important role in the interaction of the UMI E3s with UBC13A.

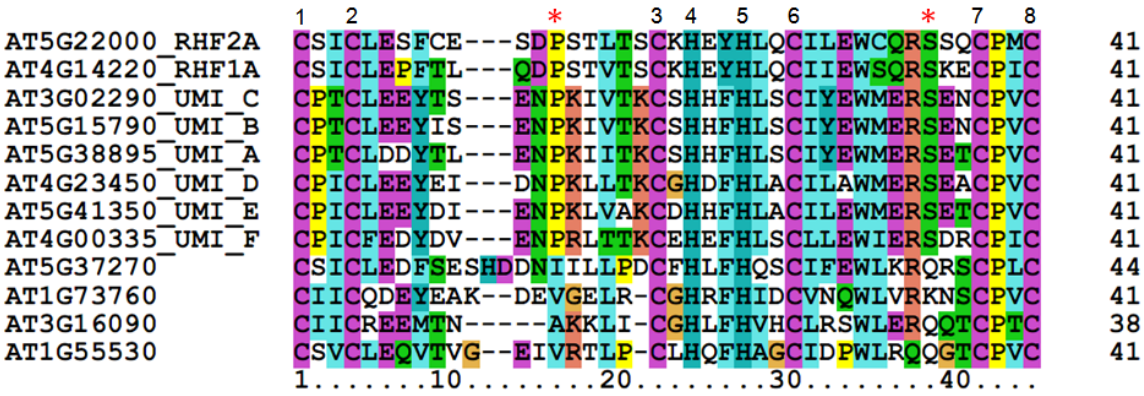

Figure 3.4 Sequence analysis of RING finger domains in UMI and other E3s. The RING domains from E3s of UMI family, RHF1a/2a, and four other E3 proteins, which are in closely related clades based on phylogenetic analysis and do not show an interaction with UBC13, were included in the analysis. Protein sequences were aligned with the program ClustalX2. The conserved Pro and Ser residues among the UMI and RHF1a/2a proteins are indicated with "*" symbols. The 8 metal ligand positions are indicated on the top of the figure.

3.2.1.3. Expression profiles of UMI E3s

To investigate the expression patterns of *UMI* genes in Arabidopsis, GENEVESTIGATOR database (https://www.genevestigator.com/gv/plant.jsp) was utilized to examine the expression of each UMI member in different development stages (Hruz et al., 2008). This resource is publicly available, and the expression profiles of many genes in Arabidopsis are based on a large set of microarray data.

The six *UMI* genes are expressed in different tissues and at various development stages (Figure 3.5). They seem to show a similar expression pattern with higher levels of expression in flowers, mature siliques, and germinated seeds, although *UMI-B (AT5G15790)* and *UMI-D (AT4G23450)* have lower levels of expression in general than the other members. The similarity in the expression pattern reflects possible functional redundancy of these six genes.

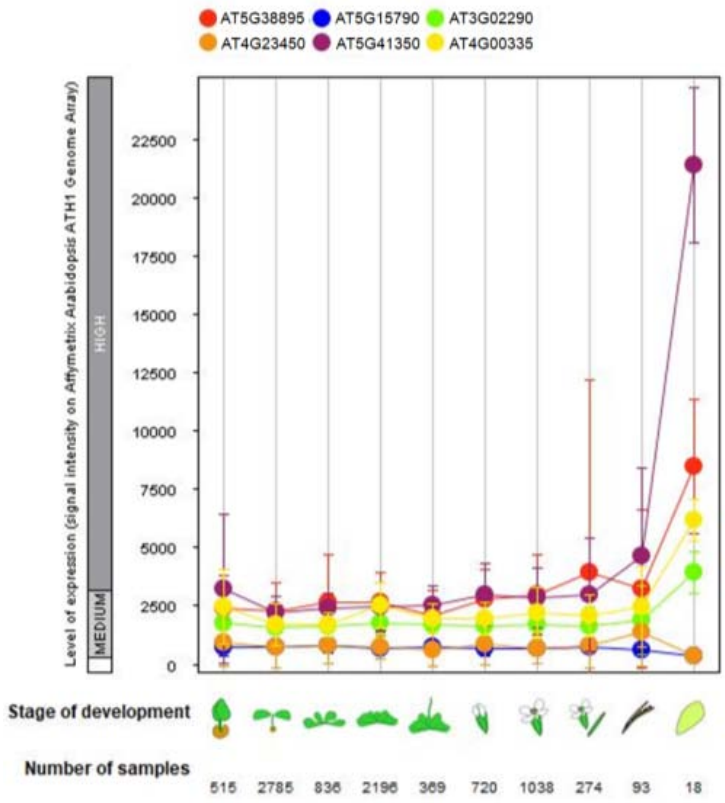

Figure 3.5 Developmental expression profiles of *UMIs*. The figure was generated by Genevestigator based on microarray expression data (https://genevestigator.com). Developmental stages and number of samples are indicated at the bottom of the figure.

3.2.1.4. Analysis of T-DNA mutants of *UMI* genes

To study their functions, T-DNA insertion mutants for this family of genes were obtained from the ABRC (Arabidopsis Biological Resources Center). The T-DNA insertion sites in the six genes were verified by genomic PCR (Figure 3.6). Homozygous lines were then obtained for each of genes. Those single homozygous lines, however, did not display any apparent phenotypic changes compared to the WT plants. To obtain double mutants, I performed crosses between various single mutants (for simplicity, the *UMI* mutants are referred to by the last letter of the gene name, for instance, *"a"* for *UMI-A* mutant) and screened the progeny plants. As a result, the double mutants, *ab*, *bc*, *df*, and *ef* were obtained,

but they did not display any phenotype either. This result is not totally surprising given the possible functional redundancy among the six closely related genes. Subsequently, I crossed two double mutants with a single mutant to create two triple mutants, *abc* and *def*. For each triple mutant, two independent lines were obtained, and no obvious phenotype was observed under normal growth conditions.

Since E3s may be involved in plant response to environmental changes and hormonal regulation, the two triple mutants were subjected to hormone treatments and stress conditions such as auxin, kinetin (KT), ethylene, jasmonic acid (JA), and salt. From the screening using a number of conditions, it was observed that the *def* triple mutants were sensitive to glucose while they were similar to the WT for all other treatments. Subsequently, a series of mutants including single, double and triple mutants (*d, e, f, df-37, ef-3, def-5,* and *def-26*) in the *UMI-DEF* subgroup were further tested. Interestingly, it was observed that in 4% glucose treatment, two triple mutant lines, *def-5* and *def-26*, had shorter roots than the WT (Figure 3.7). Also, the seedling growth of the *def-5* and *def-26* lines was inhibited by 4% glucose while the *ef-3* double mutant did not show a difference compared with the WT (Figure 3.7). The stronger sensitivity of the *def* triple mutants to glucose was further confirmed by the analysis of seed germination at different concentration of glucose and mannitol. While the *def-26* triple mutant did not show any difference from the WT at different concentrations of mannitol treatment compared to WT, it showed decreased percentages of seed germination and seedlings with green cotyledons with increasing glucose concentrations in the medium. (Figure 3.8).

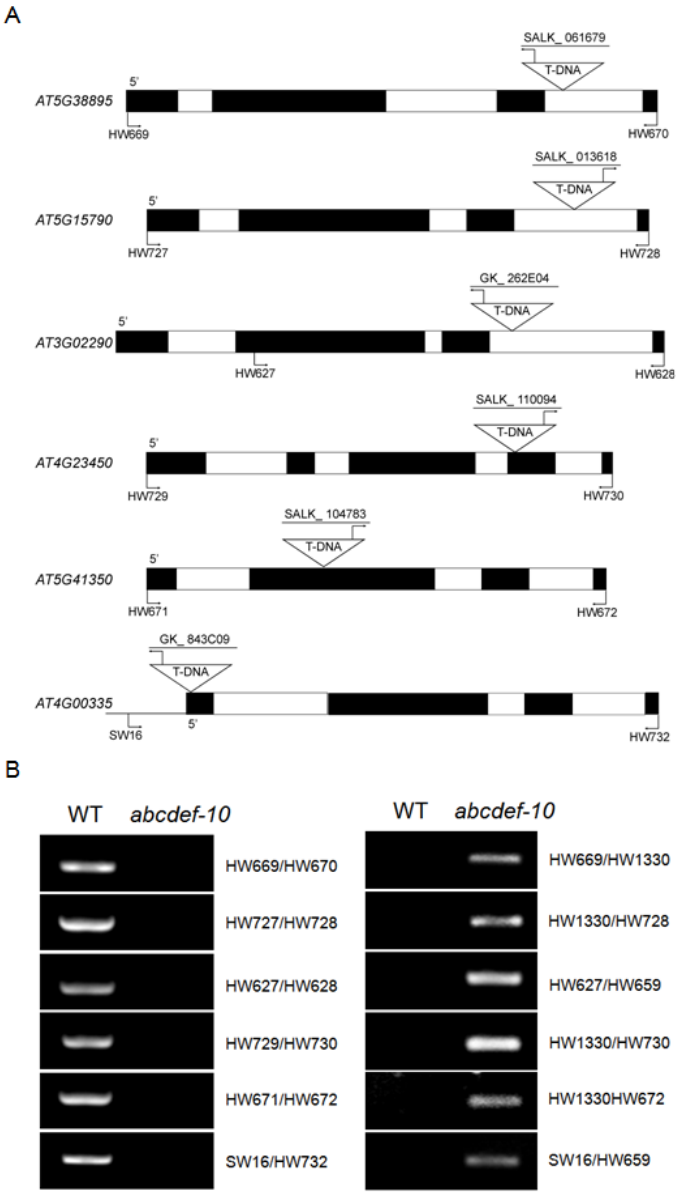

Figure 3.6 Confirmation of *UMIs* T-DNA insertion mutants. (A) Schematic representation of the genomic structure for six *UMI* genes, with the locations of primers and T-DNA insertion sites in the mutants shown. Black boxes: exons; white boxes: introns; gene-specific primers are also indicated. (B) Characterization of the hextuple mutant (*abcdef-10*) *of UMIs* by genomic PCR. Plant lines used are indicated above the panels and the primers at the right of the panels. The results of PCRs using gene-specific primers for the WT alleles are shown in the left panel and results of PCRs using one gene-specific primer, and one T-DNA primer are shown in the right panel. HW1330 is a left border primer for the SALK T-DNA lines, and HW659 is a left border primer for the GK T-DNA lines.

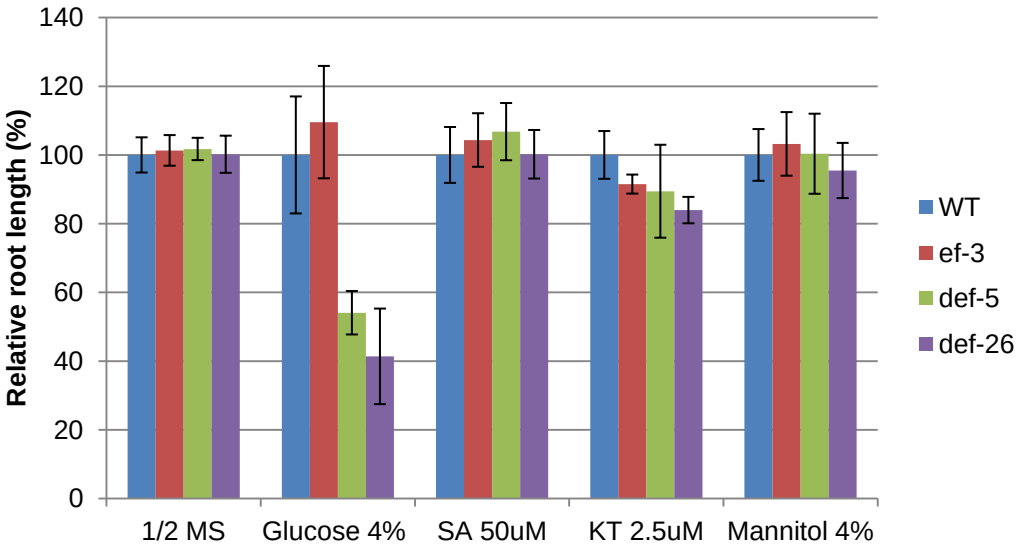

Figure 3.7 Root growth analysis of mutants compared to WT under different conditions. In each plate, mutant seedlings were grown side by side with WT seedlings as the reference. Plate images were taken when seedlings were 2-week old, and primary root length was measured using ImageJ. For each condition, at least 3 plates were used with each plate having 7-8 WT seedlings and 7-8 mutant seedlings. Y-axis indicates relative root length with the root length of the WT seedling set at 100%. The conditions used were: ½ MS, and ½ MS plus 4% glucose, 50 μM salicylic acid (SA), 2.5 μM kinetin (KT) or 4% mannitol.

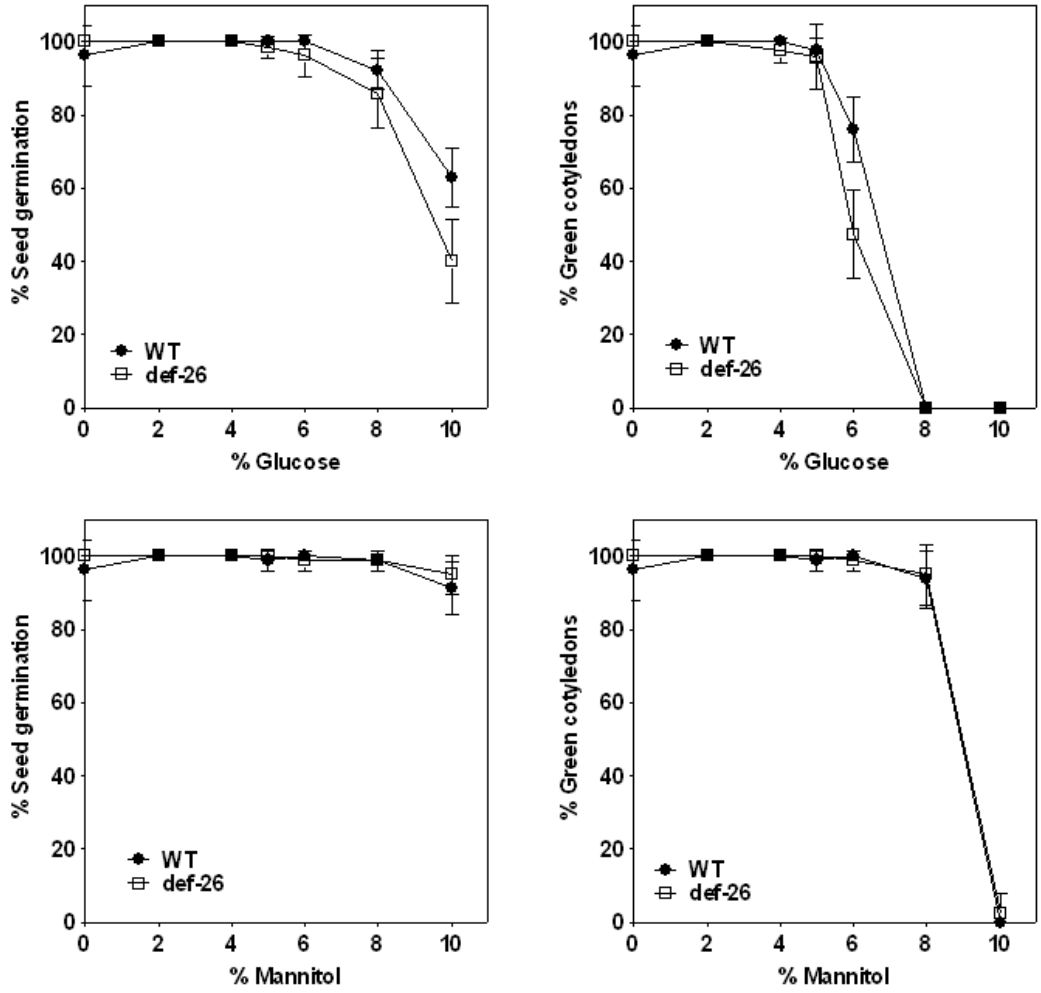

Figure 3.8 Seed germination of the *UMI-DEF* triple mutant at different concentrations of glucose and mannitol. The *UMI-DEF* triple mutant (*def-26*) and WT seedlings were grown on plates containing different concentrations of glucose and mannitol. For each condition, 5 plates were used with each plate containing 16 seedlings. Survey on seed germination and seedlings with green cotyledons was performed 12 days after seeds were sewn on the plates.

Although the *def* triple mutants displayed a phenotype in response to glucose treatment, they did not show any obvious morphological phenotype under normal conditions. The six closely related UMIs may share function redundancy, and a phenotype may require the inactivation of all six genes. Therefore, two triple mutants, *abc-14* and *def-26*, were crossed to create the hextuple mutant in which all six *UMI* genes were inactivated (Figure 3.6). Three individual homozygous lines of the hextuple mutant have been obtained. However, none showed any obvious changes in plant growth and morphology when plants were grown in soil, or when seedlings were grown in Petri plates under normal or auxin treatment conditions.

3.2.2. Analysis of overexpression of an *ARF*

It has been proposed that the levels of Aux/IAA proteins (transcriptional repressors in the TIR1/ABF-mediated auxin signaling pathway) increase in the *ubc13* double mutant (Wen et al., 2014). If the strong root phenotypes of the *ubc13* double mutant are mainly due to an increased level of Aux/IAAs, expression of a certain ARF, which is inhibited by Aux/IAA proteins, is expected to at least partially rescue the root phenotypes. Thus, several candidate ARF transcription factors (ARF5, ARF6, and ARF7) were selected for testing based on their roles in transcription activation (Tiwari et al., 2003). The plan was to firstly transform WT plant with the constructs, and transgenic lines would be selected and analyzed for *ARFs* overexpression and auxin response. The transgenic line could then be crossed with the *ubc13* double mutant to determine whether they can rescue the mutant phenotypes.

3.2.2.1. Effect of overexpressing an *ARF* on plant growth and auxin signaling

ARF5, ARF6, ARF7, and ARF19 have been shown to function as transcription activators in auxin signaling while ARF1 as a transcription suppressor when analyzed in carrot protoplasts (Tiwari et al., 2003). The activator ARFs bind to auxin-response element (AuxRE) and activate the expression of auxin-responsive genes. We used the *$DR5_{rev}$::GFP* line (from Dr. Raju Datla) as an auxin response marker. The synthetic DR5 promoter consists of 7-9 repeats of an auxin-response element (Ulmasov et al., 1997). As a result, GFP reporter expression depends on the level of endogenous auxin or auxin response. The ARF proteins are required for auxin response, and they contain four different domains: a B3 domain, an ARF domain, a variable middle region that confers activator or repressor activity, and a carboxy-terminal dimerization region involved in homo- and hetero-dimerization. The latter two domains are also referred to as domains III and IV, critical for the dimerization of ARF/ARF or IAA/ARF (Guilfoyle and Hagen, 2007). It is thought that deleting domains III and IV from ARFs may impair the interaction with the Aux/IAA proteins, leading to stronger activation of the downstream genes. Indeed, it has been reported that truncated ARF5 protein lacking domains III and IV could complement *arf5* null mutant and enhance the expression level of many auxin-inducible genes (Krogan et al., 2012). In this study, truncated forms of IAA12, ARF5, and ARF7 with domains III and IV deleted (referred to as IAA12Δ, ARF5Δ or ARF7Δ) were also included in the analysis.

To determine GFP reporter expression in Arabidopsis, each sample was prepared using a pool of independent 20-25 transformants to represent the average expression level of

the 20-25 plants. The protein samples were used in western blotting for detecting the GFP protein level. There was a basal level of GFP expression in the WT (Figure 3.9). Since the synthetic DR5 promoter contains several AuxRE elements which are the binding sites for ARFs, overexpressing *ARFs* is expected to enhance the expression of GFP protein. The overexpression of *IAA12Δ* resulted in a lower level of GFP reporter consistent with the function of IAA12 as an inhibitor of ARFs. Surprisingly, the GFP level was dramatically lower in the transformants overexpressing *ARF5Δ* or *ARF7Δ* (Figure 3.9). This result is both puzzling and interesting, and there are different possible reasons (discussion in Section 3.3.2). On the other hand, the GFP level in *ARF6*-overexpressing plants was similar to that in the WT. Since *ARF6* overexpression did not significantly lower auxin response as indicated by DR5-driven GFP based on the bulk analysis of transformants, ARF6 was selected for further investigation.

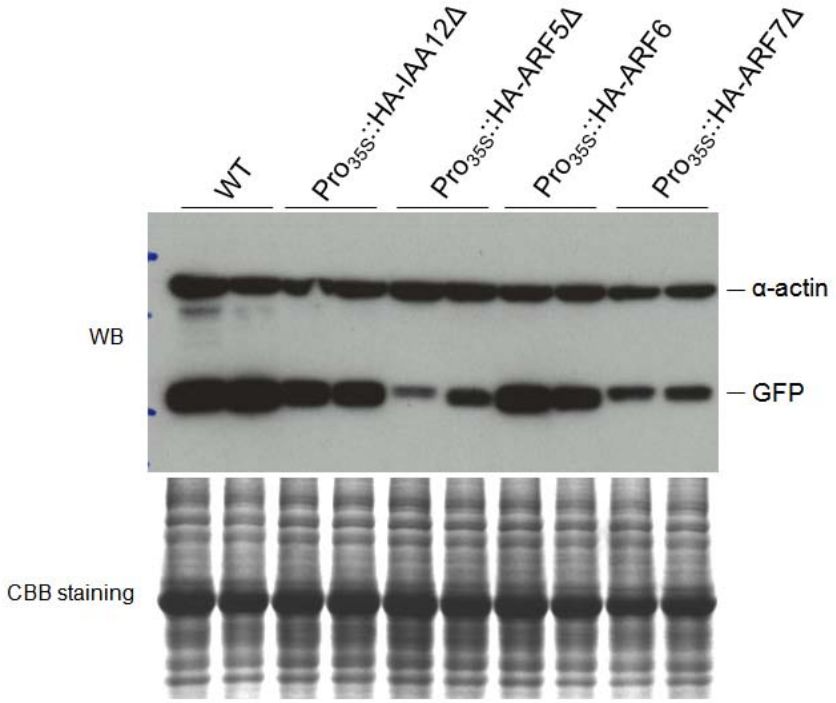

Figure 3.9 Analysis of *DR5$_{rev}$::GFP* protein level in different transgenic lines. Different constructs of *HA-IAA12*Δ, *HA-ARF5*Δ, *HA-ARF6*, and *HA-ARF7*Δ driven by the 35S promoter were used to transform the WT plants with *DR5$_{rev}$::GFP* marker. GFP protein level was determined by western blotting (WB) using an anti-GFP antibody. The β-actin was used as a loading control. Each protein sample was prepared from a pool of 20-25 transformants, and two replicates were analyzed. The bottom panel shows the Coomassie Brilliant Blue staining (CBB staining) of the gel as another loading control.

3.2.2.2. Effect of overexpressing *ARF6* on root hair growth

Since the results based on bulk transformant analysis do not reveal the variation among individual transformants, individual transgenic lines with *ARF6* overexpression (*Pro$_{35S}$::HA-ARF6* in WT carrying the *DR5$_{rev}$::GFP* marker) were screened. Since an enhanced auxin response is expected to result in a stronger GFP signal driven by the DR5 promoter, transgenic lines with enhanced auxin response could be screened conveniently under a microscope. As a result, two independent transgenic lines (997-1 and 997-2) were identified with a higher level of GFP signal in root tips (Figure 3. 10A).

These transgenic lines were further examined for their root growth. Seedlings of the WT and transgenic lines were grown side by side in plates for comparative analysis. Interestingly, these transgenic seedlings had much longer root hairs (Figure 3. 10B). At the 5-day stage after seed plating, the average root hair length of the two independent transgenic lines (997-1 and 997-2) was about 50% longer than that of the WT (Figure 3. 10C). On the other hand, the primary root length of these transgenic lines was slightly shorter than WT (Figure 3. 10D).

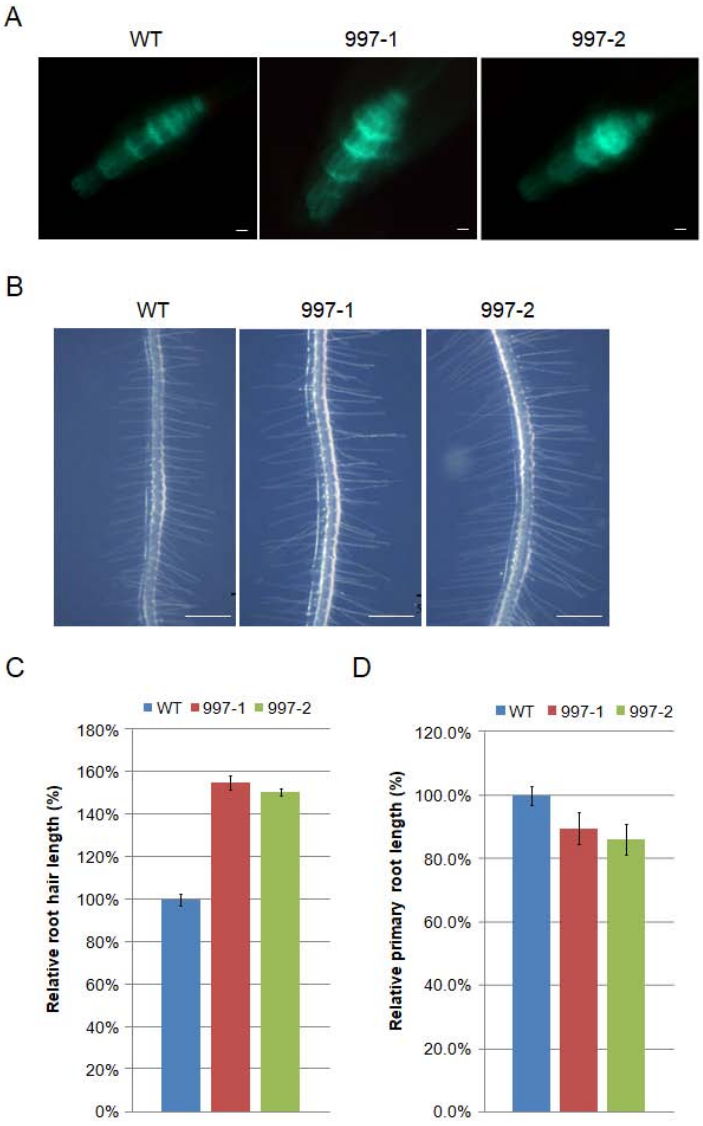

Figure 3.10 Analysis of *DR5$_{rev}$::GFP* and root growth in transgenic lines overexpressing ARF6. (A) Representative pictures of GFP signal in the root tips of two independent transgenic lines (997-1 and 997-2) overexpressing *ARF6*, and WT at the 5-day stage. Scale bar: 10 μm. (B) Representative pictures of the root hairs of two independent transgenic lines (997-1 and 997-2) overexpressing ARF6, and WT at the 5-day stage. Scale bar: 0.5 mm. (C) Relative root hair lengths of two transgenic lines (997-1 and 997-2) and WT. (D) Relative primary root length of two transgenic lines (997-1 and 997-2) and WT. Root hair and primary root lengths were expressed as the percentage of the average lengths of WT root hairs and primary roots.

3.2.2.3. Overexpression of *ARF6* in *ubc13* double mutants

The transgenic plants overexpressing *ARF6* showed an enhanced auxin response indicated by the *DR5rev::GFP* marker and longer root hairs. Thus, it would be interesting to check whether overexpressing *ARF6* could restore the hairless root phenotype of the *ubc13* double mutant. Since *ubc13* double mutant plants are weak compared to WT and difficult to be transformed, the transgenic plants with *ARF6* overexpression were crossed with the *ubc13* double mutant plants. F1 lines expressing *HA-ARF6* and carrying the *ubc13a* and *ubc13b* T-DNA inserts were retained.

In the end, one F2 line (W22-7-121) carrying the *ubc13* double mutant genes and *HA-ARF6* transgene was obtained. The seedlings of the line W22-7-121 had longer primary roots and root hairs than the *ubc13* double mutants (Figure 3.11). Since auxin can induce Aux/IAA protein degradation resulting in the release of ARFs, it may enhance the effect of overexpressing an *ARF*. Auxin is also known to inhibit primary root growth. Indeed, at the presence of 0.2 μM NAA (1-naphthaleneacetic acid, a synthetic auxin) the primary root growth was inhibited in the WT and W22-7-121 plants, but not in the *ubc13* double mutant plants (Figure 3.11A). Furthermore, root hair length of the W22-7-121 plants was similar to that of the WT at 0.2 μM NAA, while the *ubc13* double mutant seedlings barely had any root hairs (Figure 3.11A and B). Thus, these results indicate that overexpression of *ARF6* can rescue the root hair phenotype and at least partially rescue the primary root phenotype of the *ubc13* double mutant.

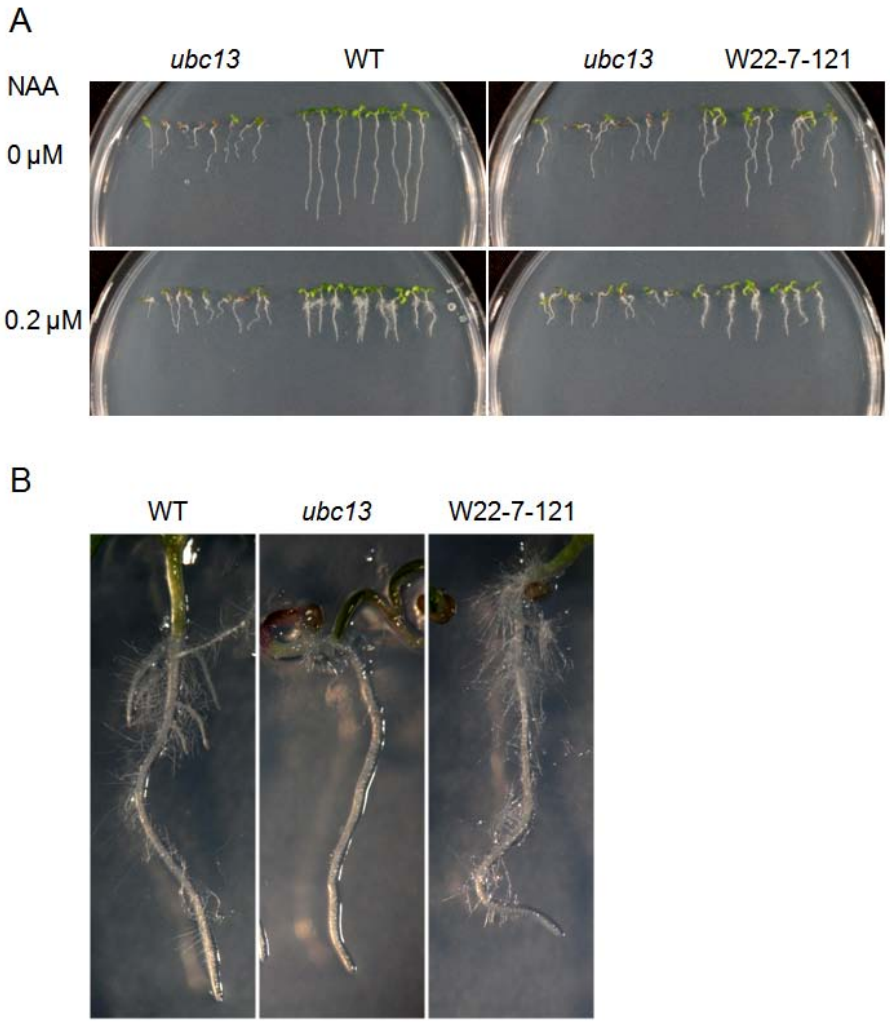

Figure 3.11 Root growth of WT, *ubc13* double mutants and *ubc13* double mutants overexpressing *ARF6* (W22-7-121). (A) WT and transgenic seedlings (line W22-7-121) overexpressing *ARF6* in the *ubc13* double mutant background were grown side by side with *ubc13* double mutants at 0 or 0.2 µM NAA. (B) Representative seedlings of WT, ubc13 mutant and W22-7-121 when grown at 0.2 µM NAA. Images were taken at the 7-day stage for both (A) and (B).

3.3. Discussion

3.3.1. UBC13-Interacting (UMI) E3s may have a function in sugar signaling

The UMI E3s showed a strong interaction with UBC13A in the yeast two-hybrid analysis, although some of them also interacted apparently more weakly with other E2s, such as UBC8 and UBC30. Since the RING domain of E3s is important for their interactions with E2s, the specific interactions of the UMI members with UBC13A and other E2s are likely due to some specific residues in this domain. Sequence analysis has identified several residues conserved among the six UMI members, which will be good candidates for further analysis on the interactions of UMI proteins with UBC13 and other E2s.

Due to the large number of E3s and very close sequence similarities among some of them, it is likely that there is wide-spread functional redundancy. Therefore, knocking out a single E3 gene may not result in obvious phenotypes while a phenotype may become discernable in double or higher orders of mutants. Indeed, down-regulation of even all six members of the *UMI* genes still could not produce any obvious phenotype in plant growth and morphology. There are two possibilities: (1) there may be still other genes which share functional redundancy with the *UMI* genes; (2) the UMI E3s are involved in a specific process, and a phenotype could only be detected under a specific condition or with a suitable technique. In this regard, seeds of good and even quality can increase the resolution of the tests. In this study, seeds of mutants and WT control were harvested from plants grown side-by-side and used to determine whether there is a phenotypic difference between the mutant and WT under different hormonal (e.g., auxin, cytokinin, abscisic acid, gibberellic acid and

salicylic acid) and abiotic stress (e.g., heat temperature, salt and oxidative) conditions.

The triple mutant with the inactivation of *UMI-D/E/F* genes was found to be more sensitive to glucose. This sensitivity is not due to poor seed quality of triple mutant since the seeds used were from plants grown side-by-side with the WT plants, and further, the triple mutants showed no difference from the WT for all other conditions tested. In plants, glucose not only serves as a carbon and energy source but also functions as a signaling molecule. In Arabidopsis, the glucose sensor hexokinase (HXK1) plays a key role in plant sugar sensing and signaling, as well as in the crosstalk between sugar and plant hormone signaling (Rolland et al., 2006). HXK1 senses and phosphorylates glucose in the cell thus mediating sugar metabolic processes. Also, in the nucleus, it controls the transcription level of a set of sugar-responsive genes. Arabidopsis mutant with down-regulation of *HXK1* displayed a glucose insensitive phenotype (Moore et al., 2003). It could be possible that the UMI E3s somehow affect sugar signaling pathway and one possible way is through controlling the protein level of HXK1. On the other hand, it is unknown whether UBC13A/B are also involved in sugar signaling.

Although the *def* triple mutant seedlings were more sensitive to glucose, the phenotype was not prominent and the underlying reason difficult to explain at the moment making it less attractive for further study. At the time when I obtained these results, the UBC22 line of work was producing very interesting results. Therefore, the main focus was gradually shifted to the studies of UBC22 (see Chapter 4 and 5).

3.3.2. Overexpression of *ARF6* can partially rescue the hairless root phenotype of *ubc13* double mutant

It has been proposed that the strong root phenotypes of the *ubc13* double mutant might be due to the increased level of Aux/IAA (Wen et al., 2014). It is thus interesting to determine whether expression of any ARFs can rescue the root phenotypes of the *ubc13* double mutant. Accordingly, ARF5, ARF6, and ARF7 were analyzed to see whether any could enhance auxin response as indicated by $DR5_{rev}$*::GFP* marker since they have been shown to be able to activate transcription of $DR5_{rev}$*::GFP* in carrot protoplast transfection assays (Tiwari et al., 2003). Unexpectedly, in the initial screening, overexpression of *ARF5Δ* or *ARF7Δ* resulted in a much lower level of the DR5-driven GFP compared to the GFP level in the WT background (Tiwari et al., 2003).

The reduced GFP expression in plants overexpressing *ARF5Δ* or *ARF7Δ* may have several possible reasons. (1) The previous results showing that ARF5, ARF6, and ARF7 are transcriptional activators were obtained using carrot protoplasts. The effects of their expression in whole plants may differ. (2) Based on the observation that the deletion of domains III and IV enhanced the effect of truncated ARF5 protein (Krogan et al., 2012), we used truncated forms of *ARF5Δ* and *ARF7Δ*. The truncated proteins may compete with WT ARFs and produce a dominant negative effect. (3) The effect may depend on the *ARF* expression level, and too high a level may disrupt hormonal signaling and inhibit plant growth. It was observed that in general *ARF5Δ* transformants were smaller in size. When plant growth was inhibited, the auxin response and thus the GFP level might be lower when

the whole plants were considered. (4) In addition, the effect may vary in different transformants, and it would be better to analyze the transformants or transgenic lines individually. The phenomenon that overexpression of *ARF5Δ* and *ARF7Δ* inhibited the expression of *DR5$_{rev}$::GFP* marker is interesting and requires further analysis.

Our main objective of this work was to identify an ARF that can enhance auxin response indicated by the *DR5rev::GFP* marker when overexpressed. Since overexpression of *ARF6* did not reduce GFP level significantly when the transformants were analyzed in pools of 20-25 transformants, they were analyzed further. I examined *ARF6*-overexpression transformants and identified lines that showed a higher level of GFP signal in root tips compared to the WT, indicating an enhanced auxin response. These results showed that overexpression of *ARF6* could enhance auxin response and root hair growth, and ARF6 is a good candidate to test whether it could restore the hairless root phenotype of the *ubc13* double mutant. Indeed, *ubc13* double mutant plants overexpressing *ARF6* had more root hairs and increased response to NAA compared to the double mutant plants, consistent with the suggestion that the strong root phenotypes in the *ubc13* double mutant may be due to increased Aux/IAA protein levels and reduced auxin response (Wen et al., 2014).

One technical problem encountered was the difficulty in directly transforming *ubc13* double mutant plants, since these plants were weak and died easily after the transformation treatment. Thus, two independent transgenic lines overexpressing *ARF6* in WT background were crossed with the *ubc13* double mutants. In the end, one line (W22-7-121) carrying the *ubc13* double mutant genes and *ARF6* transgene was obtained and showed a

complementation effect in root hair growth and in the response to auxin treatment. For the other line, however, no *ubc13* homozygous double mutant carrying the *ARF6* transgene could be obtained after screening 104 F2 progeny plants. This was surprising and might be due to a close linkage between the *ubc13* T-DNA insert and *ARF6* transgene locus. Since the indirect approach for obtaining the double mutant overexpressing *ARF6* took considerable time for having to select the *ARF6*-overexpressing lines first, then crossing them with the *ubc13* double mutant and screening the progeny plants, efforts could be spent to improve the transformation protocol so that the *ubc13* double mutant plants could be transformed directly to express *ARF6* or another gene of interest.

4. CHAPTER FOUR - CHARACTERIZATION OF ARABIDOPSIS UBIQUITIN-CONJUGATING ENZYME UBC22 IN REPRODUCTIVE DEVELOPMENT AND BIOCHEMICAL STUDIES OF UBC22

4.1. Introduction

The Arabidopsis genome is predicted to encode about 37 E2s which are grouped into 14 groups (Bachmair et al., 2001; Kraft et al., 2005). This large number of E2s may reflect functional diversity in catalyzing different ubiquitination reactions, and in the interactions with different E3s and other factors. On the other hand, the fact that some subfamilies have multiple members also suggests functional redundancy among the members (Callis, 2014b). This suggestion is supported by available, although limited, experimental evidence.

It is important to understand the specific functions for each of these E2s. Although *in vitro* results have shown that most of them possess the classical E2 activity in forming the E2-Ub complex through a thioester-linkage or could catalyze the formation of a Ub chain, very limited information is available on the specific ubiquitination reactions in which the E2s are involved. Further, the biological functions for most of them remain largely unknown. Therefore, we focus on one of the E2s, UBC22 and study its biological and biochemical functions.

Parts of the results described in this chapter have been published, with citation as follows (Wang et al., 2016).

Wang, S., Cao, L., and Wang, H. (2016). Arabidopsis ubiquitin-conjugating enzyme UBC22 is required for female gametophyte development and likely involved in Lys11-linked

ubiquitination. Journal of Experimental Botany 67, 3277-3288

For this publication, I contributed to all experimental designs, performed most experiments, analyzed the data and drafted the manuscript. Ling Cao contributed to the experimental work and data analysis as described in Figure 4.5, 4.7 and Table 4.3, 4.4. Hong Wang supervised the project, contributed to experimental designs and data analysis, and revised the manuscript.

4.2. Results

4.2.1. Characterization of Arabidopsis UBC22 and *ubc22* mutant

The 37 Arabidopsis E2s are grouped into 14 subfamilies, and many subfamilies have more than one member (Kraft et al., 2005). UBC22 (encoded by *AT5G05080*) is the sole member of the subfamily X. Interestingly, sequence analysis showed that Arabidopsis UBC22 protein is more closely related to a human E2, UBE2S, than to other Arabidopsis E2s (Figure 4.1), and it shares about 65% sequence identity with the human and animal UBE2S homologs (Figure 4.2).

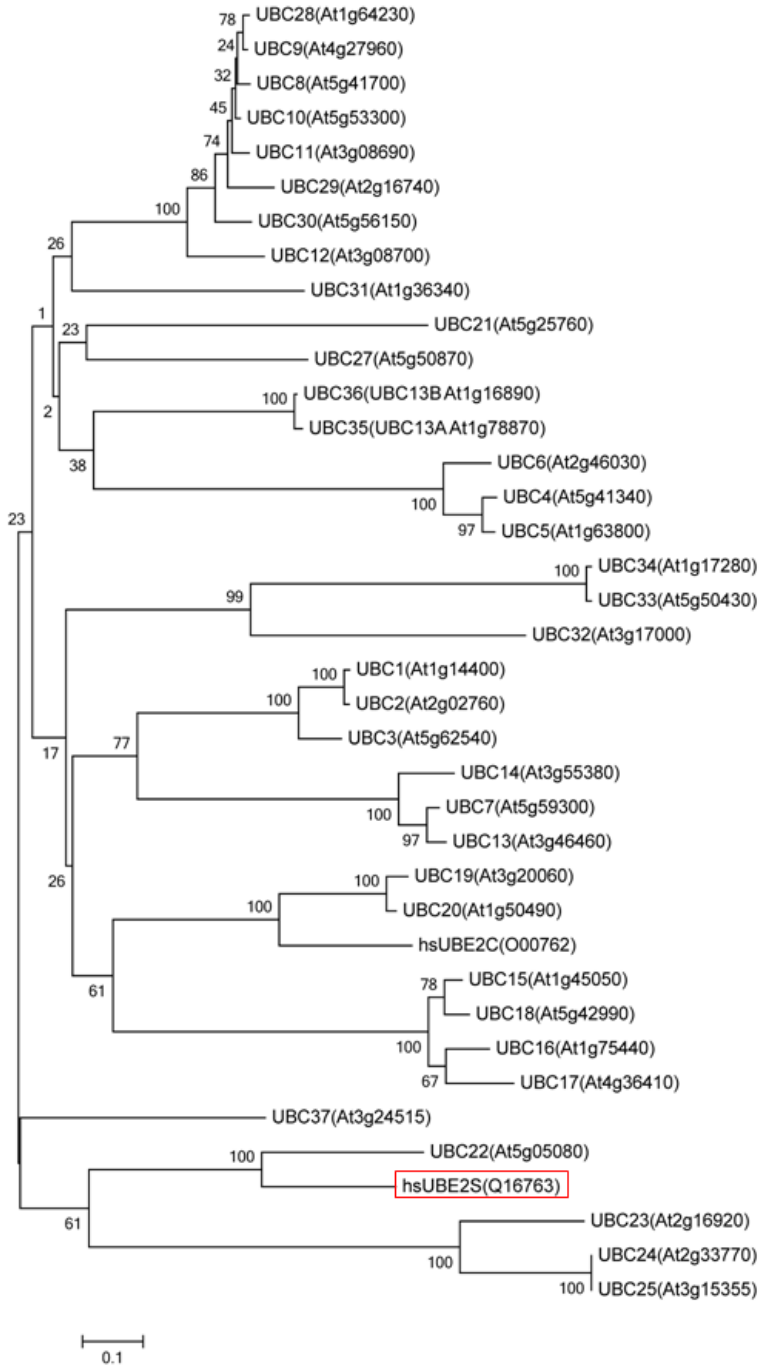

Figure 4.1 Phylogenetic analysis of Arabidopsis E2s. Thirty-six Arabidopsis E2s based on the analysis by (Kraft et al., 2005) were used, except for UBC26 which has no protein sequence data. Two human E2s, UBE2S and UBE2C were also included in the analysis. The Arabidopsis E2 proteins are listed by their accession numbers and common names. The alignment was made with ClustalX and phylogenetic tree generated with Mega 5.1. Bootstrap values from 500 replications for each branch are shown.

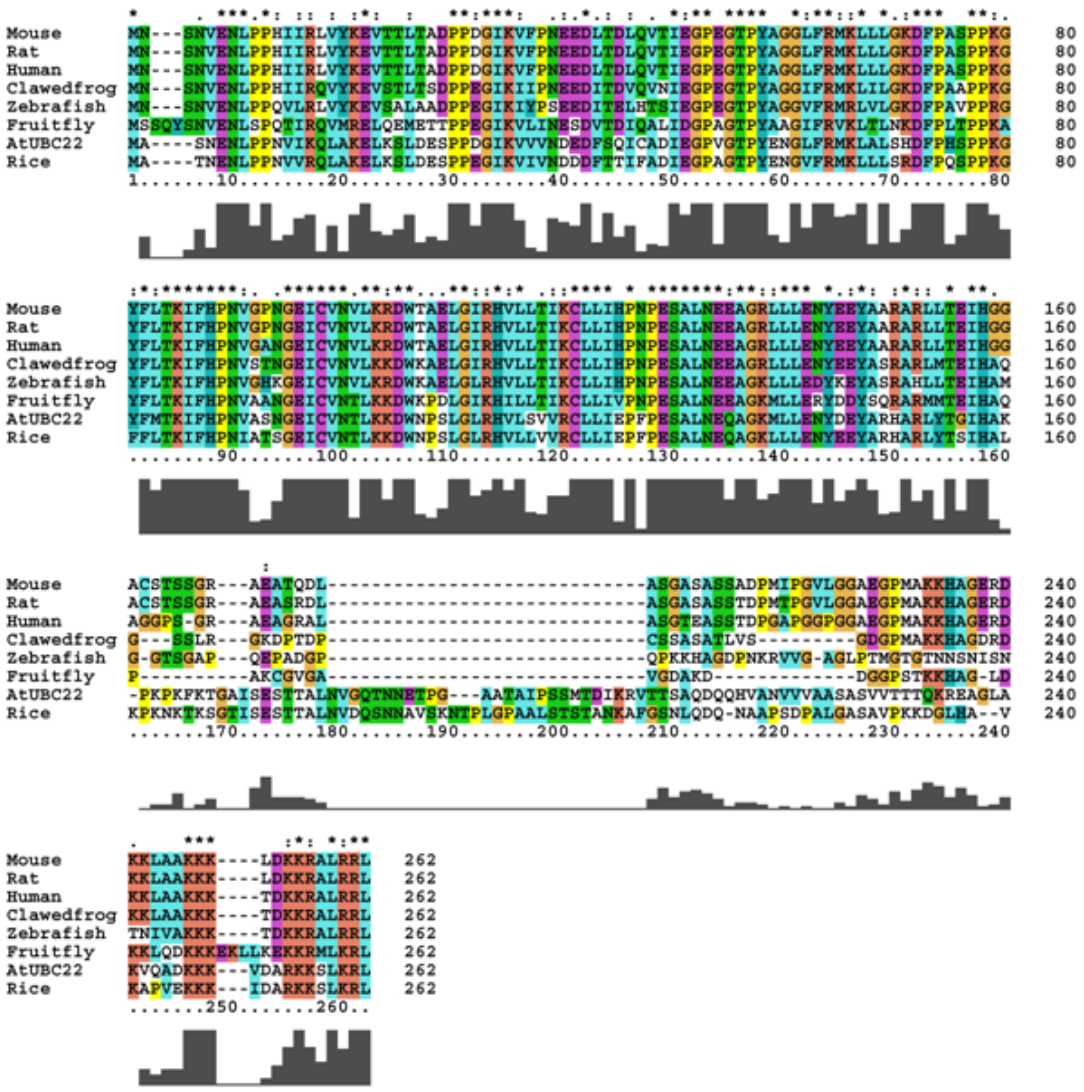

Figure 4.2 Alignment of putative UBC22 homologs from different species. Alignment was created using ClustalX using default settings. The protein sequences used are: Mouse, Q921J4; Rat, B5DFI8; Human, Q16763; Clawed frog, Q28F89; Zebrafish, Q4V908; Fruit fly, Q9VX25; Arabidopsis, At5g05080 (UBC22); Rice, Os06g0660700.

To investigate the function of Arabidopsis *UBC22*, a T-DNA insertion line (SALK_011800) was obtained from the Arabidopsis Biological Resource Center, and plants were genotyped to obtain homozygous lines. Since phenotypes were observed with this line (see below), another independent T-DNA line (GK_642C08) was also obtained from the Nottingham Arabidopsis Stock Centre (NASC). Sequence analysis of these two T-DNA insertion lines revealed that the T-DNA was inserted in the fifth exon of *UBC22* in both lines (Figure 3.3A). Genomic DNA PCR and RT-PCR using *UBC22* gene-specific primers did not amplify the full length genomic or cDNA of *UBC22* (Figure 3.3B and C). Thus, the two alleles are considered null mutation alleles and designated *ubc22-1* (SALK_011800) and *ubc22-2* (GK_642C08).

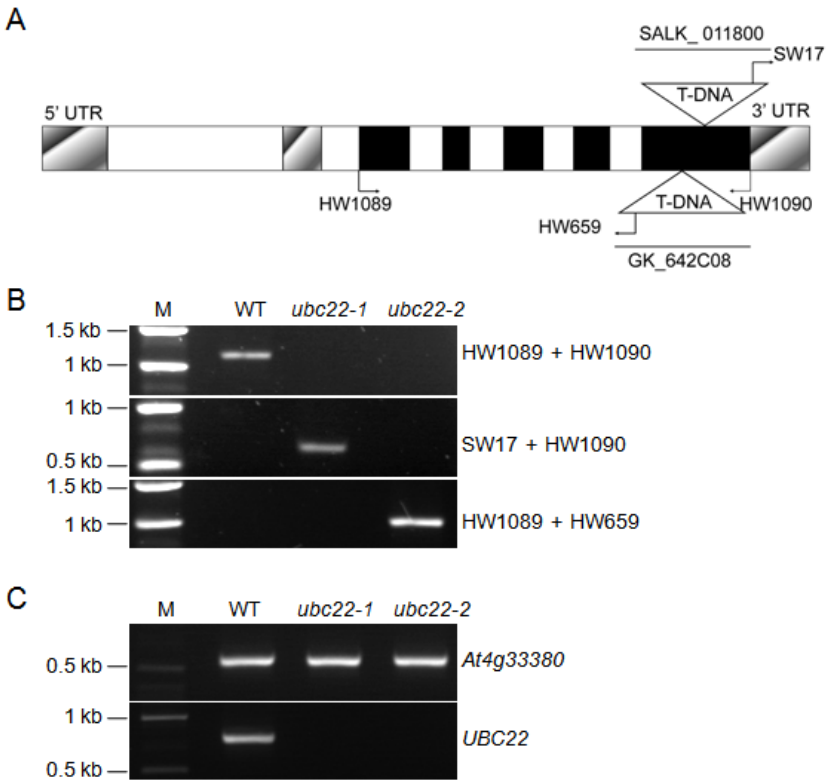

Figure 4.3 Confirmation of *ubc22* T-DNA insertion mutants. (A) Schematic representation of the *UBC22* genomic structure with the locations of primers and T-DNA insertion sites in *ubc22-1* and *ubc22-2* mutants shown. Closed boxes: exons; open boxes, introns; shadowed boxes: untranslated regions; HW1089 and HW1090, gene-specific primers for *UBC22*; SW17, a T-DNA left border primer for SALK T-DNA lines; HW659, a T-DNA left border primer for the GK lines; (B) Characterization of the *ubc22* T-DNA lines by genomic PCR. The plant lines are indicated above the panels and the primers at the right of the panels. M, DNA marker. (C) Characterization of the *ubc22* T-DNA lines by RT-PCR and 30 PCR cycles were used. PCR amplification of a reference *At4g33380* cDNA is shown at the top and amplification of *UBC22* cDNA shown at the bottom.

To characterize the phenotypes of *ubc22-1* and *ubc22-2*, plants of these two T-DNA lines were grown side by side with WT plants. The mutant plants had much shorter siliques than the WT (less than 50% in length) (Figure 4.4A and B). Further examination showed that about 88.3% of ovules were aborted in the mutant (Figure 4.2A, Table 4.1), whereas the total ovule number was not affected (Table 4.1). Reciprocal crosses between the WT and *ubc22-1* revealed that the short silique phenotype was retained when the mutant, but not the WT, was used as the female parent (Table 4.2).

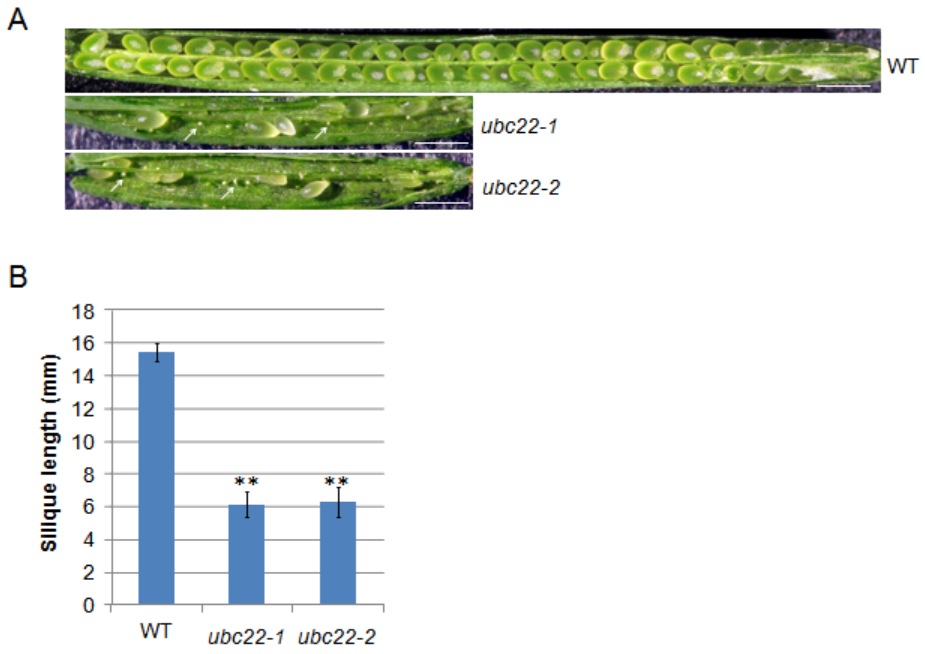

Figure 4.4 Silique phenotype of *ubc22* mutants. (A) Images to show representative siliques of WT, *ubc22-1* and *ubc22-2* mutant plants. The white arrows indicate aborted ovules. Scale bar, 1 mm. (B) Silique length of WT, *ubc22-1* and *ubc22-2* mutant plants. Four different plants, with eight fully-elongated siliques on the main inflorescent stem, were used in the analysis for each line. Student's *t*-tests were performed to determine whether there is a significant difference in silique length between the mutant and WT; ** $P<0.01$.

Table 4.1 Analysis of ovule and seed development in WT and *ubc22-1* mutant plants.

Line	Seeds /ovules counted	Normal seeds	Aborted ovules	Aborted seeds	No. of ovules per silique	No. of seeds per silique
WT	1536 (100%)	1531 (99.67%)	4 (0.26%)	1 (0.07%)	61.4 ± 2.6	61.2 ± 2.7
ubc22-1	1515 (100%)	156 (10.30%)	1337 (88.25%)	22 (1.45%)	60.6 ± 3.1	6.2 ± 2.1

Five WT and mutant plants, and for each plant the first five siliques were used in the analysis. For the number of ovules and number of seeds per silique, the data are shown with mean ± standard deviations. The difference in the number of seeds per silique between the WT and mutant was significant at the level of 0.01.

Table 4.2 Analysis of seed development in siliques from reciprocal crosses and self-fertilized siliques of the heterozygous plants

Female x male	Seeds /ovules counted	Normal seeds	Aborted ovules	Aborted ovules per silique	Aborted seeds	Silique length (mm)
WT x WT	1265 (100%)	1264 (99.92%)	1 (0.08%)	0.1 ± 0.2	0	16.2±0.2
ubc22-1 x WT	1165 (100%)	89 (7.64%)	1057 (90.73%)	52.9 ± 2.9	19 (1.63%)	6.4±1.0
WT x *ubc22-1*	1228 (100%)	1154 (93.97%)	71 (5.78%)	3.6 ± 2.5	3 (0.24%)	15.7±0.6
ubc22-1/+ x *ubc22-1/+ (self-fertilized)*	1196 (100%)	1038 (86.79%)	157 (13.13%)	7.9 ± 2.9	1 (0.08%)	14.9±0.6

Reciprocal crosses were made between the WT and homozygous *ubc22-1* mutant plants. Also, the heterozygous plants (*ubc22-1/+*) were also included in the analysis as a comparison. Twenty fully-elongated siliques from each type were used for determining the number of normal seeds, aborted ovules, and aborted seeds as well as silique length.

We analyzed the seed setting. The cross using *ubc22-1* mutant as the female parent only had about 7.6% ovules developing into normal seeds while the cross using WT as the female parent had about 94% ovules developing into normal seeds, in comparison to almost 100% in the WT plants, confirming that the major defect was due to the female parent. Further, in the self-pollinated siliques of heterozygous plants, about 13.1% ovules were aborted (Table 4.2), much less than half of that in the self-pollinated siliques of the mutant (88.3%, Table 4.1), suggesting that majority of the female gametophytes carrying the mutant allele could develop normally in the heterozygous plants. In addition, when the WT was used as the female parent and the mutant as the male parent, the siliques contained 5.8% aborted ovules (Table 4.2). Thus, we analyzed the mutant pollen and observed that the homozygous mutant plants had a slightly higher frequency of pollen with only one or no sperm nuclei (2.8% compared to 1.6% in the WT) (Figure 4.5, Table 4.3). These results indicate a minor defect in male gametogenesis of the mutant.

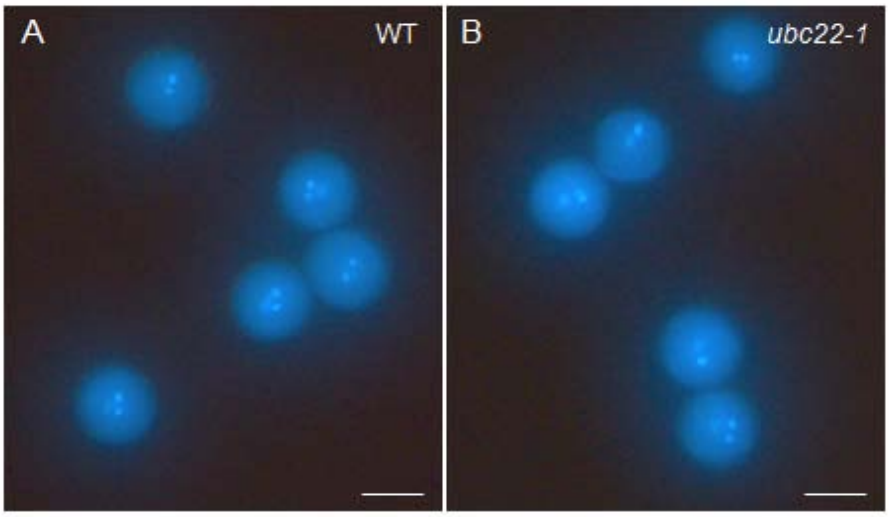

Figure 4.5 Pollen of WT and *ubc22* mutants. Pollen grains from WT (left) and *ubc22-1* mutants (right) were stained with DAPI (4′,6-diamidino-2-phenylindole) and observed under a fluorescence microscope. Scale bar, 10 μm.

Table 4.3 Analysis of pollen development in WT and *ubc22-1* mutant plants.

Line	Pollen grains counted	Pollen grains with numbers of vegetative and sperm nuclei				
		1+2	0+2	1+1	0+1	1+0
WT	1315 (100%)	1208 (91.86%)	86 (6.54%)	21 (1.60%)		
ubc22-1	1761 (100%)	1627 (92.39%)	85 (4.83%)	40 (2.27%)	2 (0.11%)	7 (0.40%)

Pollen grains were collected from newly opened flowers of WT and *ubc22-1* mutant plants. They were stained with DAPI and were grouped based on the numbers of the vegetative cell and sperm cell nuclei observed.

The observation that two independent T-DNA insertion lines showed nearly identical phenotypes strongly suggest that the phenotypes were due to the inactivation of *UBC22*. To confirm that the phenotype is due to the inactivation of *UBC22*, we expressed *UBC22* under its own promoter in *ubc22-1* mutant to see whether it could complement the mutant. Among the 21 T1 transformants obtained, three independent transformants showed nearly full complementation. Quantitative measurements using T2 plants of these lines showed that silique length in those lines was about 85% of that in the WT (Figure 4.6A). Also, the majority of the seeds in these HA-UBC22 lines developed normally (Figure 4.6B). The transcript level of *HA-UBC22* in these lines was found to be similar to the level of endogenous *UBC22* in the WT plants (Figure 4.6C).

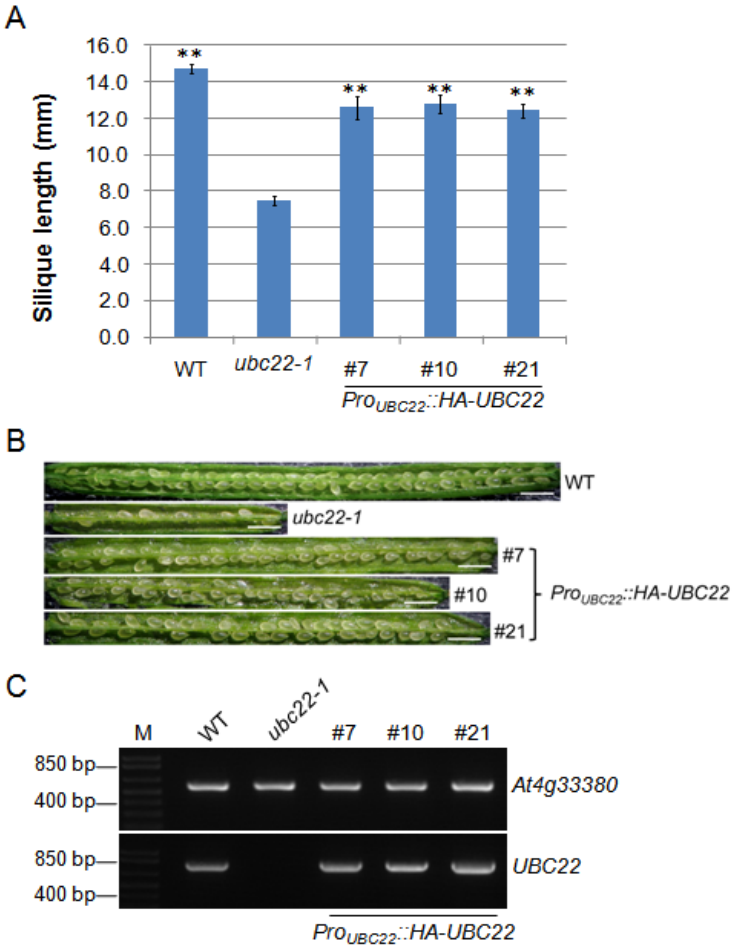

Figure 4.6 Complementation of *ubc22-1* mutant by *Pro$_{UBC22}$:: HA-UBC22*. *Pro$_{UBC22}$:: HA-UBC22* was introduced into the *ubc22-1* mutant. T2 plants of independent lines were used for further analysis. (A) Silique length of WT, *ubc22-1* and three individual complementation lines (#7, #10 and #21). About six siliques from each plant and at least four different plants in each line were measured. Student's *t*-tests were performed to determine whether there is a significant difference in silique length between the complementation lines and mutant; ** $P<0.01$. (B) Images to show representative siliques from WT, *ubc22-1* and three complementation lines. Scale bar, 1 mm. (C) RT-PCR analysis of WT, *ubc22-1* and three independent complementation lines. PCR amplification of a reference *At4g33380* cDNA is shown at the top and amplification of *UBC22* cDNA shown at the bottom. Plant lines used are indicated above the panels. M, DNA marker.

4.2.2. Gametogenesis and megasporogenesis in the *ubc22* mutant

To further characterize the ovule abortion phenotype of the *ubc22* mutant, female gametophyte development in the *ubc22-1* mutant plants was examined. At first, embryo sacs just before flowering were investigated. In the WT Arabidopsis plants, the typical embryo sac at the FG7 stage (Yadegari and Drews, 2004), the egg, central and synergid cells could be distinguished under a microscope with differential interference contrast (DIC) (Figure 4.7A). On the other hand, in the majority of mutant embryo sacs (63.8%, Table 4.4), no egg, central and synergid nuclei could be seen. Generally, these embryo sacs were smaller and narrower compared with the WT embryo sacs. In addition, contents in the mutant embryo sacs appeared grainier under the microscope (Figure 4.7B). These cellular features suggest that female gametogenesis was impaired and the gamete nuclei have degenerated in these embryo sacs. For the embryo sacs with observable gamete nuclei, most of them were also abnormal. In terms of the developmental stage, only a small proportion of them (5.7%) were at the typical FG7 stage with one central, one egg and two synergid nuclei, similar to the WT (Figure 4.7A). More (7.0%) were however at FG5 with two polar, one egg and two synergid nuclei (Figure 4.7C). Some embryo sacs were still in FG4 stage with four nuclei and one large vacuole (Figure 4.7D).

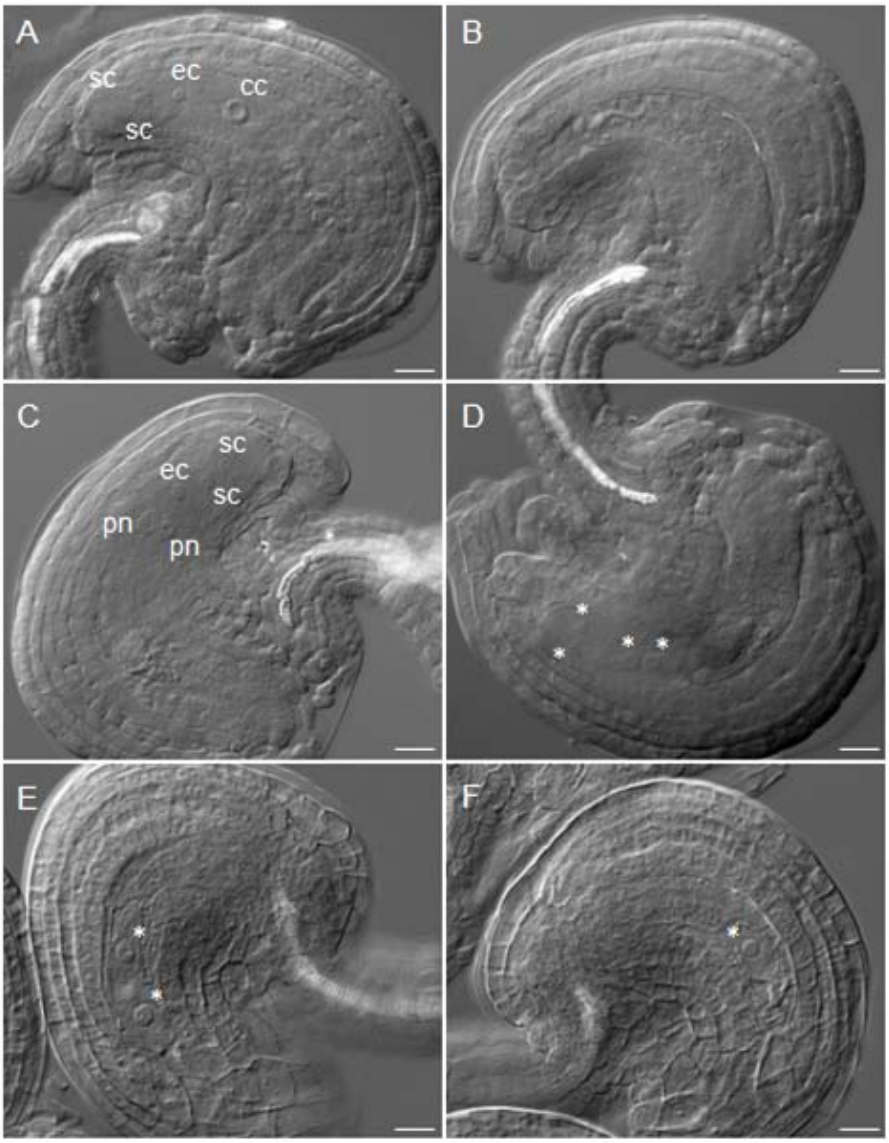

Figure 4.7 Female gametophyte development in WT and *ubc22-1*. Ovules from flowers just before opening were prepared and observed under a microscope with DIC. (A) A typical WT embryo sac (at FG7 stage) showing one central cell, one egg cell, and two synergid cells. (B-F) Abnormal embryo sacs in *ubc22-1* plants. (B) Mutant embryo sac without any nucleus and the embryo sac was smaller and narrower than the WT embryo sac. (C) Mutant embryo sac at FG5 stage. (D) Mutant embryo sac at FG4 stage, with four nuclei. (E) Mutant embryo sac FG3 stage, with two nuclei and a larger vacuole between them. (F) Mutant embryo sac with only one nucleus. Abbreviations: cc, central cell; ec, egg cell; pn, polar nuclei; sc, synergid cell. Scale bar, 10 μm.

Table 4.4 Female gametophyte development in WT and *ubc22-1* mutant plants.

Line	Total number	Female gametophyte stage							No nucleus	One nucleus	Two nuclei
		FG1	FG2	FG3	FG4	FG5	FG6	FG7			
WT (%)	270 (100)	0	0	0	0	1 (0.4)	0	268 (99.3)	1 (0.4)	0	0
ubc22-1 (%)	331 (100)	2 (0.6)	2 (0.6)	4 (1.2)	8 (2.4)	23 (7.0)	3 (0.9)	19 (5.7)	211 (63.8)	47 (14.2)	12 (3.6)

Embryo sacs from flowers just before opening were dissected, prepared and then observed under a microscope equipped with differential interference contrast (DIC) optics. The stages of embryo sacs were based on the number of cells and their configurations according to the description of (Christensen et al., 1997).

The ovules at earlier stages of development were examined to determine the stage at which ovule development of the mutants departs from that of WT. During megasporogenesis, a megaspore mother cell (MMC) or megameiocyte is produced through differentiation by one subepidermal cell. In ovules at stage 2-II (Schneitz et al., 1995) with the inner integument initiating, there was no obvious difference between the WT and mutant (Figure 4.8A, B, Table 4.5). Therefore, the development of functional megaspore (FM) was examined. In the WT, following meiosis, the megaspore closest to the chalazal end enlarges and gives rise to the FM, whereas the other three megaspores degenerate. We examined the ovules at about stage 3-I according to (Schneitz et al., 1995) (with the inner integument near and just below the top of the nucellus). Most of the WT ovules examined contained a typical FM with the nucleus having a clear edge under DIC, a round shape and often an easily recognizable nucleolus (Figure 4.8C). In contrast, in about 37% mutant ovules, no FM was observed (Table 4.6, Figure 4.8D). In 35% mutant ovules, FMs could be identified but appeared abnormal. Their nuclei did not have an easily recognized boundary, appeared thin in nuclear

content, and/or did not have a spherical shape (Figure 4.8E). In some cases, the nuclei of FMs appeared thin and “flat” under the DIC optics with the nuclear-cytoplasm boundary barely visible (Figure 4.8F), suggesting that they might be at late stages of degeneration. These observations indicate that the FM in some mutant ovules was undergoing degeneration or had degenerated, resulting in no nucleus being observed. Thus, these results indicate that the abnormality during female gametophyte development in the *ubc22-1* mutant likely started with the degeneration of the FM.

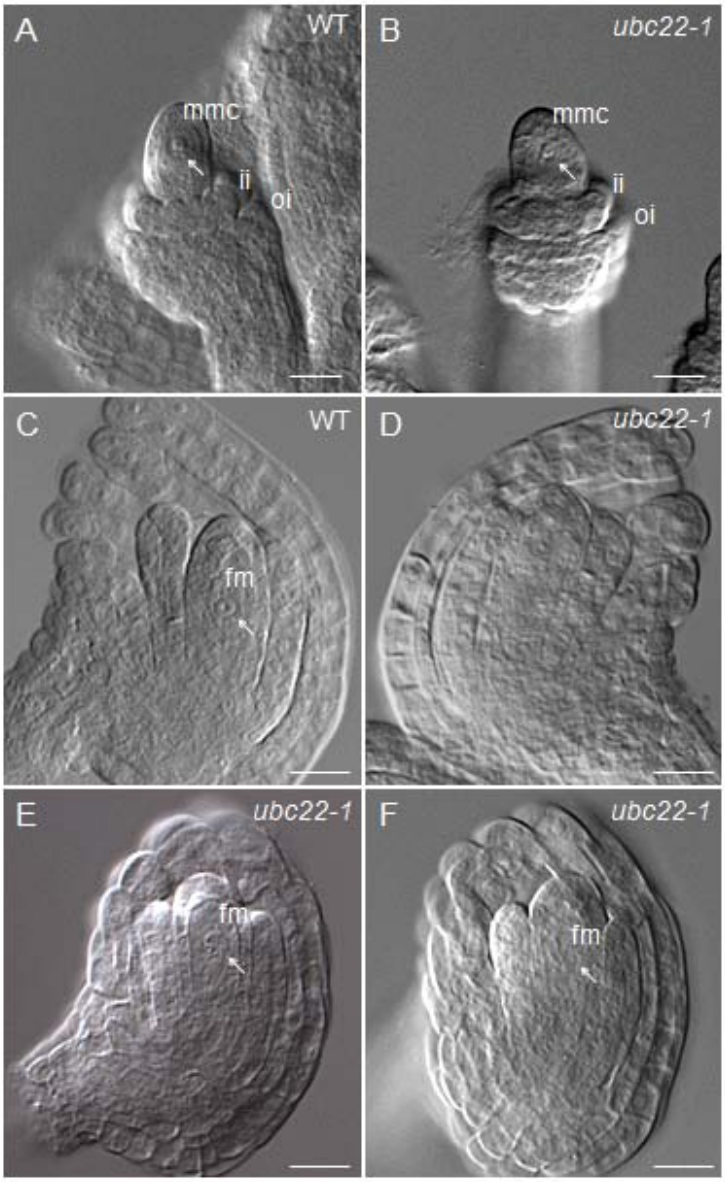

Figure 4.8 Megaspore mother cell (MMC) and functional megaspore (FM) development in WT and *ubc22-1*. Ovules from the flowers buds were prepared and observed under a microscope with DIC. (A, B) WT (A) and *ubc22-1* mutant (B) ovules with a typical MMC. ii, inner integument; oi, outer integument. (C-F) Ovules at the FM stage. (C) WT ovule with a typical FM. (D) A *ubc22-1* ovule without an observable FM. (E-F) *ubc22-1* ovules with an abnormal FM. The FM in (E) is visible, but the boundary is not clear, and the shape is abnormal. The FM in (F) is barely visible under the microscope. White arrows indicate the MMC in (A, B) or FM in (C, E & F). Scale bar, 10 μm.

Table 4.5 Megaspore mother cell (MMC) development in WT and the *ubc22-1* mutant.

Line	Total number	No MMC	One MMC	Two MMCs
WT	267 (100%)	40 (15.0%)	211 (79.0%)	16 (6.0%)
ubc22-1	138 (100%)	20 (14.5%)	112 (81.2%)	6 (4.3%)

Flowering buds were first checked for the ovule developmental stages, and the sixth bud from the newly opened flower was used. The buds were dissected, prepared and then observed under a microscope equipped with DIC optics. Ovules were grouped based on the number of MMC-like cells in each ovule.

Table 4.6 Functional megaspore development in WT and *ubc22-1* mutant ovules.

Line	Ovules observed	Typical FM (Type I)	Visible FM with abnormalities (Type II)	FM not observable (Type III)
WT (%)	114 (100)	99 (86.8)	10 (8.8)	5 (4.4)
ubc22-1 (%)	123 (100)	34 (27.6)	43 (35.0)	46 (37.5)

Flowering buds (the fifth bud from the newly opened flower) were dissected, prepared and then observed under a microscope equipped with DIC optics. Ovules at functional megaspore (FM) stage (with the inner integument near, but below the top of the nucellus) were included in the analysis. Three types of ovules were observed. Type I (normal): A typical FM had one prominent nucleus with a round shape and clear nuclear-cytoplasm boundary. Type II: The FM was visible. However, the nuclear-cytoplasm boundary was not clear, and/or the nucleoplasm appeared to be disorganized. In the *ubc22-1* mutant, the FM was often barely visible (see Figure 4.8E, 4.8F). Type III: No FM could be observed.

To further investigate more specifically the effect of *UBC22* inactivation on megasporogenesis, a biological marker, callose, is utilized to monitor this process. Callose, a polysaccharide composed of glucose residues linked through β-1,3-linkages, is present at the cell plate during meiosis prior to cytokinesis. The presence of callose can be visualized based on fluorescence signal following aniline blue staining. It has been used as a convenient cytological marker for meiosis in an MMC (Rodkiewicz, 1970). In the WT MMC, before meiosis there was some callose deposition along the cell wall (Figure 4.9B). After the first meiotic division, the fluorescence signal became concentrated at the site of the cell plate, appearing as a band (Figure 4.9C). Following the second meiotic division, an extra callose band beneath the first callose band appeared, as a result of the division by the nucleus close to the chalazal end (Figure 4.9D). Later, the fluorescence signal was concentrated at the micropylar end where the degenerating megaspores were located and finally disappeared (Figure 4.10C). Thus, based on the callose staining pattern, we could infer approximately the stages of an MMC during meiosis in WT ovules.

We thus examined ovules during early stages of meiosis to determine whether there is any difference between the *ubc22* mutant and WT. Ovules with the inner integument just emerging to below the half-length of nucellus were examined. In WT, 28.2% and 46.2% of ovules showed one and two clear callose band(s), respectively (Figure 4.9C and D). In total, 74.4% of the WT ovules had clear callose band(s) (Table 4.7). In contrast, only 10.7% of the mutant ovules showed one or two clear callose bands; further 17.5% of mutant ovules had a callose band, but also had strong callose staining in other locations (Figure 4.9F) or an odd

pattern (Figure 4.9H). A large portion (36.9%) of mutant ovules did not have a clear callose band, and instead showed a much disorganized and diffused callose staining (Figure 4.9G). After meiosis, the fluorescence signal finally disappeared in WT ovules. However, a large portion of mutant ovules (62.6%) still had disorganized and strong callose staining (Figure 4.10 and Table 4.8). These results suggest that the abnormality during female megasporogenesis in the *ubc22-1* mutant likely started during the first meiotic division and continued into the later stages of megasporogenesis.

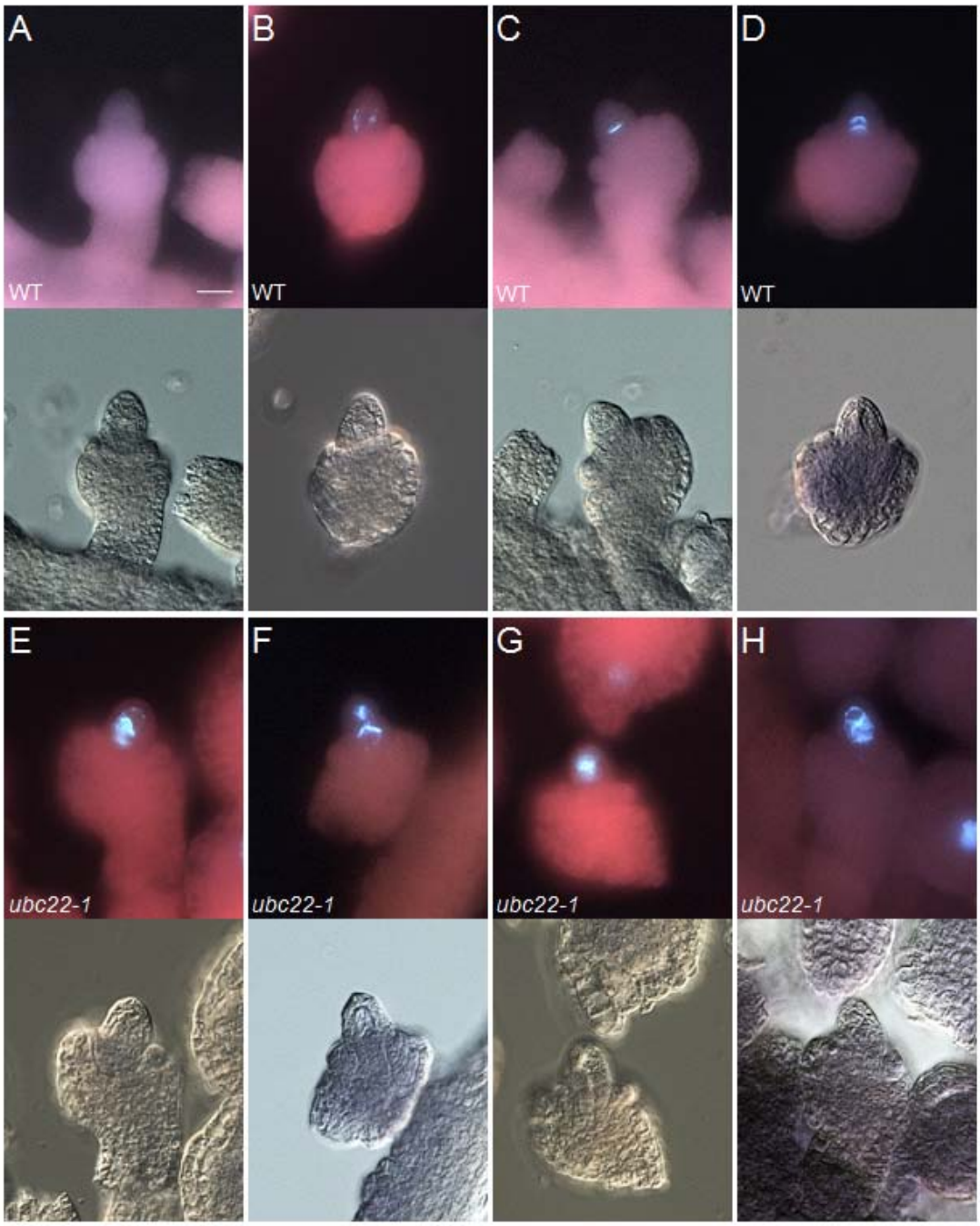

Figure 4.9 Callose formation at early stages of megasporogenesis in WT and *ubc22-1* mutant ovules. For each ovule, the callose fluorescent image is shown on the top, and the bright-field image is shown on the bottom. WT (A-D) and *ubc22-1* mutant (E-H). Scale bar: 10 μm.

(A) No callose staining in a WT ovule before meiosis

(B) Deposition of callose along the cell wall of a WT MMC

(C) A clear callose band indicating the place of newly formed cell plate from the first meiotic division by a WT MMC

(D) Two clear callose bands as a result of the first meiotic division and the second division by

the nucleus close to the chalazal end
(E) A callose band with diffused callose disposition in a *ubc22-1* MMC
(F) A callose band and also callose deposition in other locations of a *ubc22-1* MMC
(G) Strong callose staining in the center of a *ubc22-1* MMC, but the callose band is not clear.
(H) Disorganized callose deposition without a clear band in a *ubc22-1* MMC

Table 4.7 Callose formation at early stages of megasporogenesis in WT and *ubc22-1* mutant ovules

Line	Ovules observed	Callose staining along meiocyte cell wall (Type I)	Clear callose band (s) (Type II)	Recognizable callose band with staining in other places (Type III)	Disorganized callose deposition without a clear band (Type IV)
WT	117 (100%)	30 (25.6%)	87 (74.4%)	0	0
ubc22-1	103 (100%)	36 (35.0%)	11 (10.7%)	18 (17.5%)	38 (36.9%)

Flowering buds (the sixth bud counting from the newly opened flower on an inflorescence stem) were dissected, stained, prepared and then observed under a microscope equipped with DIC optics. Ovules at the early stage of meiotic division (with the inner integument below the half-length of nucellus) were included in the analysis. Four types of ovules were counted. Type I: weak callose staining observed along the cell wall of an MMC before meiosis. Type II: One or two clear callose bands observed during meiosis of an ovule. Type III: One or two callose bands were recognizable, but diffused callose signal was observed in other locations as well. Type V: Callose deposition was disorganized, and no clear callose bands were observed (Figure 4.9G). A large portion of the mutant ovules had diffused or disorganized callose deposition compared to the WT ovules that showed one or two clear bands.

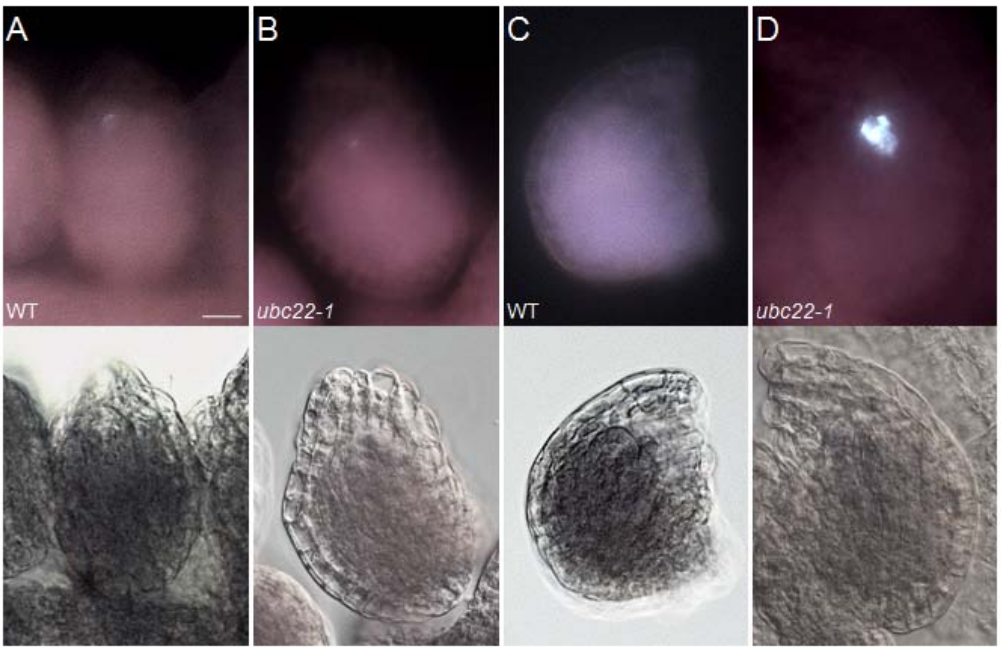

Figure 4.10 Presence of callose at late stages of megasporogenesis in WT and *ubc22-1* mutant ovules. For each ovule, the callose fluorescent image is shown on the top, and the bright-field image is shown on the bottom. WT (A and C) and *ubc22-1* mutant (B and D). Scale bar: 10 μm.

(A) Weak callose staining at the micropylar end in a WT ovule after meiosis.

(B) Weak callose staining at the micropylar end in a *ubc22-1* mutant ovule after meiosis.

(C) No callose signal in a WT ovule.

(D) Strong disorganized callose staining in a *ubc22-1* ovule

Table 4.8 Presence of callose at late stages of megasporogenesis in WT and *ubc22-1* mutant ovules

Line	Ovules observed	fluorescence signal as two bands (Type I)	fluorescence signal as a line or a spot at the micropylar end (Type II)	No fluorescence signal (Type III)	Strongly disorganized signal (Type IV)
WT	126 (100%)	2 (1.6%)	65 (51.6%)	59 (46.8%)	
ubc22-1	131 (100%)	1 (0.8%)	39 (29.8%)	9 (6.9%)	82 (62.6%)

Flowering buds (the fourth bud from the newly opened flower) were dissected, stained, prepared and then observed under a microscope equipped with DIC optics. Ovules at the functional megaspore (FM) stage (with the inner integument close or just below the top of nucellus) were included in the analysis. Four types of callose staining pattern were observed. Type I: the presence of two callose bands near the micropylar end. Type II: one callose band or spot at the micropylar end. Type III: no callose staining observed. Type V: strongly disorganized callose staining (Figure 4.10D). A large portion of mutant ovules had strongly diffused or disorganized callose staining compared to WT ovules which had weak or none callose staining.

4.2.3. Expression of *UBC22* in different tissues and developmental stages

To understand the expression of *UBC22*, we first examined the microarray data available from Genevestigator (Zimmermann et al., 2004). As shown in Figure 4.11, *UBC22* is expressed in different tissues with a higher expression level in senescence leaves. To more specifically determine the location of *UBC22* expression, we fused its promoter to the GUS reporter and the expression patterns were analyzed by histochemical GUS staining. In 10-day old seedlings, strong GUS signal was detected in vascular tissues, root tips and lateral root primordia (Figure 4.12A-C). Similar results were obtained from the 20-day old seedlings. In the reproductive organs, GUS signal was observed in stigmas, filaments, and veins of sepals, but very little in petals and pollen (Figure 4.12D). Also, the GUS signal was detected in ovules of the different developmental stages (Figure 4.12E-G). These data indicate that *UBC22* is expressed in a variety of tissues.

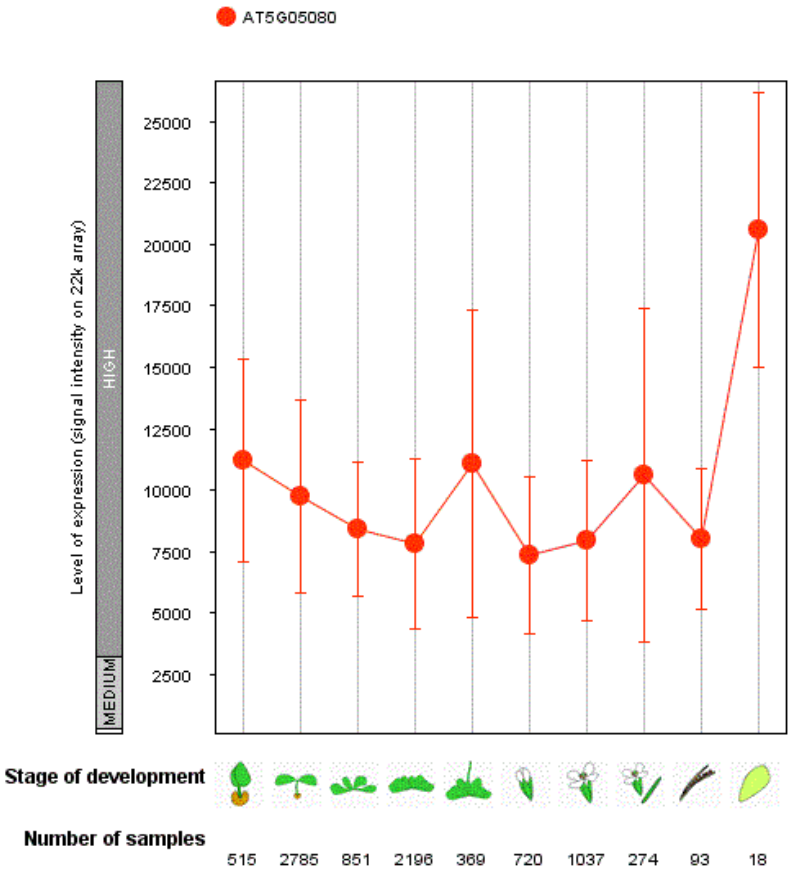

Figure 4.11 Developmental expression profile of *UBC22*. The figure based on microarray expression data was generated by Genevestigator (https://genevestigator.com). Developmental stages and sample numbers are indicated at the bottom of the figure.

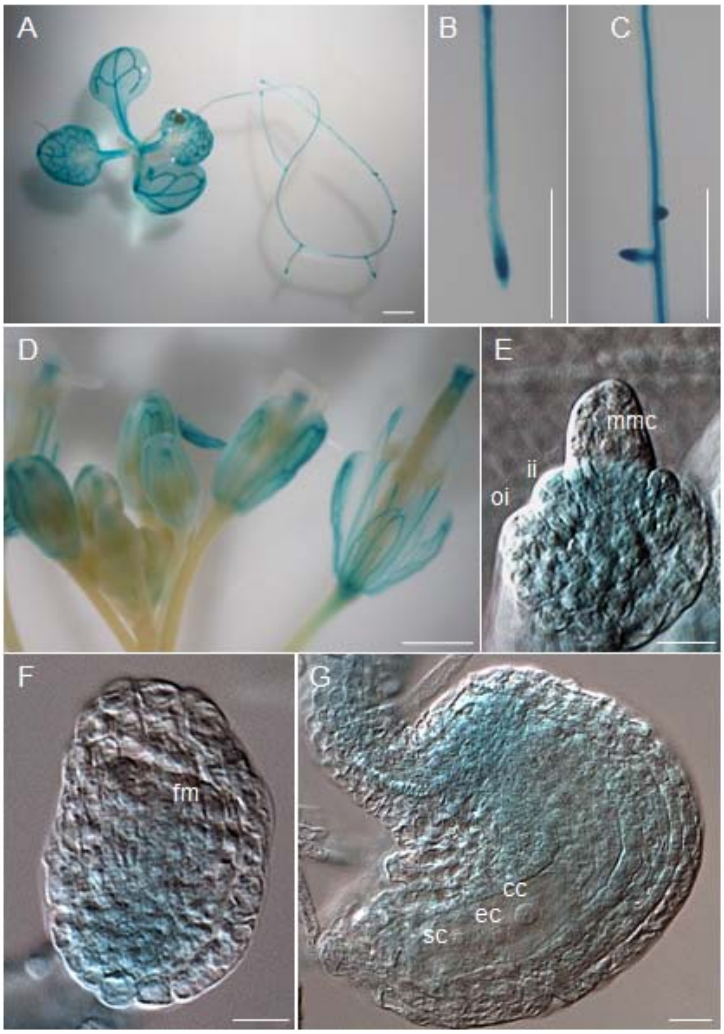

Figure 4.12 GUS staining of transgenic *Pro$_{UBC22}$::GUS* plants. Seedling or different tissues from transgenic *Pro$_{UBC22}$::GUS* plants were analyzed by histochemical GUS staining. Similar patterns were observed in independent transgenic lines although the intensity may vary among the lines. Images from representative plants are shown here. (A) A 10-day old seedling. (B) Root tip and (C) lateral root primordia from a 10-day old seedling. (D) Flower organs from a 6-week old plant. Scale bar, 1 mm. (E, F & G) Ovules at megaspore mother cell (E), functional megaspore (F) and FG7 (G) stages. Abbreviations: mmc, megaspore mother cell; ii, inner integument; oi, outer integument; fm, functional megaspore; cc, central cell; ec, egg cell; sc, synergid cell. Scale bar, 10 μm.

To further investigate the expression profile of *UBC22* during megasporogenesis, YFP (yellow fluorescent protein) with a nuclear localization sequence (nls) was fused to C-terminus of UBC22 for better visualization in cells. The construct *Pro$_{UBC22}$::UBC22-nlsYFP* was introduced into WT plants, and transgenic plants carrying YFP signal were obtained. UBC22-nlsYFP fusion protein was nuclear localized and strongly expressed in different cells in the ovule (Figure 4.13). In stage 1-II ovule, UBC22-nlsYFP was preferentially expressed in L1 cells and started to accumulate in the MMC of the stage 2 ovules (Figure 4.13A, B, and C). During meiosis, UBC22-nlsYFP was present in a dyad (Figure 4.13D, E, and F) and tetrad cells (Figure 4.13G, H and I). Further, stronger YFP signal could be detected in the nucleus at the chalazal end. After meiosis, stronger YFP was observed in the FM, while the degenerative megaspores had a very weak signal. The expression pattern is consistent with UBC22 playing an important role in FM formation.

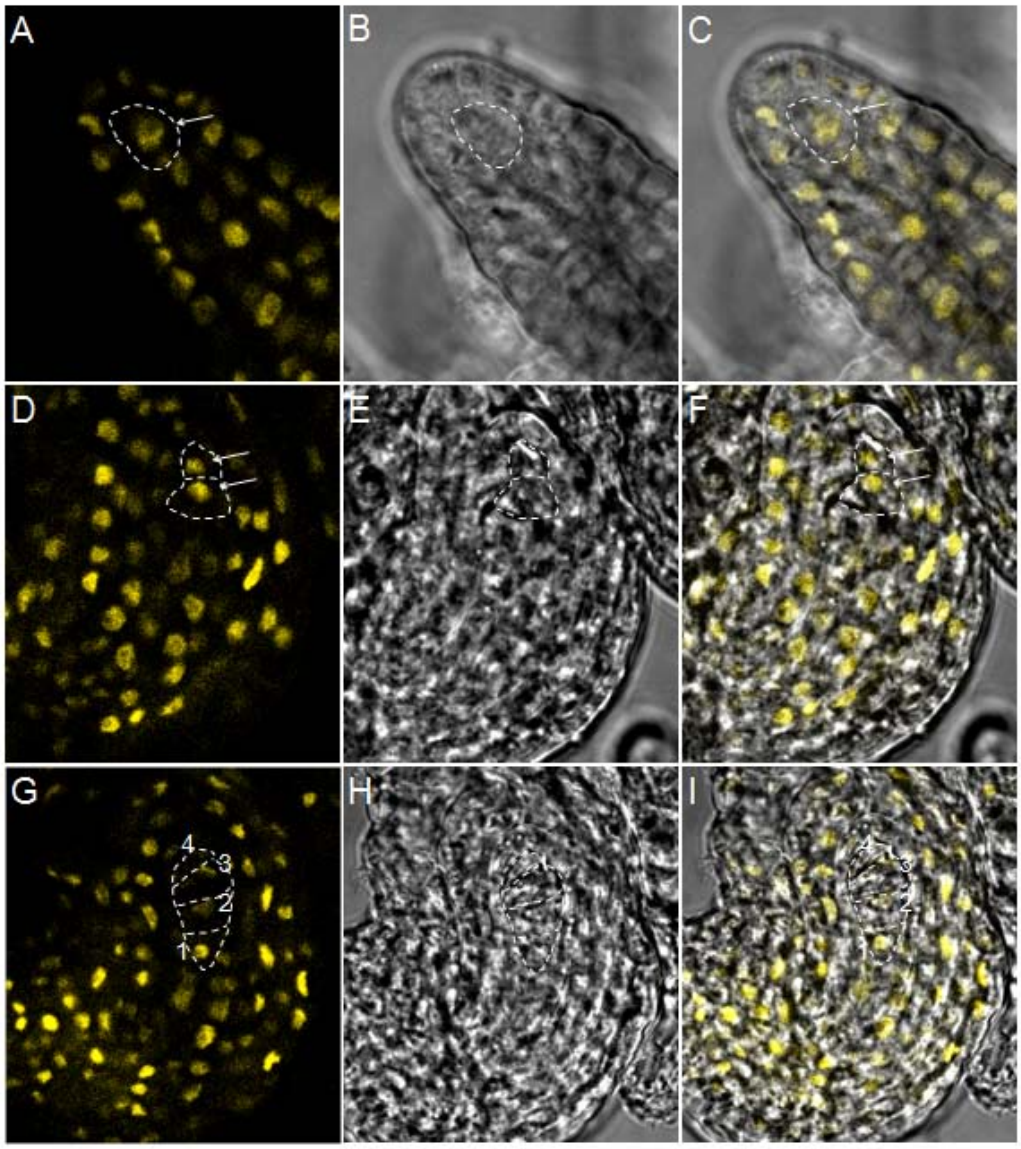

Figure 4.13 UBC22-nlsYFP expression during megasporogenesis. Developing ovules of the UBC22-nlsYFP transgenic line (WT background) were observed under a confocal microscope. (A, D, G) show confocal images, (B, E, H) show bright field images, and (C, F, I) show the overlays of the confocal and bright field images. (A, B, C) A stage 2-II ovule. (D, E, F) A stage 2-IV ovule. (G, H, I) A stage 3-I ovule after meiosis. The arrow in (A, C) shows the position of an MMC. The arrows in (D, F) show the positions of two nuclei in a dyad. The numbers in (G, I) indicate the positions of megaspores counting from the chalazal end.

4.2.4. Biochemical studies of UBC22

4.2.4.1. UBC22 catalyzing K11-linked Ub dimer formation *in vitro*

The observation that Arabidopsis UBC22 is more closely related to human UBE2S (65% of identity) than to other Arabidopsis E2s (Figure 4.2) suggests functional conservation between the Arabidopsis and human proteins. In addition, the N-terminal region of about 160 amino acids shares high levels of similarity with the human UBE2S and putative UBE2S homologs from other species (Figure 4.1). It has been shown that human UBE2S is capable of generating K11-linked Ub dimers and chains (Wickliffe et al., 2011a). We thus determined whether UBC22 could catalyze Ub dimer formation *in vitro* using recombinant UBC22 protein. As shown in Figure 4.14, Ub dimers were formed when His-UBC22 was present in the reaction (lane 2 of Figure 4.14). Furthermore, when the Ub-K11R mutant that lacks K11 residue was used (lanes 3 and 4), little dimer was produced while dimer formation was not affected when the Ub-K63R mutant that lacks the K63 residue was used (lane 5 and 6). The results indicate that UBC22 could catalyze dimer formation *in vitro* specifically through the K11 residue of the Ub.

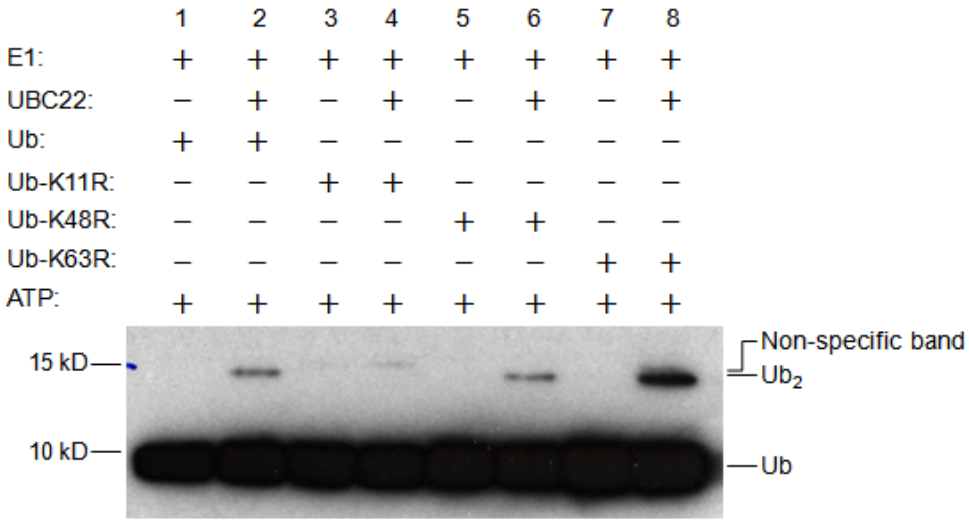

Figure 4.14 Ub dimer formation assay by His-UBC22. An *in vitro* Ub dimer formation assay was performed by adding with (lane 2, 4, 6 and 8) or without His-UBC22 (lane 1, 3, 5 and 7). Components added in different reactions are indicated on the top of the figure. The conjugation reactions were performed at 30 °C for 4 hours. Assay samples were subjected to SDS-PAGE. Ub and Ub dimers were detected by Western blotting using an anti-Ub antibody. Free Ub (Ub) and Ub dimers (Ub_2) were indicated on the right side of the figure. For K11R mutant, no new Ub dimer formation was seen when His-UBC22 protein was added. Due to slight impurity in the recombinant K11R protein, one weak band was present which is slightly higher than the Ub dimer synthesized when His-UBC22 was added. Three experiments were performed and produced similar results.

4.2.4.2. Analysis of UBC22 interaction with subunits of APC/C complex

Since the APC/C complex is conserved between plants and animals, and most subunits of the human APC/C have at least one homolog in Arabidopsis (Heyman and De Veylder, 2012), one interesting question is whether Arabidopsis UBC22 interacts with the APC/C complex, any of its subunits, or associated proteins such as CDC20 and CDH1. Based on sequence analysis, a dozen of candidates, mostly the components of the APC/C, were selected and their coding sequences were cloned into pGAD424, a yeast two-hybrid vector with the GAL4 DNA activation domain. The full-length coding sequence of UBC22 was

cloned into pGBT9, a yeast two-hybrid vector with the GAL4 DNA binding domain. Yeast two-hybrid assay was performed, and no interaction between the full-length UBC22 and any of the proteins was detected (Table 4.9). In the yeast two-hybrid system, a lack of interaction could be due to improper expression or folding of the heterologous proteins. Since the UBC domain is involved in E1-E2 and E2-E3 interactions while the lysine-rich (Lys-rich) C-terminal tail of UBE2S, the putative homolog of UBC22 in human, was found to be important for the interaction with APC/C complex (Brown et al., 2014), the N-terminal and C-terminal fragments ($UBC22^{1-155}$ and $UBC22^{156-252}$) were cloned separately into pGBT9. The yeast two-hybrid assay was then performed to test the interaction between the truncated forms of UBC22 and components of APC/C complex. However, no interaction could be observed either (Table 4.9).

Table 4.9 Analysis of interactions between Arabidopsis UBC22 and APC/C subunits in the yeast two-hybrid system.

DNA-activating domain constructs	DNA-binding domain constructs		
	UBC22	$UBC22^{1-155}$	$UBC22^{156-252}$
APC2	-	-	-
APC3b/HOBBIT	-	-	-
APC4	-	-	-
APC6/NOMEGA	-	-	-
APC8	-	-	-
APC11	-	-	-
CDC20-1	-	-	-
CCS52A1(CDH1)	-	-	-

cDNAs of Arabidopsis APC/C subunits were cloned into a GAL4 DNA activation domain yeast two-hybrid vector, while Arabidopsis *UBC22* and its truncated forms were cloned into a GAL DNA-binding domain vector (from pGBT9). The constructs were used to transform the yeast strain PJ69-4A. The transformants were grown on different synthetic defined (SD) medium plates and evaluated for cell growth. "-" means that no cell growth was observed on the plates lacking leucine, tryptophan, and histidine (-Leu-Trp-His). All transformants could grow normally on SD-Leu-Trp plates.

4.2.4.3. Analysis of UBC22 stability

The GUS expression in the transgenic *Pro$_{UBC22}$::GUS* plants (Figure 4.12) suggests a wide expression pattern of *UBC22*. On the other hand, in the *ubc22-1* mutant lines that were mostly complemented by expressing *Pro$_{UBC22}$::HA-UBC22*, it was very difficult to detect the HA-UBC22 protein despite the fact that *HA-UBC22* transcripts in the transgenic plants were at a similar level to that of the native *UBC22* transcript in the WT plants. This observation suggests that UBC22 protein may be under tight regulation or unstable. To examine the expression of UBC22 protein, the coding sequences for full-length UBC22, C-terminal, and N-terminal domains were cloned into a yeast expression vector with a GFP tag, modified from pYES2. These constructs were expressed in yeast cells. In the initial analysis, GFP-fused UBC22 (GFP-UBC22) could barely be detected and a faint band on the gel indicated possibly the full-length GFP-UBC22 with the expected size (Figure 4.15B, lane 2, the expected sizes for GFP and UBC22 are about 26 kD and 28 kD, respectively). Interestingly, GFP-fused UBC domain of UBC22 (GFP-UBC22$^{1-155}$) was easily detected with a clear protein band (Figure 4.15B, lane 3). These results indicate that GFP-UBC22$^{1-155}$ is more stable than GFP-UBC22, and suggest that the Lys-rich C-terminal domain might render UBC22 less stable. However, this observation is preliminary and requires further confirmation.

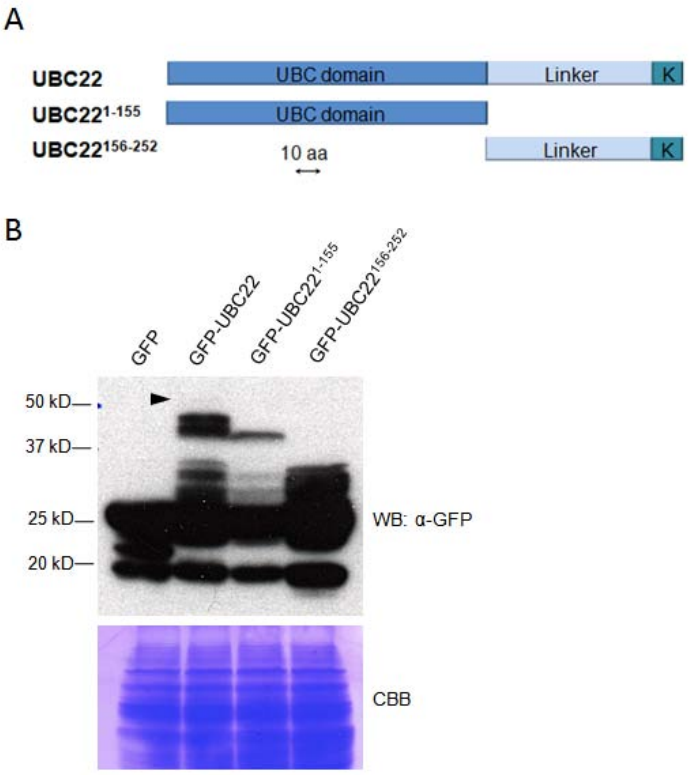

Figure 4.15 Expression of UBC22 and two truncated UBC22 in yeast. (A) Schematic display of sequences of UBC22 and UBC22 fragments used in the analysis. (B) The constructs were introduced into yeast cells, and protein expression was induced by incubating cells in the galactose-containing medium for 4 h. GFP-fusion proteins were detected by western blotting with an anti-GFP antibody. The Coomassie Brilliant Blue (CBB) stained gel was shown in the bottom to indicate the loading evenness. The arrow head points a faint band which may represent the full-length GFP-UBC22.

4.3. Discussion

4.3.1. UBC22 plays an important role in female gametophyte development

During megasporogenesis in plants, the MMC is developed from one subepidermal cell in the young ovule. In the great majority of angiosperms, following meiosis, the megaspore closest to the chalazal end enlarges and gives rise to the FM, while the other three megaspores degenerate (Yadegari and Drews, 2004). This developmental feature that only

one megaspore survives ensures that there will only be one embryo sac with one egg cell and one central cell in each ovule. In the *ubc22* mutants, the MMC develops normally based on the observations of developing ovules at the stage 2-II (Schneitz et al., 1995); however about 37% ovules at the stage 3-I (with the outer integuments near the top of nucellus) did not have an FM. Under the present conditions, in a small portion of ovules (4.4%), the FM could not be observed, which was likely due to developmental variation among ovules or simply to the limitation of the microscope optics. Since FM was present in most of WT ovules at this developmental stage, but absent in a large portion of the mutant ovules, we infer that a key point for UBC22 to function is during female megasporogenesis, specifically from MMC to the formation of FM.

There are two possible causes for the absence of the FM in the *ubc22* mutant: (1) arrest or inhibition of meiosis and (2) degeneration of the FM together with the other three megaspores. It has been shown that the non-functional megaspores degenerate likely through programmed cell death (Citterio et al., 2005). In the *ubc22* mutant, many FMs appeared to be at different stages of degeneration from unclear nuclear-cytoplasm boundary to almost completely disappearing. This observation together with the absence of FM in a large percentage of ovules suggests the degeneration of the FM along with the three non-functional megaspores in the mutant.

In addition to the absence of an FM, defects also occurred during female gametogenesis in the *ubc22* mutant. Over 60% of mutant embryo sac at flowering stage did not contain any gamete nuclei likely due to degeneration either during megasporogenesis or

gametogenesis. Further, in about 30% of embryo sacs in which gamete nuclei were observed, the embryo sacs were at various stages of gametogenesis with a relatively high proportion in FG5 (Table 4.4), compared to the WT embryo sacs which were almost all at FG7, indicating that megagametogenesis in the mutant ovules was delayed to various extents. The defects in female megasporogenesis and gametogenesis in the *ubc22* mutant indicate that *UBC22* plays a critical role in female gametophyte development. It could be postulated that the inactivation of UBC22 inhibits female gametophyte development likely due to impaired degradation of certain substrate proteins. Since the extent of inhibition varies among ovules, strong inhibition in some ovules leads to degeneration at the FM stage while weaker inhibition allows FM development but affects female gametogenesis. The stronger expression of UBC22-nlsYFP in the FM indicates its important role in FM formation.

Although major defects were observed in female gametophyte development of the *ubc22* mutant plants, results from the reciprocal crosses and the analysis of mutant pollen also revealed a relatively minor effect of *UBC22* inactivation on male gametogenesis. In addition, results from the promoter-GUS expression (Figure 4.12) showed that *UBC22* was expressed in various tissues, suggesting that UBC22 may have functions in other tissues.

4.3.2. UBC22 likely catalyzes K11-linked protein ubiquitination

UBC22 is the sole member of the subfamily X among the 37 Arabidopsis E2s (Kraft et al., 2005), implying that it has a unique function in plants. Several studies suggest that UBC22 may be involved in polyubiquitination in Arabidopsis and could catalyze E3-independent ubiquitination *in vitro* (Kraft et al., 2005; Takahashi et al., 2009; Zhao et al.,

2013). Additionally, an E2 conjugating assay showed the formation of a thioester linkage between Ub and UBC22 (Zhao et al., 2013). Our results further show that UBC22 can catalyze Ub dimer formation *in vitro* independent of an E3.

The close sequence similarity of Arabidopsis UBC22 with the human and animal UBE2S homologs (Figure 4.1) suggests functional conservation. Results from different studies have shown that human UBE2S plays a unique function in K11-linked polyubiquitination together with the APC/C (anaphase-promoting complex/cyclosome), a large complex consisting about 13 subunits, targeting cell cycle proteins for degradation (Garnett et al., 2009; Wickliffe et al., 2011a; Williamson et al., 2009). So far, UBE2S is the only E2 known to be able to catalyze K11-linked ubiquitination and a major role for K11-linked ubiquitination is in the regulation of mitosis (Wickliffe et al., 2011b). We showed that the formation of Ub dimers *in vitro* is K11-specific. This finding together with the sequence conservation with the mammalian UBE2S homologs strongly supports the notion that UBC22 catalyzes K11-linked ubiquitination in plants.

APC/C acts as a platform to recruit substrates to E2s for their polyubiquitination. In mammalian cells, UBE2S conjugates the C terminus of a donor Ub to the K11 of an acceptor Ub (Wickliffe et al., 2011a). APC/C provides acceptor-Ub binding sites for UBE2S. The APC/C is highly conserved in plants and different APC/C subunits from Arabidopsis are able to complement the corresponding yeast mutants (Capron et al., 2003; Eloy et al., 2011; Wang et al., 2012). Results from Arabidopsis indicate that APC/C functions in regulating the cell cycle by targeting cell cycle proteins containing the specific D- or KEN/GxEN-box

destruction signals (Heyman and De Veylder, 2012). In Arabidopsis, APC/C complex consists of at least 11 components, and some Arabidopsis APC/C mutants display defects in female gametogenesis. The ovules of *apc2* and *apc6* mutants are arrested at the two-nucleus stage of megagametogenesis (Capron et al., 2003; Kwee and Sundaresan, 2003), while defects at different stages of megagametogenesis are found in the *apc1* and *apc4* mutants (Wang et al., 2012; Wang et al., 2013).

From the studies of human UBE2S, APC/C complex could be potential interactors of Arabidopsis UBC22. However, the yeast two-hybrid analysis did not show an interaction of UBC22 with any of the APC/C components tested, even when truncated forms of UBC22 were used. The lack of an interaction could be due to improper expression or folding of the heterologous proteins in yeast, or because one subunit of APC/C complex might not be sufficient for the interaction with UBC22. Further, the GFP-UBC22 expression analysis in yeast cells suggests that UBC22 is not stable *in vivo* since no full-length of GFP-UBC22 could be detected. Thus, different approaches, such as *in vitr*o pulldown assay using recombinant proteins, may be needed to analyze whether there is an interaction between UBC22 and APC/C complex.

In humans, the UBE2S is considered as an “elongation” E2 which extends the Ub chain through K11-linkages, following the initial ubiquitination of the substrate by another E2 (UBE2C) together with APC/C (Primorac and Musacchio, 2013). In Arabidopsis, UBC19 and UBC20 have been identified as the homologs of UBE2C based on sequence relatedness and the ability to complement a yeast mutant (Criqui et al., 2002). However, there is no

information regarding the specific ubiquitination that UBC19 and UBC20 are involved in plants currently. The present results have provided the initial experimental evidence for the existence of the atypical K11-linked protein ubiquitination in plants and identified a critical role of UBC22 in female gametophyte. It will be interesting to determine whether a module similar to the animal UBE2S-APC/C module is conserved in plants, and also possible differences between the plant and animal E2 homologs involved in K11-specific ubiquitination.

5. CHAPTER FIVE - FUNCTIONS OF UBC22 IN VEGETATIVE DEVELOPMENT

5.1. Introduction

UBC22 is the sole member in the subfamily X and was found to play a critical role in female gametophyte development as described in the previous chapter. The *ubc22* mutants had much shorter siliques with about 90% ovules aborted. Analysis of ovules at different developmental stages revealed the degeneration of FM and various abnormalities during megagametogenesis in the mutant plants. Further, *in vitro* Ub dimer assay demonstrated that UBC22 can catalyze the Lys11-specific Ub dimer formation, suggesting that UBC22 is involved in Lys11-linked ubiquitination in plants (Wang et al., 2016). The analysis using promoter-GUS reporter showed that *UBC22* is ubiquitously expressed, not only in reproductive tissues but also in vegetative tissues, indicating UBC22 may play roles in other tissues or developmental processes as well. In this study, *ubc22* mutants were further characterized in vegetative development. Interestingly, four different subtypes of mutant plants were observed. RNA-seq analysis of four subtypes of mutant plants revealed that multiple signaling pathways were affected in *ubc22* mutants. Further analyses indicated the possible roles of UBC22 in plant-pathogen interaction and hormonal responses.

5.2. Results

5.2.1. Characterization of four subtypes of *ubc22* mutant plants

In our previous study, the characterization of two individual T-DNA insertion mutant lines *ubc22-1* and *ubc22-2* revealed that inactivation of *UBC22* affects female gametophyte development (Wang et al., 2016). In terms of vegetative characteristics such as leaf size and

morphology, although the majority of *ubc22* mutant plants appeared similar to WT plants, we found that some *ubc22* mutant plants were very different from WT plants (Figure 5.1A). Based on leaf size and shape, *ubc22-1* mutant plants could be categorized into four different subtypes (Table 5.1). (1) Type I: This subtype includes the majority (~70%) of *ubc22* mutant plants. These plants had much shorter siliques due to defects in female gametophyte development as described earlier. However, leaf morphology was similar to the WT plants, although the mutant plants appeared slightly larger. (2) Type II: This type of plants represented about 16% of the mutant plants. They had wider and rounder leaves. The petioles were shorter, and thus leaves appeared more compact compared to WT plants. When plants grew older, the color of mature leaves appeared dark green. The flowering time was dramatically delayed (Figure 5.1B), and seed setting was reduced. (3) Type III: The percentage of this subtype is about 7%. Leaves of this type of plants appeared narrower and leaf surface was smoother. Leaves on older plants appeared paler and started to senesce earlier compared to WT plants. Very few seeds could be collected from this type of plants. (4) Type IV (7%): Mutant plants in this category were much smaller. The leaves appeared narrow, wrinkled, and normally had obvious serrations. Early senescence was also observed in old leaves. Moreover, the plants were almost completely sterile. These four subtypes of plants with similar percentages were also observed in a different T-DNA insertion mutant line *ubc22-2* (Table 5.1). Furthermore, interestingly, the four subtypes of plants reappeared in the progeny of any subtype, particularly Type I and Type II, since few seeds could be collected from Type III and Type IV plants due to sterility.

We observed that the female gametophyte phenotypes of the *ubc22* mutant could be mostly rescued by the expression of the *Pro$_{UBC22}$::HA-UBC22* construct. Thus, we set out to determine whether the subtype phenotypes would also be rescued. This complementation line had been characterized previously and its silique length was similar to that of the WT (Wang et al., 2016). About 96% plants of the complementation line belonged to Type I category and they appeared similar to the WT in term of leaf morphology. The percentages of Type II, III and IV plants were highly reduced at 1.8%, 1.2%, and 1.0%, compared to 16.0%, 11.5% and 6% in *ubc22-1* mutants, respectively (Table 5.1). Thus, the expression of *Pro$_{UBC22}$::HA-UBC22* in the *ubc22-1* mutant rescued mostly the phenotypes of different subtypes, similar to the rescue of the female gametophyte phenotypes. To further confirm that the occurrences of four subtypes in mutant plants are due to *UBC22* inactivation, we created yet another UBC22 mutant using CRISPR (Clustered Regularly Interspaced Short Palindromic Repeats)/Cas9 system (Ma et al., 2015). This mutant (W76-1) had an "AG" two-nucleotide deletion in the *UBC22* open-reading frame causing a frame shift in UBC22 at the position of amino acid Asp28 (Figure 5.2A). In this mutant line, the same four subtypes of mutant plants were also observed as in the two T-DNA insertion mutant lines, *ubc22-1* and *ubc22-2* (Figure 5.2B). Collectively, these data clearly indicate that the appearance of four different subtypes of mutant plants is not due to the variation in plant growth or inactivation of a non-target gene, but to the inactivation of *UBC22*.

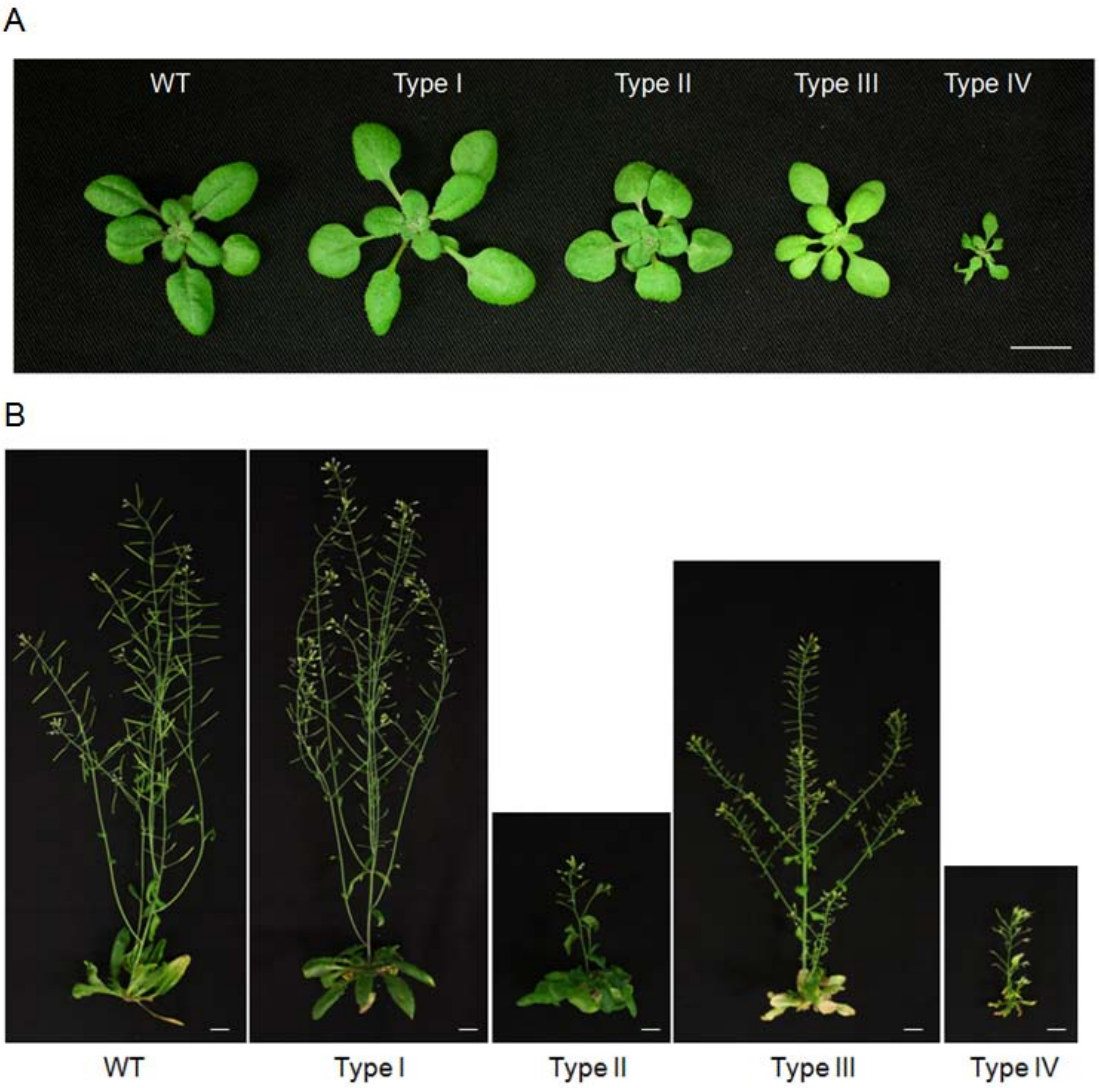

Figure 5.1 Four subtypes of *ubc22-1* mutant plants. Images were taken of one representative plant from each subtype at 3-week (A) and 8-week (B) stages. From left to right: WT, Type I, Type II, Type III and Type IV. Scale bar: 1 cm.

Table 5.1 Percentage of four different subtypes of mutant plants in WT and *ubc22* mutant lines as well as a complementation line expressing *UBC22*.

Line	Total number of plants	Type I	Type II	Type III	Type IV
WT	224 (100%)	N/A	N/A	N/A	N/A
ubc22-1	989 (100%)	693 (70.1%)	159 (16.1%)	70 (7.1%)	67 (6.8%)
ubc22-2	321 (100%)	210 (65.4%)	53 (16.5%)	37 (11.5%)	21 (6.5%)
ubc22-1/ Pro$_{UBC22}$::HA-UBC22	904 (100%)	868 (96.0%)	16 (1.8%)	11 (1.2%)	9 (1.0%)

Seeds from different lines were planted directly into the soil. After two weeks, plants were surveyed and grouped into the subtypes based on leaf size, shape, and color.

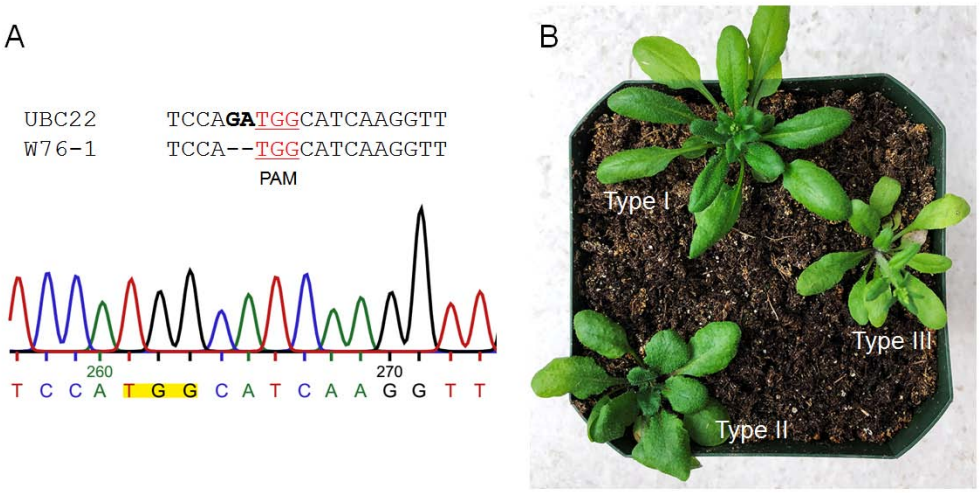

Figure 5.2 Characterization of the *ubc22* mutant created through CRISPR/Cas9 technology. (A) Alignment of genomic sequences of *UBC22* from WT and *UBC22*-CRISPR/cas9 line (W76-1) near the edited sites. The electropherogram at the bottom shows the DNA sequence near the edited site from W76-1. The PAM (Protospacer Adjacent Motif) NGG site is highlighted. (B) The same subtypes of plants were observed in the progeny plants from W76-1. Images were taken at 5-week stage of the plants.

5.2.2. RNA-seq analysis of four subtypes of mutant plants

The occurrence of different subtypes of *ubc22* mutants suggests that inactivation of UBC22 affects plants differently in the different types. To understand which genes were affected in different subtypes of plants and differences among the subtypes, we used RNA-seq technique to analyze gene expression profile (transcriptome) at the whole-genome level (Wang et al., 2009). To that end, rosette leaves from different subtypes of *ubc22-1* plants at the 3-week stage were collected, RNAs were isolated, and three biological replicates collected from different plants were used for each subtype.

Analysis of the RNA-seq data revealed a total of 2,525 differentially expressed genes DEGs) in *ubc22-1* mutants. The numbers of DEGs varied among the subtypes. There were only 44 DEGs found in Type I mutant plants, while Type II, III, and IV mutant plants had 321, 1968, and 827 DEGs, respectively, compared to the WT. This finding was not surprising, since Type I mutant plants were the most similar to the WT plants in terms of leaf morphology and plant size, while the other subtypes of mutant plants had more obvious phenotypic changes, including leaf shape, leaf color and flowering time. Venn diagram showed that a large number of DEGs were specific for Type II, III and IV mutant plants (206, 1429, and 313) compared to WT plants, suggested that each subtype has a unique profile of gene expression (Figure 5.3A). Interestingly, a total of 487 DEGs were shared by both Type III and Type IV plants, while the Type II plants shared much fewer DEGs with either Type III or Type IV mutant plants. There were 10 DEGs shared by four different subtypes of mutant plants (Figure 5.3A). However, they could not be grouped under a specific biological process

and most of them did not show significant changes compared to WT. Thus, they were not analyzed further.

Cluster analysis was performed to identify the gene expression patterns in four subtypes of mutant plants. In total, 9 clusters were identified based on the changes in gene expression compared to the WT (Figure 5.3B). Genes in cluster 1 did not show much change in Type I and II plants, but down-regulated in Type III mutant plants. Genes in cluster 2 had a higher level of expression in Type II plants, but a lower level in Type III plants. Genes in cluster 3 had a reduced level in Type II plants but a higher level in Type III plants. Genes in cluster 4 and 6 were expressed at a higher level in Type III plants, while genes in cluster 5 were expressed at a higher level in Type IV. Genes in cluster 7 and 9 were expressed at a lower level in Type III and Type IV plants, while genes in cluster 8 did not show obvious changes among different subtypes.

GO enrichment analysis showed that cluster 1 was enriched with genes in secondary metabolisms, such as flavonoid metabolic process, and cluster 4 with genes in carbohydrate metabolic process, suggesting that flavonoid and carbohydrate metabolic pathways were affected in Type III mutant plants. Interestingly, cluster 2 was highly enriched with genes in defense response, systemic acquired resistance and response to biotic stress. Genes in this cluster showed a higher level of expression in Type II mutant plants, but a lower level in Type III mutant plants, implying that these genes might be regulated differently in these two subtypes (Figure 5.3C). The subsequent analyses focused mainly on Type I and Type II mutant plants since they counted for over 80% of the mutant plants and also very few seeds

were produced from Type III and Type IV plants.

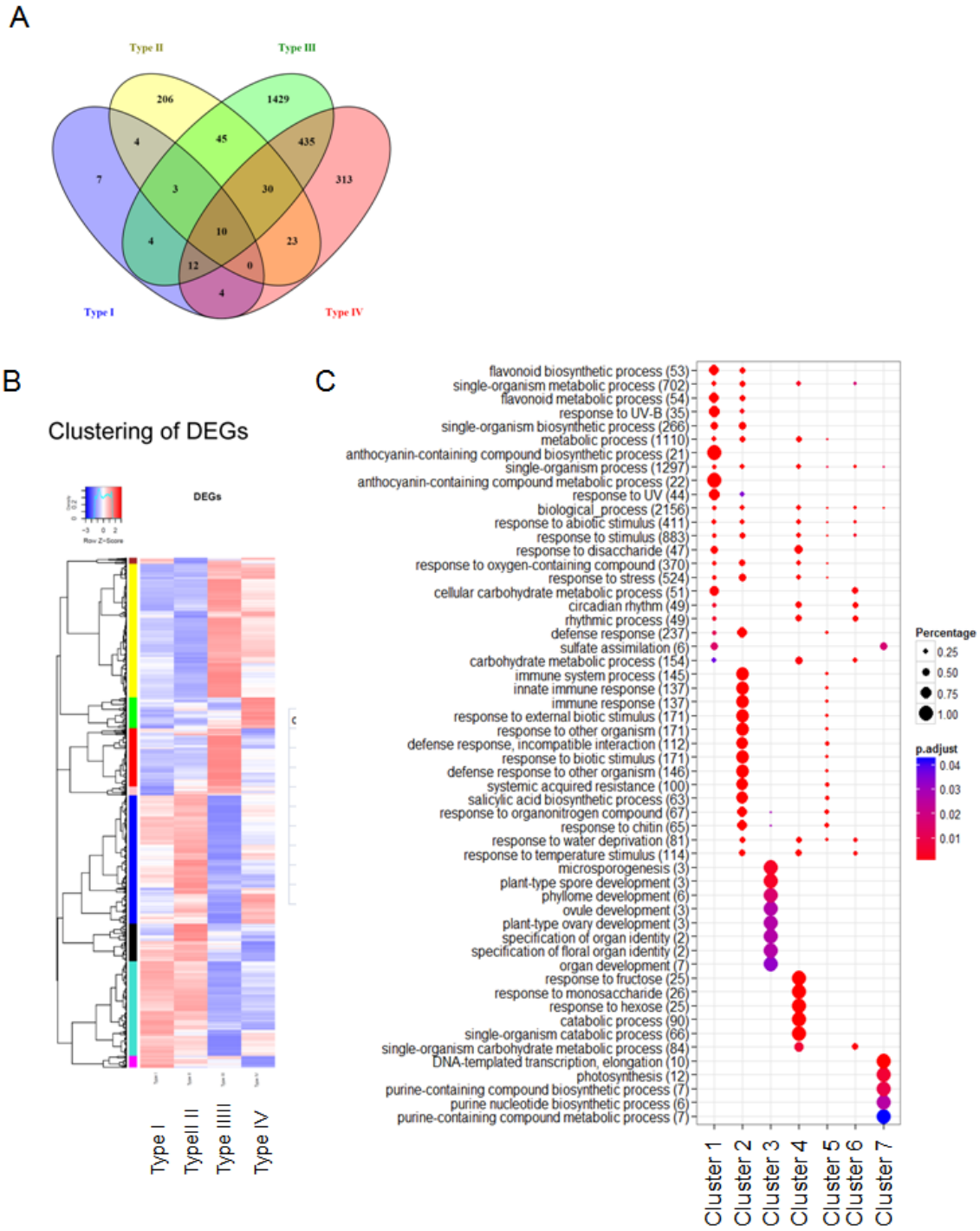

Figure 5.3 Transcriptome analysis of the four subtypes of *ubc22* mutant plants. (A) Venn diagram of differentially expressed genes (DEGs) in Type I, Type II, Type III and Type IV mutant plants. DEGs were identified as $\log_2$ fold change (mutant vs WT) >= 1 or <= -1 and

adjusted p-value < 0.01. (B) Hierarchical clustering analysis for DEGs in *ubc22* mutant plants. Clustering was performed with $\log_2$ fold change values between the mutants and WT. A total of 9 clusters indicated by different colors were identified from the four subtypes of *ubc22* mutant plants. Colors from cluster 1 to 9: turquoise, blue, brown, yellow, green, red, black, pink and magenta. (C) Gene Ontology (GO) enrichment analysis. Y-axis represents GO terms in biological processes, and X-axis stands for each cluster (no significant GO terms in cluster 8 and 9). Significantly enriched GO terms are shown (adjusted p-value < 0.05).

5.2.3. Plant-pathogen interaction in the *ubc22* mutant

Interestingly, the expression of a set of *PDF* (Plant Defensin) genes was drastically increased in Type II mutant plants (Table 5.2). For instance, *PDF1.3* and *1.2*, two plant defense-encoding genes, were up-regulated by 42.3 and 21.0 folds. This change was only observed in Type II mutant plants, but not in other subtypes of mutant plants. The dramatic changes in *PDF* gene expression led us to investigate whether the other plant defense genes might also be up-regulated in Type II mutant plants. To have a better understanding, DEGs from Type II mutant were applied with a cut-off p-value of <0.01. Among the 180 DEGs, 151 DEGs were up-regulated and the average fold change was 3.0. Furthermore, 34 defense-related genes were up-regulated and the average fold change was 5.0 (Table 5.2). In addition to *PDF* genes, *AT4G16260*, *LAL5 (AT3G23550)*, and *DIN11 (AT3G49620)* were also up-regulated by about 7.7, 6.8, and 5.5 folds, respectively. The change in the expression of *PDF1.2* was validated by qPCR (Figure 5.4A). Together, these results indicate clearly the up-regulation of defense-related genes in Type II mutant plants.

Table 5.2 Up-regulation of defense-related genes in one subtype (Type II) of *ubc22* mutant plants

AGI	Gene Name	Product Description	Fold changes	Reference
AT2G26010	PDF1.3	Plant defensin 1.3	42.3	(Pre et al., 2008)
AT5G44420	PDF1.2	Plant defensin 1.2	21.0	(Pre et al., 2008)
AT5G44430	PDF1.2c	Plant defensin 1.2C	12.2	(Pre et al., 2008)
AT4G16260	AT4G16260	Glycosyl hydrolase superfamily protein	7.7	(Pre et al., 2008)
AT3G23550	LAL5	MATE efflux family protein	6.8	(Pre et al., 2008)
AT3G49620	DIN11	2-oxoglutarate (2OG) and Fe(II)-dependent oxygenase superfamily protein	5.5	(Pre et al., 2008)
AT2G43590	AT2G43590	Chitinase family protein	3.8	(Pre et al., 2008)
AT2G43510	ATTI1	Trypsin inhibitor protein 1	3.7	(Clauss and Mitchell-Olds, 2004)
AT1G26390	AT1G26390	FAD-binding Berberine family protein	3.5	(Rajniak et al., 2015)
AT2G33380	RD20	Caleosin-related family protein	2.9	(Hanano et al., 2015)
AT3G04720	PR-4	Pathogenesis-related 4	2.8	(Pre et al., 2008)
AT3G16530	AT3G16530	Legume lectin family protein	2.8	(Pre et al., 2008)
AT2G22330	CYP79B3	Cytochrome P450, family 79, subfamily B, polypeptide 3	2.8	(Naur et al., 2003)
AT4G12480	pEARLI 1	Bifunctional inhibitor/lipid-transfer protein/seed storage 2S albumin superfamily protein	2.7	(Li et al., 2012)
AT3G16460	AT3G16460	Mannose-binding lectin superfamily protein	2.7	(Yamada et al., 2011)
AT3G16450	AT3G16450	Mannose-binding lectin superfamily protein	2.7	(Yamada et al., 2011)
AT4G15440	HPL1	Hydroperoxide lyase 1	2.6	(Scala et al., 2013)
AT3G15356	AT3G15356	Legume lectin family protein	2.5	(Pre et al., 2008)
AT4G23600	CORI3	Tyrosine transaminase family protein	2.5	(Kim et al., 2013a)
AT2G39030	NATA1	Acyl-CoA N-acyltransferases (NAT) superfamily protein	2.5	(Adio et al., 2011)
AT2G26560	PLP2	Phospholipase A 2A	2.4	(Pre et al., 2008)
AT2G46240	BAG6	BCL-2-associated athanogene 6	2.4	(Li et al., 2016b)
AT5G13220	JAZ10	jasmonate-zim-domain protein 10	2.4	(Demianski et al., 2012)
AT3G09260	PYK10	Glycosyl hydrolase superfamily protein	2.3	(Yamada et al., 2011)
AT5G57220	CYP81F2	Cytochrome P450, family 81, subfamily F, polypeptide 2	2.2	(Clay et al., 2009)

AT2G37130	PER21	Peroxidase superfamily protein	2.1	(Maleck et al., 2000)
AT2G43620	AT2G43620	Chitinase family protein	2.1	(Desveaux et al., 2005)
AT3G16420	PBP1	PYK10-binding protein 1	2.1	(Yamada et al., 2011)
AT2G31230	ATERF15	Ethylene-responsive element binding factor 15	2.1	(Pre et al., 2008)
AT2G34490	CYP710A2	Cytochrome P450, family 710, subfamily A, polypeptide 2	2.1	(Griebel and Zeier, 2010)
AT2G20340	AT2G20340	Pyridoxal phosphate (PLP)-dependent transferases superfamily protein	2.0	(Gutensohn et al., 2011)
AT2G29525	AtIPCS3	Arabidopsis Inositol phosphorylceramide synthase 3	2.0	(Wang et al., 2008)
AT2G18170	ATMPK7	ATMPK7_MPK7_MAP kinase 7	2.0	(Zhang et al., 2007)

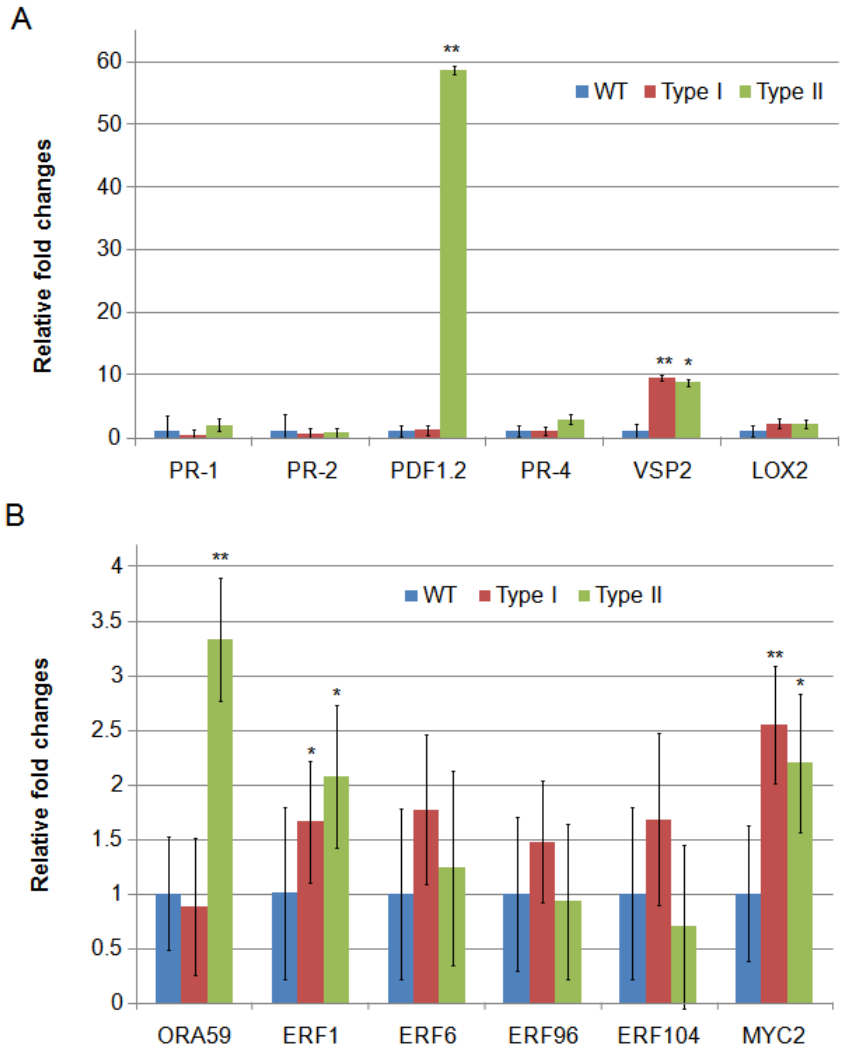

Figure 5.4 Real-time quantitative PCR analysis of gene expression in different subtypes of *ubc22* mutant plants. (A) A set of marker genes involved in different pathways were tested. Salicylic acid pathway: *PR-1* and *PR-2*; Jasmonic acid (JA) pathway: *PDF1.2*, *PR-4*, *VSP2*, and *LOX2*. (B) The genes encoding transcription factors involved in JA signaling pathway were selected for the RT-PCR analysis. Each datum represents the average of three biological replicates. Error bars indicate standard errors. Student's t-tests were performed to determine whether there is a significant difference between different subtypes and WT for each of the genes analyzed. **: p-value < 0.01; *: p-value < 0.05.

The clear increases in the expression of many defense-related genes raise a question whether the Type II mutant plants had increased resistance to pathogens. The plant microbial pathogens can be divided into three major groups according to their life styles: necrotrophic, biotrophic, and hemi-biotrophic pathogens. Necrotrophic pathogens invade plant tissue and kill it rapidly, and then live on the dead tissues. In contrast, biotrophic pathogens exist and propagate in living cells and derive nutrient from the cells. The hemi-biotrophic pathogens have combined features of the necrotrophic and biotrophic pathogenes. It is widely known that plant hormones, especially salicylic acid (SA), jasmonic acid (JA) and ethylene (ET), play major roles in plant-pathogen interactions (Pieterse et al., 2009; Pieterse et al., 2012). The SA response pathway is typically effective against microbial biotrophic pathogens, with the expression of a robust marker gene *PR-1*, whereas JA and ET pathways have a synergistic effect in the resistance to necrotrophic pathogens (Pieterse et al., 2009; Pieterse et al., 2012). The activation of a marker gene *PDF1.2* expression is controlled by both JA and ET signaling (Pre et al., 2008). The up-regulation of JA or/and ET pathways, as indicated by the expression of a number of plant defense genes, including *PDF1.2*, is important for the resistance to the necrotrophic pathogens. *Botrytis cinerea*, also known as grey mold, is considered as a typical necrotrophic pathogen and can infect more than 200 crop species worldwide. This pathogen has been widely used for studying plant-pathogen interactions in Arabidopsis (Williamson et al., 2007).

Thus, we determined whether Type II mutant plants have an enhanced resistance to necrotrophic pathogens such as *Botrytis cinerea*. Following the inoculation of the pathogen,

the detached leaves from Type II mutant plants developed smaller areas of lesions compared to larger areas of lesions on the WT leaves (Figure 5.5A and B). The increased resistance of Type II mutant plants to *Botrytis cinerea* was also observed following the inoculation of the pathogen on whole plants (Figure 5.6). Trypan blue staining showed that the growth of fungal hyphae on leaves of Type II mutant plants was much less than that on the leaves of Type I and WT plants (Figure 5.5C). Thus, Type II mutant plants had an enhanced resistance to *Botrytis cinerea* compared to WT and Type I plants.

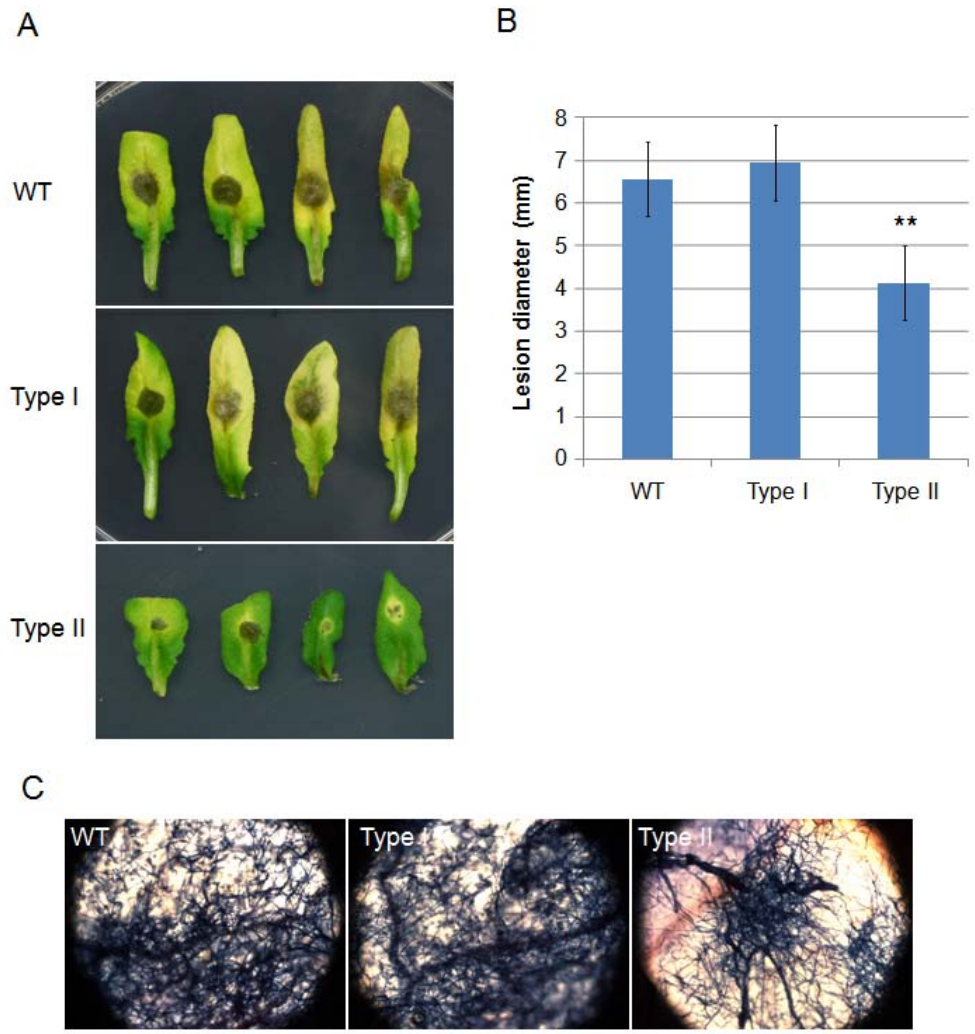

Figure 5.5 Response of Type I and Type II plants of the *ubc22* mutant to necrotrophic pathogen *Botrytis cinerea*. (A) Infection lesions observed at 4 dpi (days post-inoculation) on leaves inoculated with *B. cinerea*. (B) Quantitative analysis of the leaf lesion size at 3 dpi with *B. cinerea* (n >=10). Error bars indicate standard errors. **: p-value < 0.01. (C) Visualization of fungal hyphae growth in leaves of WT, Type I and Type II mutant plants after trypan blue staining at 4 dpi with *B. cinerea*.

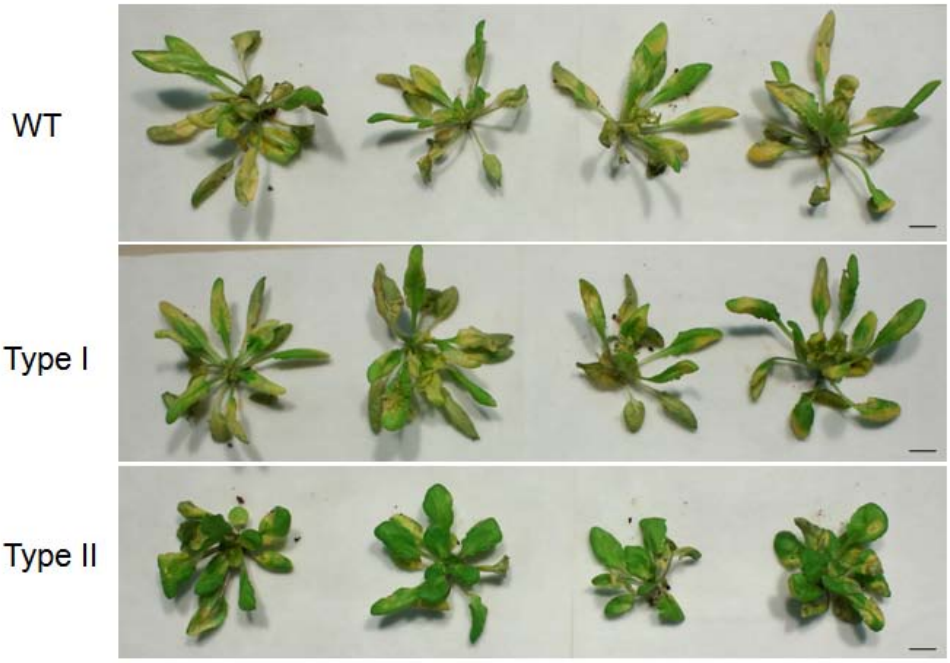

Figure 5.6 Symptoms of pathogen infection on leaves of WT, Type I and Type II *ubc22* mutant plants after *B. cinerea* inoculation. WT, Type I and Type II mutant plants (4-week) grown in the soil were inoculated with *B. cinerea*. Images were taken at four days after inoculation.

5.2.4. Responses of the *ubc22* mutant to different hormonal and stress conditions

Real-time qPCR analysis confirmed that only in Type II mutant plants the expression of *PDF1.2* was dramatically up-regulated. Also, the expression of transcription factor MYC2 as well as its target, the JA-responsive gene *VSP2* (*Vegetative Storage Protein 2*), increased in Type I and Type II plants (Figure 5.4). It has been shown that MYC2 is not only involved in JA, but also in ABA signaling. For instance, MYC2 acts as a positive regulator of ABA signaling and *MYC2* overexpressing plants showed increased ABA sensitivity (Abe et al., 2003). The increased level of *MYC2* in both Type I and Type II mutant plants may suggest an alternation in ABA signaling. Moreover, ubiquitination is known to play important roles in diverse plant responses to hormonal and stress conditions (Kelley and Estelle, 2012; Stone, 2014).

Therefore, a series of conditions were tested to determine possible changes in the responses of the *ubc22* mutant. These conditions were based on the previous analysis performed in our lab, including salinity, oxidative stress, osmotic stress and different hormones. WT and mutant seedlings were grown on 1/2 MS agar medium supplemented with one of the test reagents: naphthaleneacetic acid (NAA, a synthetic auxin), kinetin (KN, one of the cytokinins), methyl jasmonate (MeJA, a derivate of jasmonic acid), salicylic acid (SA), an analog of abscisic acid (ABA), 1-Aminocyclopropane-1-carboxylic acid (ACC, a precursor of ethylene), mannitol (as an osmolyte), and N,N′-dimethyl-4,4′-bipyridinium dichloride (paraquat, to produce oxidative stress). To reduce variation in plant growth among different plates, WT seedlings were grown side by side with mutant seedlings in the same plate. The

primary root length was measured to evaluate the difference between WT and mutant seedlings. From the initial screening, *ubc22* mutant did not show any difference compared to the WT in most conditions, except for an ABA analog, PBI425 which is more stable than ABA (Cutler et al., 2000) (Figure 5.8). Under 1 µM PBI425, *ubc22* mutant seedlings had more reduction in primary root length compared to the WT seedlings (Figure 5.9A). To confirm the hypersensitivity of the *ubc22* mutant to PBI425, different concentrations of PBI425 were tested. Seed germination (emerging of the radicle) and green cotyledon were surveyed. In the plates containing no PBI425, there was no difference in frequency of seed germination between the WT and *ubc22* mutant. However, in the presence of 1.25 µM PBI425, the frequency of germination was much lower for the mutant (35.0%) compared to that of WT (80.0%) (Figure 5.9B). Additionally, the percentage of mutant seedlings with green cotyledons was also lower for the mutant (55.6%) at 0.5 µM PBI425, compared to the WT (99.2%) (Figure 5.9C). These results confirm that the *ubc22* mutant is more sensitive to exogenous ABA during seed germination.

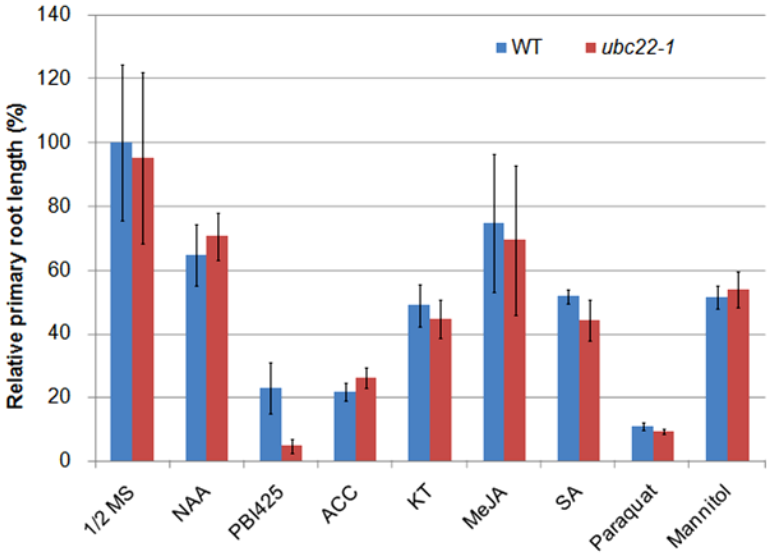

Figure 5.7 Responses of the *ubc22-1* mutant to various hormonal and stress conditions. WT and mutant seedlings were grown side by side in ½ MS medium agar plates. At day 10 after seed plating, images were taken of the seedlings and lengths of primary roots measured with ImageJ. The root length was relative to that of the WT seedlings in the control plates which was set at 100%. For each treatment, at least 3 plates were used. NAA: naphthaleneacetic acid, a synthetic auxin; PBI425: an analog of abscisic acid; ACC: 1-aminocyclopropane-1-carboxylic acid, a precursor of ethylene; KT: kinetin, one of the cytokinins; MeJA: methyl jasmonate, a derivate of jasmonic acid; SA: salicylic acid; paraquat: N,N′-dimethyl-4,4′-bipyridinium dichloride, a chemical to produce oxidative stress.

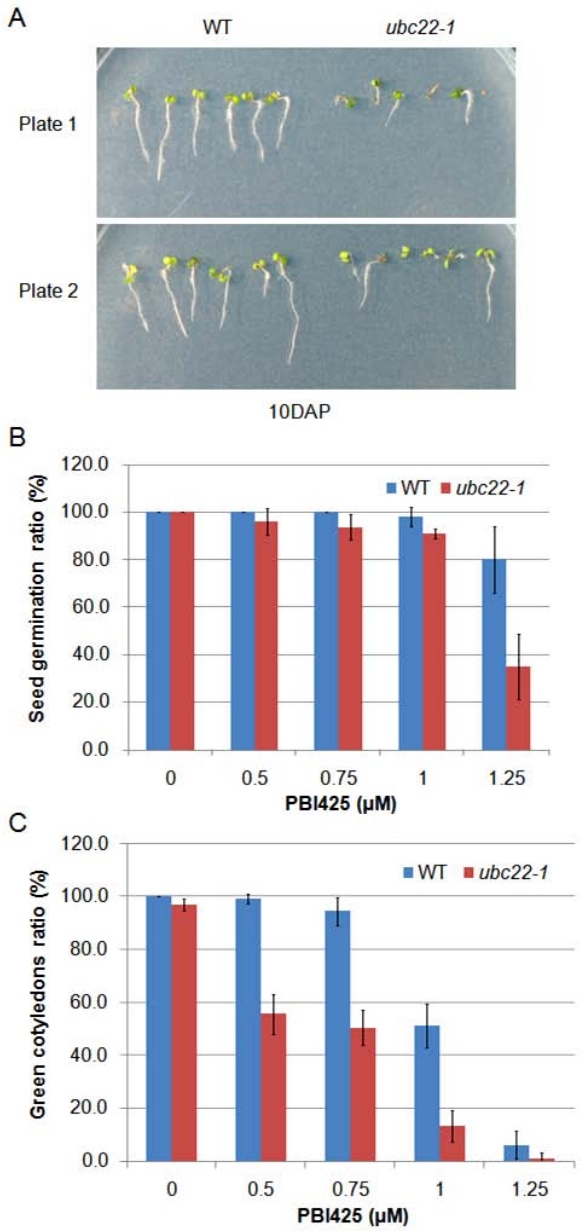

Figure 5.8 Sensitivity of the *ubc22-1* mutant to PBI425, a synthetic ABA analog. (A) Two representative images showing the root growth of WT and *ubc22* mutant seedlings grown on plates containing 1 μM PBI425 at 10-day stage after seed plating. (B) Germination frequencies of the WT and *ubc22* mutant at different concentrations of PBI425. Germination was surveyed at day 7 after seed plating. (C) Percentages of WT and *ubc22* seedlings with green cotyledons at 7-day stage after seed plating at different concentrations of PBI425. For (B) and (C), each treatment had at least 3 plates.

5.3. Discussion

5.3.1. UBC22 is involved in different pathways

Most of the *ubc22* mutant plants appeared to be similar to the WT plants throughout the vegetative growth and development. However, further careful examination of the *ubc22* mutant plants revealed multiple subtypes. The occurrence of four subtypes of mutant plants is deemed to be due to *UBC22* inactivation for the following reasons. First, three independent *ubc22* mutant lines (two T-DNA insertion lines and one CRISPR/Cas9 line) all showed the four subtypes with similar percentages. Further, when a Pro_{UBC22}*::HA-UBC22* construct was introduced in the *ubc22-1* mutant, the silique length and seed setting phenotypes were mostly rescued, and there were very few plants in Type II, III and IV. These results indicate that the four subtypes are not due to the inactivation of an unknown off-target gene. Third, when seeds from Type I or Type II mutant plants were planted, the four subtypes reappeared similarly. Fourth, distinct changes in gene expression were observed in the four subtypes of plants compared to the WT. These results indicate that the four subtypes of plants are not due to a difference in seed quality or growth conditions, but they are accompanied by specific changes in gene expression.

In gene functional studies, it is common that the inactivation of one single gene may have pleiotropic effects on different aspects of plant growth and development, but all the mutant plants usually have similar types of changes although they may differ in the severity of the phenotypes. For the *ubc22* mutant plants, although most of the plants appeared normal morphologically to the WT plants, some of them appeared very different. The phenomenon of

having several different subtypes of plants from one single gene inactivation is rarely reported and not often studied.

The numbers of E1, E2 and E3 proteins in eukaryotic species display a pyramid structure, for instance, with 2 E1s, 37 E2s and over 1000 E3s in Arabidopsis. It is understandable that one E2 may work with different E3s targeting different substrates. Thus, E2s in generally would have a broader spectrum of functions in different pathways than E3s, although some E3 could also interact with more than one E2 or target different substrates (Mazzucotelli et al., 2006). Indeed, RNA-seq analysis of different subtypes of the *ubc22* mutant plants indicated a large number of DEGs in one subtype, suggesting that expression of certain genes is uniquely altered in different subtypes. It can be envisioned that UBC22 as a sole member of the E2 subfamily X, along with cognate E3s, could target different substrate proteins involved in different pathways and cellular processes. Ubiquitination of these proteins could affect their cellular levels or functional properties such as interactions with other proteins. De-regulation of these substrate proteins due to *UBC22* inactivation could result in different phenotypic effects.

Multiple phenotypic effects are often observed with important players in cell signaling. The observation that *ubc22* mutant plants have four different subtypes each with different phenotypic features is rarely observed with other mutants. One possible explanation is that the de-regulation of certain proteins as a result of UBC22 inactivation could affect the stability of more than one signaling pathways or the balance among different pathways. There may be changes occurring in most of the mutant plants. In Type I and Type II mutant plants,

the genes encoding the transcription factor MYC2 and its target *VSP2* were both found up-regulated, indicating that a common pathway was affected in these two subtypes which constitute the majority of *ubc22* mutant plants. On the other hand, in certain mutant plants, the changes to one particular pathway might become more prominent, leading to distinct phenotypes in the subtype. For example, in Type II mutant plants, the pathways involved in pathogen responses were more prominently affected.

5.3.2. UBC22 is most likely involved in JA pathway

Plant hormones, especially SA, JA, and ET, play critical roles in plant-pathogen interactions. The SA response pathway plays a major role against biotrophic pathogens. An important regulator in the SA signaling pathway is NPR1, which upon activation by SA acts as a transcriptional coactivator for a large set of defense-related genes (Dong, 2004). *PR-1* is one of the well characterized *PR* genes, which is often used as a marker for SA-responsive gene expression (Glazebrook, 2001). JA and ET pathways have a synergistic effect on the resistance to necrotrophic pathogens. The expression of the marker gene *PDF1.2* is controlled by both JA and ET signaling (Glazebrook, 2001). In Type II mutant plants, the expression level of *PR-1* was similar to WT, suggesting that the SA pathway was not affected. On the other hand, the transcript levels of *PDFs* were much higher in Type II mutant plants and enhanced resistance to *Botrytis cinerea* was observed. These results indicate that JA and/or ET pathways were activated in Type II mutant plants.

In Arabidopsis, the JA signaling pathway consists of two major branches: the ERF branch and MYC branch. The ERF branch is regulated by members of the AP2/ERF

(Apetala2/Ethylene Response Factor) family of transcription factors, such as ERF1 and ORA59 (Octadecanoid-Responsive Arabidopsis 59) (Pre et al., 2008). The expression of JA-responsive marker gene *PDF1.2* is dependent on ERF1 or/and ORA59. Activation of the ERF branch requires either JA or ET. The MYC branch is controlled by MYC-family transcription factors such as MYC2. MYC2 acts as a positive regulator of JA-responsive genes, such as *VSP2*, whereas it negatively controls the expression level of ERF-regulated *PDF1.2* (Lorenzo et al., 2004). In general, the ERF branch of the JA pathway is associated with enhanced resistance to necrotrophic pathogens, whereas the MYC branch of the JA pathway is associated with the wound response and defense against insect herbivores (Verhage et al., 2011). In Type II mutant plants, the up-regulation of *PDF1.2* and *VSP2,* as well as the transcription factor ORA59 and MYC2, indicated that both the ERF branch and MYC2 branch of JA signaling were activated. The increased resistance to *Botrytis cinerea* observed in Type II mutant plants is consistent with an activated ERF branch. Moreover, ET signaling may also be involved in the up-regulation of *PDF1.2* since it can greatly affect JA response synergistically on the expression of ERF1 and ORA9 in the ERF branch of JA signaling pathway (Pre et al., 2008).

5.3.3. UBC22 may play a role in the ABA signaling pathway

ABA is a plant hormone that is important for many aspects of plant growth and development. Also, it is an important factor for plant responses to environmental conditions and abiotic stresses. The transcription factor MYC2 not only functions as an important player in the JA signaling but also acts a positive regulator in the ABA signaling. The plants

overexpressing *MYC2* showed an increased ABA sensitivity while *myc2* mutant appeared to have a reduced sensitivity of ABA (Abe et al., 2003; Lorenzo et al., 2004). Further, the ABA-responsive genes were up-regulated in plants overexpressing *MYC2* (Abe et al., 2003). In *ubc22* mutant plants, the up-regulation of *MYC2* could be a possible reason for the *ubc22* mutant seeds to be more sensitive to an analog of ABA.

Currently, it is still unclear regarding how MYC2 is regulated in the ABA signaling pathway. In the ABA signaling pathway, ABA binds to the receptor proteins, the PYL (Pyrabactin Resistance (PYR) 1-like)/RCA (Regulatory Component of ABA receptor) proteins. ABA binding facilitates the binding of ABA receptor proteins to PP2Cs (type 2C Protein Phosphatases), inhibits the phosphatase activities of PP2Cs and subsequently increases the level of phosphorylated SnRK2 (SNF1-Related protein Kinase 2) (Hubbard et al., 2010). Then, phosphorylated SnRK2 activates ABA-responsive transcription factors, such as ABI5 (ABA-Insensitive 5), responsible for downstream gene expression. A recent study showed that PYL6, one of the ABA receptor proteins, interacted with MYC2 in a yeast two-hybrid assay and the interaction was enhanced when ABA was present (Aleman et al., 2016). However, the expression level of MYC2 was not demonstrated in the *pyl6* mutant. Regarding the *ubc22* mutant, it is unknown which component or step in ABA signaling pathway is affected. It is attempting to speculate that UBC22 may target MYC2 for degradation and MYC2 protein would accumulate in the *ubc22* mutant thus causing the hypersensitivity to ABA during seed germination.

The occurrence of four different subtypes of *ubc22* mutant plants and responses of the

ubc22 mutant to the pathogen and hormonal treatments strongly suggest that UBC22 plays important and multiple roles in plant vegetative development. As the sole member of the subfamily X and with the ability to catalyze Lys11-linked ubiquitination, its functions in different pathways or processes are understandable, since Lys11-linked Ub chain is found as the third most abundant chain type in Arabidopsis (Kim et al., 2013b; Maor et al., 2007). To understand how UBC22 may function in different pathways and processes, it is important to identify the interacting-E3s as well as the substrates.

6. CHAPTER SIX - CONCLUSIONS AND FUTURE DIRECTIONS

It has been estimated that about 5% of the Arabidopsis genome encodes various components of the Ub-proteasome system. There are about 37 genes encoding Ub-conjugating E2 enzymes. Functions for most of them remain largely unknown. Further, in protein ubiquitination, polyubiquitin chains can be linked through different Lys residues of Ub and have different functional properties. While Lys48-linked ubiquitination is well known in targeting substrate proteins for degradation by the 26S proteasome, there is a paucity of information regarding the functions of ubiquitination linked through others Lys residues of Ub in plants. This project was set to gain understanding on the E2s and related components involved in unconventional ubiquitination in plants using Arabidopsis as the model.

Previously, Arabidopsis UBC13A/B have been identified to be the E2s capable of catalyzing the Lys63-linked Ub chain assembly and play an important role in DNA damage repair. Arabidopsis *ubc13* double mutants display strong phenotypes in major aspects of root development. Results from the knockout mutant study and also another study suggest that UBC13 may function through auxin signaling pathway as well as auxin transport. Many questions regarding the UBC13-mediated pathway and functions of Lys63-linked ubiquitination in plants remain. In one aspect, it is important to identify other components in the UBC13-mediated pathway. Thus, one line of this work was to identify E3s that can interact with UBC13. Using the yeast two-hybrid approach, a group of six E3s referred to as UMIs were identified and they showed a clear interaction with UBC13A. The six UMIs can be grouped into two subgroups based on sequence similarity. Phenotype screening using a

series of treatments revealed that the triple T-DNA knockout mutant for one subgroup of genes (*UMI-D/E/F*) showed an increased sensitivity to glucose. However, none of the mutants from double to the hextuple mutant in which all six UMI genes were inactivated showed a clear phenotype in plant growth and development. The absence of a significant phenotype may be because there are other genes that share functional redundancy with the UMIs or they have functions in plant development or other processes that were discernible under the present conditions used for phenotype screening.

It has been proposed based on previous results that UBC13 affects auxin signaling pathway through stabilizing Aux/IAA proteins thus inhibiting the activities of ARFs. Based on this proposal, we reasoned that an *ARF* that could enhance auxin response should be able to rescue the root phenotypes of the *ubc13* mutant. Thus, several *ARFs* were selected for overexpression in WT plants and investigated for their effect on auxin response indicated by the auxin-responsive *DR5rev::GFP* marker. *ARF6* was found to be able to enhance auxin response and also root hair growth in WT plants. Further, an *ARF6* overexpressing line was crossed with the *ubc13* double mutant, and the progeny plants had more and longer root hairs as well as increased response to the synthetic auxin NAA, compared to the *ubc13* double mutant, indicating that the expression of *ARF6* can complement the hairless root phenotype of the *ubc13* double mutant. Further work is needed to confirm whether *ARF6* and other *ARFs* are involved in the UBC13 mediated-auxin signaling pathway. In studying *ARF* overexpression, our results also show that different *ARFs* may have different effects and clear understanding on the specific roles of the *ARFs* will be important.

The polyubiquitin chains in protein ubiquitination can be linked through different Lys residues of Ub. In Arabidopsis, the top three types of linkages in terms of abundance were found to be: Lys48-, Lys63- and Lys11-linked Ub chains. The functions of the conventional ubiquitination presumably through Lys48-linkage are well documented. Some initial understanding has been gained on the functions of Lys63-mediated ubiquitination and particular the E2 involved. There had been no documented report prior to this study on the E2 for Lys11-linked ubiquitination in plants. In this study, we identified Arabidopsis UBC22 to be the first plant E2 for Lys11-linked ubiquitination based on sequence similarity with similar E2s from yeast and humans, and more importantly, the results that UBC22 could catalyze the formation of Ub dimers in a Lys11-dependent matter.

UBC22 is the sole member of the subfamily X among the 37 E2s in Arabidopsis. This observation and its unique biochemical function in catalyzing Lys11-linked ubiquitination imply that UBC22 should have important and perhaps unique functions in plants. Indeed, we found that UBC22 is important for the differentiation of the FM during megasporogenesis. In most plants, the transition from vegetative to female reproductive development starts with the formation of a distinct MMC in each ovule. The MMC produces four megaspores through meiosis, and one of the four megaspores survives to become the FM. The FM then develops into an embryo sac required for fertilization and seed production. In the *ubc22* knockout mutant plants, while the mutant ovules were similar to WT ovules at MMC stage, the FM was not present or appeared abnormal in a large portion of mutant ovules, and nearly 90% ovules were aborted, suggesting a crucial role of UBC22 in FM formation and embryo sac

development. The analysis of callose deposition pattern during megasporogenesis indicates that some defects started in meiosis I in the mutant ovules. Inactivation of *UBC22* not only caused the degeneration of the FM but also affected the later stages of megagametogenesis since the percentage of mature embryo sacs without any gamete nuclei was much greater than the percentage of developing ovules without an FM.

The analysis of UBC22 expression based on microarray data and promoter-reporter approach revealed that it is expressed in different plants tissues, suggesting that it may have other functions in addition to its function in female gametophyte development. Interestingly, although the majority of *ubc22* knockout mutants were similar to the WT plants in terms of plant size and leaf morphology, careful examination revealed four different subtypes of mutant plants based on leaf size, shape, and color. The observations that four subtypes of plants occurred with similar percentages in all three independent mutant lines (two T-DNA and one CRISPR/Cas9 lines) and the mutant phenotypes largely disappeared when *UBC22* was re-introduced into the mutant, confirming that the occurrence of the four subtypes was due to inactivation of *UBC22*. The trancriptomic analysis by RNA-seq revealed distinct changes in gene expression in four subtypes of the mutant plants. For example, Type II mutant plants showed a specific and significant increase in the expression of plant defense genes, such as *PDF1.2*. It was further observed that Type II mutant plants had an increased resistance to a necrotrophic fungus *Botrytis cinerea*, indicating a possible role of UBC22 in plant-pathogen interactions. In addition, the *ubc22* mutant seedlings were more sensitive to the treatment with an analog of the hormone ABA. Collectively, these results show that

UBC22 has multiple functions in plants. It is conceivable that UBC22 along with certain E3s can target different substrates and regulate their levels and functions. The finding that *ubc22* mutants have four different subtypes is interesting and somewhat surprising. It is possible that in some mutant plants, changes in one pathway are more prominent or the balance among different pathways is affected differently so that they display distinct phenotypes compared to other mutant plants.

This study has made some interesting and novel findings related to UBC13 and on UBC22. However, many questions remain. Regarding the UBC13-mediated pathway, information on the cognate E3s and substrates is still very limited. Further insight will certainly be gained from the identification of more E3s that interact with UBC13 and functional studies of these E3s. In this regard, it may be worth to further analyze the UMI mutants to see whether a phenotype could be identified using different conditions. Regarding UBC13 and auxin signaling, it will be interesting to determine whether expression of other ARFs can also rescue the mutant phenotypes of the *ubc13* mutant and, if they do, which Aux/IAA proteins they interact with and what the downstream target genes are. Our results also identified UBC22 as the first plant E2 for the Lys11-linked ubiquitination, opening the door for future studies on the functions of this unique type of E2s and the Lys11-linked ubiquitination in plants. Other components in the UBC22-mediated pathway(s) remain to be discovered including the interacting E3s, major substrates, and regulation of UBC22. Further analyses of UBC22 along with the E3s and substrates will certainly lead to better and insightful understanding on the functions of Lys11-linked ubiquitination in plants.

REFERENCES

Abe, H., Urao, T., Ito, T., Seki, M., Shinozaki, K., and Yamaguchi-Shinozaki, K. (2003). Arabidopsis AtMYC2 (bHLH) and AtMYB2 (MYB) function as transcriptional activators in abscisic acid signaling. Plant Cell *15*, 63-78.

Adhikari, A., and Chen, Z.J. (2009). Diversity of polyubiquitin chains. Dev Cell *16*, 485-486.

Adio, A.M., Casteel, C.L., De Vos, M., Kim, J.H., Joshi, V., Li, B., Juery, C., Daron, J., Kliebenstein, D.J., and Jander, G. (2011). Biosynthesis and defensive function of Ndelta-acetylornithine, a jasmonate-induced Arabidopsis metabolite. Plant Cell *23*, 3303-3318.

Aleman, F., Yazaki, J., Lee, M., Takahashi, Y., Kim, A.Y., Li, Z., Kinoshita, T., Ecker, J.R., and Schroeder, J.I. (2016). An ABA-increased interaction of the PYL6 ABA receptor with MYC2 Transcription Factor: A putative link of ABA and JA signaling. Sci Rep *6*, 28941.

Anders, S., Pyl, P.T., and Huber, W. (2015). HTSeq--a Python framework to work with high-throughput sequencing data. Bioinformatics *31*, 166-169.

Andersen, P.L., Xu, F., and Xiao, W. (2008). Eukaryotic DNA damage tolerance and translesion synthesis through covalent modifications of PCNA. Cell Res *18*, 162-173.

Aung, K., Lin, S.I., Wu, C.C., Huang, Y.T., Su, C.L., and Chiou, T.J. (2006). pho2, a phosphate overaccumulator, is caused by a nonsense mutation in a MicroRNA399 target gene. Plant Physiology *141*, 1000-1011.

Baboshina, O.V., and Haas, A.L. (1996). Novel multiubiquitin chain linkages catalyzed by the conjugating enzymes E2EPF and RAD6 are recognized by 26 S proteasome subunit 5. J Biol Chem *271*, 2823-2831.

Babu, J.R., Geetha, T., and Wooten, M.W. (2005). Sequestosome 1/p62 shuttles polyubiquitinated tau for proteasomal degradation. J Neurochem *94*, 192-203.

Bachmair, A., Novatchkova, M., Potuschak, T., and Eisenhaber, F. (2001). Ubiquitylation in plants: a post-genomic look at a post-translational modification. Trends in Plant Science *6*, 463-470.

Bari, R., Datt Pant, B., Stitt, M., and Scheible, W.R. (2006). PHO2, microRNA399, and PHR1 define a phosphate-signaling pathway in plants. Plant Physiol *141*, 988-999.

Bates, P.W., and Vierstra, R.D. (1999). UPL1 and 2, two 405 kDa ubiquitin-protein ligases from Arabidopsis thaliana related to the HECT-domain protein family. Plant J *20*, 183-195.

Berrocal-Lobo, M., Molina, A., and Solano, R. (2002). Constitutive expression of ETHYLENE-RESPONSE-FACTOR1 in Arabidopsis confers resistance to several necrotrophic fungi. Plant J *29*, 23-32.

Bolger, A.M., Lohse, M., and Usadel, B. (2014). Trimmomatic: a flexible trimmer for Illumina sequence data. Bioinformatics *30*, 2114-2120.

Bradford, M. (1976). A Rapid and Sensitive Method for the Quantitation of Microgram Quantities of Protein Utilizing the Principle of Protein-Dye Binding. Anal Biochem, 248-254.

Brown, N.G., VanderLinden, R., Watson, E.R., Weissmann, F., Ordureau, A., Wu, K.P., Zhang, W., Yu, S., Mercredi, P.Y., Harrison, J.S., *et al.* (2016). Dual RING E3 Architectures Regulate Multiubiquitination and Ubiquitin Chain Elongation by APC/C. Cell *165*, 1440-1453.

Brown, N.G., Watson, E.R., Weissmann, F., Jarvis, M.A., VanderLinden, R., Grace, C.R., Frye, J.J., Qiao, R., Dube, P., Petzold, G., *et al.* (2014). Mechanism of polyubiquitination by human anaphase-promoting complex: RING repurposing for ubiquitin chain assembly. Mol Cell *56*, 246-260.

Burroughs, A.M., Jaffee, M., Iyer, L.M., and Aravind, L. (2008). Anatomy of the E2 ligase fold: implications for enzymology and evolution of ubiquitin/Ub-like protein conjugation. J Struct Biol *162*, 205-218.

Callis, J. (2014). The ubiquitination machinery of the ubiquitin system. Arabidopsis Book *12*, e0174.

Callis, J., Carpenter, T., Sun, C.W., and Vierstra, R.D. (1995). Structure and evolution of genes encoding polyubiquitin and ubiquitin-like proteins in Arabidopsis thaliana ecotype Columbia. Genetics *139*, 921-939.

Callis, J., Raasch, J.A., and Vierstra, R.D. (1990). Ubiquitin extension proteins of Arabidopsis thaliana. Structure, localization, and expression of their promoters in transgenic tobacco. J Biol Chem *265*, 12486-12493.

Cao, Y., Dai, Y., Cui, S., and Ma, L. (2008). Histone H2B monoubiquitination in the chromatin of FLOWERING LOCUS C regulates flowering time in Arabidopsis. Plant Cell *20*, 2586-2602.

Capron, A., Serralbo, O., Fulop, K., Frugier, F., Parmentier, Y., Dong, A., Lecureuil, A., Guerche, P., Kondorosi, E., Scheres, B., *et al.* (2003). The Arabidopsis anaphase-promoting complex or cyclosome: molecular and genetic characterization of the APC2 subunit. Plant Cell *15*, 2370-2382.

Chau, V., Tobias, J.W., Bachmair, A., Marriott, D., Ecker, D.J., Gonda, D.K., and Varshavsky, A. (1989). A multiubiquitin chain is confined to specific lysine in a targeted short-lived protein. Science *243*, 1576-1583.

Chen, Q., Liu, R., Wang, Q., and Xie, Q. (2017). ERAD Tuning of the HRD1 Complex Component AtOS9 Is Modulated by an ER-Bound E2, UBC32. Mol Plant *10*, 891-894.

Chen, Z., Hagler, J., Palombella, V.J., Melandri, F., Scherer, D., Ballard, D., and Maniatis, T. (1995). Signal-induced site-specific phosphorylation targets I kappa B alpha to the ubiquitin-proteasome pathway. Genes Dev *9*, 1586-1597.

Chen, Z.J., and Sun, L.J. (2009). Nonproteolytic functions of ubiquitin in cell signaling. Mol

Cell *33*, 275-286.

Cheng, M.C., Hsieh, E.J., Chen, J.H., Chen, H.Y., and Lin, T.P. (2012). Arabidopsis RGLG2, functioning as a RING E3 ligase, interacts with AtERF53 and negatively regulates the plant drought stress response. Plant Physiol *158*, 363-375.

Cheng, M.C., Kuo, W.C., Wang, Y.M., Chen, H.Y., and Lin, T.P. (2017). UBC18 mediates ERF1 degradation under light-dark cycles. New Phytol *213*, 1156-1167.

Choi, C.M., Gray, W.M., Mooney, S., and Hellmann, H. (2014). Composition, roles, and regulation of cullin-based ubiquitin e3 ligases. Arabidopsis Book *12*, e0175.

Christensen, C.A., King, E.J., Jordan, J.R., and Drews, G.N. (1997). Megagametogenesis in Arabidopsis wild type and the Gf mutant. Sexual Plant Reproduction *10*, 49-64.

Citterio, S., Albertini, E., Varotto, S., Feltrin, E., Soattin, M., Marconi, G., Sgorbati, S., Lucchin, M., and Barcaccia, G. (2005). Alfalfa Mob1-like genes are expressed in reproductive organs during meiosis and gametogenesis. Plant Molecular Biology *58*, 789-807.

Clauss, M.J., and Mitchell-Olds, T. (2004). Functional divergence in tandemly duplicated Arabidopsis thaliana trypsin inhibitor genes. Genetics *166*, 1419-1436.

Clay, N.K., Adio, A.M., Denoux, C., Jander, G., and Ausubel, F.M. (2009). Glucosinolate metabolites required for an Arabidopsis innate immune response. Science *323*, 95-101.

Criqui, M.C., de Almeida Engler, J., Camasses, A., Capron, A., Parmentier, Y., Inze, D., and Genschik, P. (2002). Molecular characterization of plant ubiquitin-conjugating enzymes belonging to the UbcP4/E2-C/UBCx/UbcH10 gene family. Plant Physiol *130*, 1230-1240.

Cui, F., Liu, L., Zhao, Q., Zhang, Z., Li, Q., Lin, B., Wu, Y., Tang, S., and Xie, Q. (2012). Arabidopsis ubiquitin conjugase UBC32 is an ERAD component that functions in brassinosteroid-mediated salt stress tolerance. Plant Cell *24*, 233-244.

Cutler, A.J., Rose, P.A., Squires, T.M., Loewen, M.K., Shaw, A.C., Quail, J.W., Krochko, J.E., and Abrams, S.R. (2000). Inhibitors of abscisic acid 8'-hydroxylase. Biochemistry *39*, 13614-13624.

Cyr, D.M., Hohfeld, J., and Patterson, C. (2002). Protein quality control: U-box-containing E3 ubiquitin ligases join the fold. Trends Biochem Sci *27*, 368-375.

Dammer, E.B., Na, C.H., Xu, P., Seyfried, N.T., Duong, D.M., Cheng, D., Gearing, M., Rees, H., Lah, J.J., Levey, A.I., *et al.* (2011). Polyubiquitin linkage profiles in three models of proteolytic stress suggest the etiology of Alzheimer disease. J Biol Chem *286*, 10457-10465.

Demianski, A.J., Chung, K.M., and Kunkel, B.N. (2012). Analysis of Arabidopsis JAZ gene expression during Pseudomonas syringae pathogenesis. Mol Plant Pathol *13*, 46-57.

Deshaies, R.J., and Joazeiro, C.A. (2009). RING domain E3 ubiquitin ligases. Annu Rev Biochem *78*, 399-434.

Desveaux, D., Marechal, A., and Brisson, N. (2005). Whirly transcription factors: defense gene regulation and beyond. Trends Plant Sci *10*, 95-102.

Dikic, I., Wakatsuki, S., and Walters, K.J. (2009). Ubiquitin-binding domains - from structures to functions. Nat Rev Mol Cell Biol *10*, 659-671.

Dobin, A., Davis, C.A., Schlesinger, F., Drenkow, J., Zaleski, C., Jha, S., Batut, P., Chaisson, M., and Gingeras, T.R. (2013). STAR: ultrafast universal RNA-seq aligner. Bioinformatics *29*, 15-21.

Dong, X. (2004). NPR1, all things considered. Curr Opin Plant Biol *7*, 547-552.

Downes, B.P., Stupar, R.M., Gingerich, D.J., and Vierstra, R.D. (2003). The HECT ubiquitin-protein ligase (UPL) family in Arabidopsis: UPL3 has a specific role in trichome development. Plant J *35*, 729-742.

Eddins, M.J., Carlile, C.M., Gomez, K.M., Pickart, C.M., and Wolberger, C. (2006). Mms2-Ubc13 covalently bound to ubiquitin reveals the structural basis of linkage-specific polyubiquitin chain formation. Nat Struct Mol Biol *13*, 915-920.

Edwards, K., Johnstone, C., and Thompson, C. (1991). A simple and rapid method for the preparation of plant genomic DNA for PCR analysis. Nucleic Acids Res *19*, 1349.

El Refy, A., Perazza, D., Zekraoui, L., Valay, J.G., Bechtold, N., Brown, S., Hulskamp, M., Herzog, M., and Bonneville, J.M. (2003). The Arabidopsis KAKTUS gene encodes a HECT protein and controls the number of endoreduplication cycles. Mol Genet Genomics *270*, 403-414.

Eloy, N.B., de Freitas Lima, M., Van Damme, D., Vanhaeren, H., Gonzalez, N., De Milde, L., Hemerly, A.S., Beemster, G.T., Inze, D., and Ferreira, P.C. (2011). The APC/C subunit 10 plays an essential role in cell proliferation during leaf development. Plant J *68*, 351-363.

Finley, D., Bartel, B., and Varshavsky, A. (1989). The tails of ubiquitin precursors are ribosomal proteins whose fusion to ubiquitin facilitates ribosome biogenesis. Nature *338*, 394-401.

Finley, D., Sadis, S., Monia, B.P., Boucher, P., Ecker, D.J., Crooke, S.T., and Chau, V. (1994). Inhibition of proteolysis and cell cycle progression in a multiubiquitination-deficient yeast mutant. Mol Cell Biol *14*, 5501-5509.

Finley, D., Ulrich, H.D., Sommer, T., and Kaiser, P. (2012). The ubiquitin-proteasome system of Saccharomyces cerevisiae. Genetics *192*, 319-360.

Flick, K., Raasi, S., Zhang, H., Yen, J.L., and Kaiser, P. (2006). A ubiquitin-interacting motif protects polyubiquitinated Met4 from degradation by the 26S proteasome. Nat Cell Biol *8*, 509-515.

Freemont, P.S. (1993). The RING finger. A novel protein sequence motif related to the zinc finger. Ann N Y Acad Sci *684*, 174-192.

Fukaki, H., Tameda, S., Masuda, H., and Tasaka, M. (2002). Lateral root formation is blocked by a gain-of-function mutation in the SOLITARY-ROOT/IAA14 gene of Arabidopsis. Plant J *29*, 153-168.

Galan, J.M., and Haguenauer-Tsapis, R. (1997). Ubiquitin lys63 is involved in ubiquitination of a yeast plasma membrane protein. EMBO J *16*, 5847-5854.

Garnett, M.J., Mansfeld, J., Godwin, C., Matsusaka, T., Wu, J., Russell, P., Pines, J., and Venkitaraman, A.R. (2009). UBE2S elongates ubiquitin chains on APC/C substrates to promote mitotic exit. Nat Cell Biol *11*, 1363-1369.

Ghaboosi, N., and Deshaies, R.J. (2007). A conditional yeast E1 mutant blocks the ubiquitin-proteasome pathway and reveals a role for ubiquitin conjugates in targeting Rad23 to the proteasome. Mol Biol Cell *18*, 1953-1963.

Glazebrook, J. (2001). Genes controlling expression of defense responses in Arabidopsis--2001 status. Curr Opin Plant Biol *4*, 301-308.

Goritschnig, S., Zhang, Y., and Li, X. (2007). The ubiquitin pathway is required for innate immunity in Arabidopsis. Plant J *49*, 540-551.

Gray, W.M., Hellmann, H., Dharmasiri, S., and Estelle, M. (2002). Role of the Arabidopsis RING-H2 protein RBX1 in RUB modification and SCF function. Plant Cell *14*, 2137-2144.

Gray, W.M., Kepinski, S., Rouse, D., Leyser, O., and Estelle, M. (2001). Auxin regulates SCF(TIR1)-dependent degradation of AUX/IAA proteins. Nature *414*, 271-276.

Griebel, T., and Zeier, J. (2010). A role for beta-sitosterol to stigmasterol conversion in plant-pathogen interactions. Plant J *63*, 254-268.

Groen, E.J.N., and Gillingwater, T.H. (2015). UBA1: At the Crossroads of Ubiquitin Homeostasis and Neurodegeneration. Trends Mol Med *21*, 622-632.

Gu, X., Jiang, D., Wang, Y., Bachmair, A., and He, Y. (2009). Repression of the floral transition via histone H2B monoubiquitination. Plant J *57*, 522-533.

Guilfoyle, T.J., and Hagen, G. (2007). Auxin response factors. Curr Opin Plant Biol *10*, 453-460.

Gutensohn, M., Klempien, A., Kaminaga, Y., Nagegowda, D.A., Negre-Zakharov, F., Huh, J.H., Luo, H., Weizbauer, R., Mengiste, T., Tholl, D., *et al.* (2011). Role of aromatic aldehyde synthase in wounding/herbivory response and flower scent production in different Arabidopsis ecotypes. Plant J *66*, 591-602.

Hamann, T., Benkova, E., Baurle, I., Kientz, M., and Jurgens, G. (2002). The Arabidopsis BODENLOS gene encodes an auxin response protein inhibiting MONOPTEROS-mediated embryo patterning. Genes Dev *16*, 1610-1615.

Hanano, A., Bessoule, J.J., Heitz, T., and Blee, E. (2015). Involvement of the

caleosin/peroxygenase RD20 in the control of cell death during Arabidopsis responses to pathogens. Plant Signal Behav *10*, e991574.

Hardtke, C.S., and Berleth, T. (1998). The Arabidopsis gene MONOPTEROS encodes a transcription factor mediating embryo axis formation and vascular development. EMBO J *17*, 1405-1411.

Hatakeyama, S., and Nakayama, K.I. (2003). U-box proteins as a new family of ubiquitin ligases. Biochem Biophys Res Commun *302*, 635-645.

Hatfield, P.M., Gosink, M.M., Carpenter, T.B., and Vierstra, R.D. (1997). The ubiquitin-activating enzyme (E1) gene family in Arabidopsis thaliana. Plant J *11*, 213-226.

Hay, R.T. (2005). SUMO: a history of modification. Mol Cell *18*, 1-12.

Heyman, J., and De Veylder, L. (2012). The anaphase-promoting complex/cyclosome in control of plant development. Mol Plant *5*, 1182-1194.

Hibbert, R.G., Huang, A., Boelens, R., and Sixma, T.K. (2011). E3 ligase Rad18 promotes monoubiquitination rather than ubiquitin chain formation by E2 enzyme Rad6. Proc Natl Acad Sci U S A *108*, 5590-5595.

Hicke, L., and Dunn, R. (2003). Regulation of membrane protein transport by ubiquitin and ubiquitin-binding proteins. Annu Rev Cell Dev Biol *19*, 141-172.

Hill, J., Donald, K.A., and Griffiths, D.E. (1991). DMSO-enhanced whole cell yeast transformation. Nucleic Acids Res *19*, 5791.

Hoege, C., Pfander, B., Moldovan, G.L., Pyrowolakis, G., and Jentsch, S. (2002). RAD6-dependent DNA repair is linked to modification of PCNA by ubiquitin and SUMO. Nature *419*, 135-141.

Hofmann, R.M., and Pickart, C.M. (1999). Noncanonical MMS2-encoded ubiquitin-conjugating enzyme functions in assembly of novel polyubiquitin chains for DNA repair. Cell *96*, 645-653.

Hotton, S.K., and Callis, J. (2008). Regulation of cullin RING ligases. Annu Rev Plant Biol *59*, 467-489.

Hruz, T., Laule, O., Szabo, G., Wessendorp, F., Bleuler, S., Oertle, L., Widmayer, P., Gruissem, W., and Zimmermann, P. (2008). Genevestigator v3: a reference expression database for the meta-analysis of transcriptomes. Adv Bioinformatics *2008*, 420747.

Hu, J., Baker, A., Bartel, B., Linka, N., Mullen, R.T., Reumann, S., and Zolman, B.K. (2012). Plant peroxisomes: biogenesis and function. Plant Cell *24*, 2279-2303.

Hua, Z., and Vierstra, R.D. (2011). The cullin-RING ubiquitin-protein ligases. Annu Rev Plant Biol *62*, 299-334.

Huang, D.T., Hunt, H.W., Zhuang, M., Ohi, M.D., Holton, J.M., and Schulman, B.A. (2007a).

Basis for a ubiquitin-like protein thioester switch toggling E1-E2 affinity. Nature *445*, 394-398.

Huang, F., Goh, L.K., and Sorkin, A. (2007b). EGF receptor ubiquitination is not necessary for its internalization. Proc Natl Acad Sci U S A *104*, 16904-16909.

Huang, L., Kinnucan, E., Wang, G., Beaudenon, S., Howley, P.M., Huibregtse, J.M., and Pavletich, N.P. (1999). Structure of an E6AP-UbcH7 complex: insights into ubiquitination by the E2-E3 enzyme cascade. Science *286*, 1321-1326.

Hubbard, K.E., Nishimura, N., Hitomi, K., Getzoff, E.D., and Schroeder, J.I. (2010). Early abscisic acid signal transduction mechanisms: newly discovered components and newly emerging questions. Genes Dev *24*, 1695-1708.

Husnjak, K., and Dikic, I. (2012). Ubiquitin-binding proteins: decoders of ubiquitin-mediated cellular functions. Annu Rev Biochem *81*, 291-322.

Ishida, T., Kurata, T., Okada, K., and Wada, T. (2008). A genetic regulatory network in the development of trichomes and root hairs. Annu Rev Plant Biol *59*, 365-386.

Iwai, K., and Tanaka, K. (2014). Ubiquitin chain elongation: an intriguing strategy. Mol Cell *56*, 189-191.

James, P., Halladay, J., and Craig, E.A. (1996). Genomic libraries and a host strain designed for highly efficient two-hybrid selection in yeast. Genetics *144*, 1425-1436.

Jefferson, R.A. (1987). Assaying chimeric genes in plants: the GU S gene fusion system. Plant Molecular Biology Reporter *5*, 387-405.

Jin, J., Li, X., Gygi, S.P., and Harper, J.W. (2007). Dual E1 activation systems for ubiquitin differentially regulate E2 enzyme charging. Nature *447*, 1135-1138.

Jin, L., Williamson, A., Banerjee, S., Philipp, I., and Rape, M. (2008). Mechanism of ubiquitin-chain formation by the human anaphase-promoting complex. Cell *133*, 653-665.

Jung, C., Zhao, P., Seo, J.S., Mitsuda, N., Deng, S., and Chua, N.H. (2015). PLANT U-BOX PROTEIN10 Regulates MYC2 Stability in Arabidopsis. Plant Cell *27*, 2016-2031.

Kaiser, P., Flick, K., Wittenberg, C., and Reed, S.I. (2000). Regulation of transcription by ubiquitination without proteolysis: Cdc34/SCF(Met30)-mediated inactivation of the transcription factor Met4. Cell *102*, 303-314.

Kao, C.F., Hillyer, C., Tsukuda, T., Henry, K., Berger, S., and Osley, M.A. (2004). Rad6 plays a role in transcriptional activation through ubiquitylation of histone H2B. Genes Dev *18*, 184-195.

Kelley, D.R., and Estelle, M. (2012). Ubiquitin-mediated control of plant hormone signaling. Plant Physiol *160*, 47-55.

Kim, B., Fujioka, S., Kwon, M., Jeon, J., and Choe, S. (2013a). Arabidopsis brassinosteroid-

overproducing gulliver3-D/dwarf4-D mutants exhibit altered responses to jasmonic acid and pathogen. Plant Cell Rep *32*, 1139-1149.

Kim, D.Y., Scalf, M., Smith, L.M., and Vierstra, R.D. (2013b). Advanced proteomic analyses yield a deep catalog of ubiquitylation targets in Arabidopsis. Plant Cell *25*, 1523-1540.

Kim, W., Bennett, E.J., Huttlin, E.L., Guo, A., Li, J., Possemato, A., Sowa, M.E., Rad, R., Rush, J., Comb, M.J., *et al.* (2011). Systematic and quantitative assessment of the ubiquitin-modified proteome. Mol Cell *44*, 325-340.

Kinkema, M., Fan, W., and Dong, X. (2000). Nuclear localization of NPR1 is required for activation of PR gene expression. Plant Cell *12*, 2339-2350.

Knox, K., Grierson, C.S., and Leyser, O. (2003). AXR3 and SHY2 interact to regulate root hair development. Development *130*, 5769-5777.

Komander, D., and Rape, M. (2012). The ubiquitin code. Annu Rev Biochem *81*, 203-229.

Kraft, E., Stone, S.L., Ma, L., Su, N., Gao, Y., Lau, O.S., Deng, X.W., and Callis, J. (2005). Genome analysis and functional characterization of the E2 and RING-type E3 ligase ubiquitination enzymes of Arabidopsis. Plant Physiol *139*, 1597-1611.

Krogan, N.T., Ckurshumova, W., Marcos, D., Caragea, A.E., and Berleth, T. (2012). Deletion of MP/ARF5 domains III and IV reveals a requirement for Aux/IAA regulation in Arabidopsis leaf vascular patterning. New Phytol *194*, 391-401.

Kulathu, Y., and Komander, D. (2012). Atypical ubiquitylation - the unexplored world of polyubiquitin beyond Lys48 and Lys63 linkages. Nat Rev Mol Cell Biol *13*, 508-523.

Kwee, H.S., and Sundaresan, V. (2003). The NOMEGA gene required for female gametophyte development encodes the putative APC6/CDC16 component of the Anaphase Promoting Complex in Arabidopsis. Plant J *36*, 853-866.

Lechner, E., Xie, D., Grava, S., Pigaglio, E., Planchais, S., Murray, J.A., Parmentier, Y., Mutterer, J., Dubreucq, B., Shen, W.H., *et al.* (2002). The AtRbx1 protein is part of plant SCF complexes, and its down-regulation causes severe growth and developmental defects. J Biol Chem *277*, 50069-50080.

Lee, I., and Schindelin, H. (2008). Structural insights into E1-catalyzed ubiquitin activation and transfer to conjugating enzymes. Cell *134*, 268-278.

Lee, P.C., Dodart, J.C., Aron, L., Finley, L.W., Bronson, R.T., Haigis, M.C., Yankner, B.A., and Harper, J.W. (2013). Altered social behavior and neuronal development in mice lacking the Uba6-Use1 ubiquitin transfer system. Mol Cell *50*, 172-184.

Leitner, J., Petrasek, J., Tomanov, K., Retzer, K., Parezova, M., Korbei, B., Bachmair, A., Zazimalova, E., and Luschnig, C. (2012). Lysine63-linked ubiquitylation of PIN2 auxin carrier protein governs hormonally controlled adaptation of Arabidopsis root growth. Proc Natl Acad Sci U S A *109*, 8322-8327.

Li, L., Zhang, C., Xu, D., Schlappi, M., and Xu, Z.Q. (2012). Expression of recombinant EARLI1, a hybrid proline-rich protein of Arabidopsis, in Escherichia coli and its inhibition effect to the growth of fungal pathogens and Saccharomyces cerevisiae. Gene *506*, 50-61.

Li, Q., Shi, X., Ye, S., Wang, S., Chan, R., Harkness, T., and Wang, H. (2016a). A short motif in Arabidopsis CDK inhibitor ICK1 decreases the protein level, probably through a ubiquitin-independent mechanism. Plant J *87*, 617-628.

Li, W., Bengtson, M.H., Ulbrich, A., Matsuda, A., Reddy, V.A., Orth, A., Chanda, S.K., Batalov, S., and Joazeiro, C.A. (2008). Genome-wide and functional annotation of human E3 ubiquitin ligases identifies MULAN, a mitochondrial E3 that regulates the organelle's dynamics and signaling. PLoS One *3*, e1487.

Li, W., and Schmidt, W. (2010). A lysine-63-linked ubiquitin chain-forming conjugase, UBC13, promotes the developmental responses to iron deficiency in Arabidopsis roots. Plant J *62*, 330-343.

Li, X., Clarke, J.D., Zhang, Y., and Dong, X. (2001). Activation of an EDS1-mediated R-gene pathway in the snc1 mutant leads to constitutive, NPR1-independent pathogen resistance. Mol Plant Microbe Interact *14*, 1131-1139.

Li, Y., Kabbage, M., Liu, W., and Dickman, M.B. (2016b). Aspartyl Protease-Mediated Cleavage of BAG6 Is Necessary for Autophagy and Fungal Resistance in Plants. Plant Cell *28*, 233-247.

Lin, W.Y., Huang, T.K., and Chiou, T.J. (2013). Nitrogen limitation adaptation, a target of microRNA827, mediates degradation of plasma membrane-localized phosphate transporters to maintain phosphate homeostasis in Arabidopsis. Plant Cell *25*, 4061-4074.

Ling, R., Colon, E., Dahmus, M.E., and Callis, J. (2000). Histidine-tagged ubiquitin substitutes for wild-type ubiquitin in Saccharomyces cerevisiae and facilitates isolation and identification of in vivo substrates of the ubiquitin pathway. Anal Biochem *282*, 54-64.

Liu, J., Zhang, Y., Qin, G., Tsuge, T., Sakaguchi, N., Luo, G., Sun, K., Shi, D., Aki, S., Zheng, N., *et al.* (2008). Targeted degradation of the cyclin-dependent kinase inhibitor ICK4/KRP6 by RING-type E3 ligases is essential for mitotic cell cycle progression during Arabidopsis gametogenesis. Plant Cell *20*, 1538-1554.

Lorenzo, O., Chico, J.M., Sanchez-Serrano, J.J., and Solano, R. (2004). JASMONATE-INSENSITIVE1 encodes a MYC transcription factor essential to discriminate between different jasmonate-regulated defense responses in Arabidopsis. Plant Cell *16*, 1938-1950.

Love, M.I., Huber, W., and Anders, S. (2014). Moderated estimation of fold change and dispersion for RNA-seq data with DESeq2. Genome Biol *15*, 550.

Ma, X., Zhang, Q., Zhu, Q., Liu, W., Chen, Y., Qiu, R., Wang, B., Yang, Z., Li, H., Lin, Y., *et al.* (2015). A Robust CRISPR/Cas9 System for Convenient, High-Efficiency Multiplex Genome Editing in Monocot and Dicot Plants. Mol Plant *8*, 1274-1284.

Maleck, K., Levine, A., Eulgem, T., Morgan, A., Schmid, J., Lawton, K.A., Dangl, J.L., and Dietrich, R.A. (2000). The transcriptome of Arabidopsis thaliana during systemic acquired resistance. Nat Genet *26*, 403-410.

Mandelkow, E.M., and Mandelkow, E. (2012). Biochemistry and cell biology of tau protein in neurofibrillary degeneration. Cold Spring Harb Perspect Med *2*, a006247.

Maor, R., Jones, A., Nuhse, T.S., Studholme, D.J., Peck, S.C., and Shirasu, K. (2007). Multidimensional protein identification technology (MudPIT) analysis of ubiquitinated proteins in plants. Mol Cell Proteomics *6*, 601-610.

Martins, S., Dohmann, E.M., Cayrel, A., Johnson, A., Fischer, W., Pojer, F., Satiat-Jeunemaitre, B., Jaillais, Y., Chory, J., Geldner, N., *et al.* (2015). Internalization and vacuolar targeting of the brassinosteroid hormone receptor BRI1 are regulated by ubiquitination. Nat Commun *6*, 6151.

Matsumoto, M.L., Wickliffe, K.E., Dong, K.C., Yu, C., Bosanac, I., Bustos, D., Phu, L., Kirkpatrick, D.S., Hymowitz, S.G., Rape, M., *et al.* (2010). K11-linked polyubiquitination in cell cycle control revealed by a K11 linkage-specific antibody. Mol Cell *39*, 477-484.

Mazzucotelli, E., Belloni, S., Marone, D., De Leonardis, A., Guerra, D., Di Fonzo, N., Cattivelli, L., and Mastrangelo, A. (2006). The e3 ubiquitin ligase gene family in plants: regulation by degradation. Curr Genomics *7*, 509-522.

Meierhofer, D., Wang, X., Huang, L., and Kaiser, P. (2008). Quantitative analysis of global ubiquitination in HeLa cells by mass spectrometry. J Proteome Res *7*, 4566-4576.

Miao, Y., and Zentgraf, U. (2010). A HECT E3 ubiquitin ligase negatively regulates Arabidopsis leaf senescence through degradation of the transcription factor WRKY53. Plant J *63*, 179-188.

Mockaitis, K., and Estelle, M. (2008). Auxin receptors and plant development: a new signaling paradigm. Annu Rev Cell Dev Biol *24*, 55-80.

Moore, B., Zhou, L., Rolland, F., Hall, Q., Cheng, W.H., Liu, Y.X., Hwang, I., Jones, T., and Sheen, J. (2003). Role of the Arabidopsis glucose sensor HXK1 in nutrient, light, and hormonal signaling. Science *300*, 332-336.

Naur, P., Petersen, B.L., Mikkelsen, M.D., Bak, S., Rasmussen, H., Olsen, C.E., and Halkier, B.A. (2003). CYP83A1 and CYP83B1, two nonredundant cytochrome P450 enzymes metabolizing oximes in the biosynthesis of glucosinolates in Arabidopsis. Plant Physiol *133*, 63-72.

Ohtake, F., Tsuchiya, H., Saeki, Y., and Tanaka, K. (2018). K63 ubiquitylation triggers proteasomal degradation by seeding branched ubiquitin chains. Proc Natl Acad Sci U S A *115*, E1401-E1408.

Okushima, Y., Fukaki, H., Onoda, M., Theologis, A., and Tasaka, M. (2007). ARF7 and

ARF19 regulate lateral root formation via direct activation of LBD/ASL genes in Arabidopsis. Plant Cell *19*, 118-130.

Park, B.S., Seo, J.S., and Chua, N.H. (2014). NITROGEN LIMITATION ADAPTATION Recruits PHOSPHATE2 to Target the Phosphate Transporter PT2 for Degradation during the Regulation of Arabidopsis Phosphate Homeostasis. Plant Cell *26*, 454-464.

Paul, A., and Wang, B. (2017). RNF8- and Ube2S-Dependent Ubiquitin Lysine 11-Linkage Modification in Response to DNA Damage. Mol Cell *66*, 458-472 e455.

Pertea, M., Pertea, G.M., Antonescu, C.M., Chang, T.C., Mendell, J.T., and Salzberg, S.L. (2015). StringTie enables improved reconstruction of a transcriptome from RNA-seq reads. Nat Biotechnol *33*, 290-295.

Petroski, M.D., and Deshaies, R.J. (2005). Function and regulation of cullin-RING ubiquitin ligases. Nat Rev Mol Cell Biol *6*, 9-20.

Pickart, C.M. (2001). Mechanisms underlying ubiquitination. Annu Rev Biochem *70*, 503-533.

Pickart, C.M., and Eddins, M.J. (2004). Ubiquitin: structures, functions, mechanisms. Biochim Biophys Acta *1695*, 55-72.

Pieterse, C.M., Leon-Reyes, A., Van der Ent, S., and Van Wees, S.C. (2009). Networking by small-molecule hormones in plant immunity. Nat Chem Biol *5*, 308-316.

Pieterse, C.M., Van der Does, D., Zamioudis, C., Leon-Reyes, A., and Van Wees, S.C. (2012). Hormonal modulation of plant immunity. Annu Rev Cell Dev Biol *28*, 489-521.

Platta, H.W., Girzalsky, W., and Erdmann, R. (2004). Ubiquitination of the peroxisomal import receptor Pex5p. Biochem J *384*, 37-45.

Pre, M., Atallah, M., Champion, A., De Vos, M., Pieterse, C.M., and Memelink, J. (2008). The AP2/ERF domain transcription factor ORA59 integrates jasmonic acid and ethylene signals in plant defense. Plant Physiol *147*, 1347-1357.

Primorac, I., and Musacchio, A. (2013). Panta rhei: The APC/C at steady state. Journal of Cell Biology *201*, 177-189.

Qin, F., Sakuma, Y., Tran, L.S., Maruyama, K., Kidokoro, S., Fujita, Y., Fujita, M., Umezawa, T., Sawano, Y., Miyazono, K., *et al.* (2008). Arabidopsis DREB2A-interacting proteins function as RING E3 ligases and negatively regulate plant drought stress-responsive gene expression. Plant Cell *20*, 1693-1707.

Rabut, G., and Peter, M. (2008). Function and regulation of protein neddylation. 'Protein modifications: beyond the usual suspects' review series. EMBO Rep *9*, 969-976.

Rajniak, J., Barco, B., Clay, N.K., and Sattely, E.S. (2015). A new cyanogenic metabolite in Arabidopsis required for inducible pathogen defence. Nature *525*, 376-379.

Rodkiewicz, B. (1970). Callose in cell walls during megasporogenesis in angiosperms. Planta *93*, 39-47.

Rolland, F., Baena-Gonzalez, E., and Sheen, J. (2006). Sugar sensing and signaling in plants: conserved and novel mechanisms. Annu Rev Plant Biol *57*, 675-709.

Rotin, D., and Kumar, S. (2009). Physiological functions of the HECT family of ubiquitin ligases. Nat Rev Mol Cell Biol *10*, 398-409.

Sakuma, Y., Maruyama, K., Osakabe, Y., Qin, F., Seki, M., Shinozaki, K., and Yamaguchi-Shinozaki, K. (2006). Functional analysis of an Arabidopsis transcription factor, DREB2A, involved in drought-responsive gene expression. Plant Cell *18*, 1292-1309.

Sambrook, and Russell (2001). Molecular Cloning: A Laboratory Manual, 3rd ed.

Scala, A., Mirabella, R., Mugo, C., Matsui, K., Haring, M.A., and Schuurink, R.C. (2013). E-2-hexenal promotes susceptibility to Pseudomonas syringae by activating jasmonic acid pathways in Arabidopsis. Front Plant Sci *4*, 74.

Scheffner, M., and Kumar, S. (2014). Mammalian HECT ubiquitin-protein ligases: biological and pathophysiological aspects. Biochim Biophys Acta *1843*, 61-74.

Schneitz, K., Hulskamp, M., and Pruitt, R. (1995). Wild-type ovule development in Arabidopsis thaliana: a light microscope study of cleared whole-mount tissue. The Plant Journal *7*, 731-749.

Schulman, B.A., and Harper, J.W. (2009). Ubiquitin-like protein activation by E1 enzymes: the apex for downstream signalling pathways. Nat Rev Mol Cell Biol *10*, 319-331.

Sheard, L.B., Tan, X., Mao, H., Withers, J., Ben-Nissan, G., Hinds, T.R., Kobayashi, Y., Hsu, F.F., Sharon, M., Browse, J., *et al.* (2010). Jasmonate perception by inositol-phosphate-potentiated COI1-JAZ co-receptor. Nature *468*, 400-405.

Shen, G., Adam, Z., and Zhang, H. (2007a). The E3 ligase AtCHIP ubiquitylates FtsH1, a component of the chloroplast FtsH protease, and affects protein degradation in chloroplasts. Plant J *52*, 309-321.

Shen, G., Yan, J., Pasapula, V., Luo, J., He, C., Clarke, A.K., and Zhang, H. (2007b). The chloroplast protease subunit ClpP4 is a substrate of the E3 ligase AtCHIP and plays an important role in chloroplast function. Plant J *49*, 228-237.

Sivakumar, S., and Gorbsky, G.J. (2015). Spatiotemporal regulation of the anaphase-promoting complex in mitosis. Nat Rev Mol Cell Biol *16*, 82-94.

Sloper-Mould, K.E., Jemc, J.C., Pickart, C.M., and Hicke, L. (2001). Distinct functional surface regions on ubiquitin. J Biol Chem *276*, 30483-30489.

Spence, J., Gali, R.R., Dittmar, G., Sherman, F., Karin, M., and Finley, D. (2000). Cell cycle-regulated modification of the ribosome by a variant multiubiquitin chain. Cell *102*, 67-76.

Spence, J., Sadis, S., Haas, A.L., and Finley, D. (1995). A ubiquitin mutant with specific defects in DNA repair and multiubiquitination. Mol Cell Biol *15*, 1265-1273.

Spratt, D.E., Walden, H., and Shaw, G.S. (2014). RBR E3 ubiquitin ligases: new structures, new insights, new questions. Biochem J *458*, 421-437.

Stone, S.L. (2014). The role of ubiquitin and the 26S proteasome in plant abiotic stress signaling. Front Plant Sci *5*, 135.

Stone, S.L., Hauksdottir, H., Troy, A., Herschleb, J., Kraft, E., and Callis, J. (2005). Functional analysis of the RING-type ubiquitin ligase family of Arabidopsis. Plant Physiol *137*, 13-30.

Strzalka, W., Bartnicki, F., Pels, K., Jakubowska, A., Tsurimoto, T., and Tanaka, K. (2013). RAD5a ubiquitin ligase is involved in ubiquitination of Arabidopsis thaliana proliferating cell nuclear antigen. J Exp Bot *64*, 859-869.

Takahashi, H., Nozawa, A., Seki, M., Shinozaki, K., Endo, Y., and Sawasaki, T. (2009). A simple and high-sensitivity method for analysis of ubiquitination and polyubiquitination based on wheat cell-free protein synthesis. BMC Plant Biol *9*, 39.

Tan, X., Calderon-Villalobos, L.I., Sharon, M., Zheng, C., Robinson, C.V., Estelle, M., and Zheng, N. (2007). Mechanism of auxin perception by the TIR1 ubiquitin ligase. Nature *446*, 640-645.

Thrower, J.S., Hoffman, L., Rechsteiner, M., and Pickart, C.M. (2000). Recognition of the polyubiquitin proteolytic signal. EMBO J *19*, 94-102.

Tiwari, S.B., Hagen, G., and Guilfoyle, T. (2003). The roles of auxin response factor domains in auxin-responsive transcription. Plant Cell *15*, 533-543.

Trapnell, C., Roberts, A., Goff, L., Pertea, G., Kim, D., Kelley, D.R., Pimentel, H., Salzberg, S.L., Rinn, J.L., and Pachter, L. (2012). Differential gene and transcript expression analysis of RNA-seq experiments with TopHat and Cufflinks. Nat Protoc *7*, 562-578.

Trujillo, M. (2018). News from the PUB: plant U-box type E3 ubiquitin ligases. J Exp Bot *69*, 371-384.

Ulmasov, T., Murfett, J., Hagen, G., and Guilfoyle, T.J. (1997). Aux/IAA proteins repress expression of reporter genes containing natural and highly active synthetic auxin response elements. Plant Cell *9*, 1963-1971.

Ulrich, H.D., and Walden, H. (2010). Ubiquitin signalling in DNA replication and repair. Nat Rev Mol Cell Biol *11*, 479-489.

Verhage, A., Vlaardingerbroek, I., Raaymakers, C., Van Dam, N.M., Dicke, M., Van Wees, S.C., and Pieterse, C.M. (2011). Rewiring of the Jasmonate Signaling Pathway in Arabidopsis during Insect Herbivory. Front Plant Sci *2*, 47.

Verma, R., Annan, R.S., Huddleston, M.J., Carr, S.A., Reynard, G., and Deshaies, R.J. (1997). Phosphorylation of Sic1p by G1 Cdk required for its degradation and entry into S phase. Science *278*, 455-460.

Vijay-Kumar, S., Bugg, C.E., and Cook, W.J. (1987). Structure of ubiquitin refined at 1.8 A resolution. J Mol Biol *194*, 531-544.

Wang, C., Deng, L., Hong, M., Akkaraju, G.R., Inoue, J., and Chen, Z.J. (2001). TAK1 is a ubiquitin-dependent kinase of MKK and IKK. Nature *412*, 346-351.

Wang, J., Yu, H., Xiong, G., Lu, Z., Jiao, Y., Meng, X., Liu, G., Chen, X., Wang, Y., and Li, J. (2017). Tissue-Specific Ubiquitination by IPA1 INTERACTING PROTEIN1 Modulates IPA1 Protein Levels to Regulate Plant Architecture in Rice. Plant Cell *29*, 697-707.

Wang, S., Cao, L., and Wang, H. (2016). Arabidopsis ubiquitin-conjugating enzyme UBC22 is required for female gametophyte development and likely involved in Lys11-linked ubiquitination. J Exp Bot *67*, 3277-3288.

Wang, W., Yang, X., Tangchaiburana, S., Ndeh, R., Markham, J.E., Tsegaye, Y., Dunn, T.M., Wang, G.L., Bellizzi, M., Parsons, J.F., *et al.* (2008). An inositolphosphorylceramide synthase is involved in regulation of plant programmed cell death associated with defense in Arabidopsis. Plant Cell *20*, 3163-3179.

Wang, Y., Hou, Y., Gu, H., Kang, D., Chen, Z., Liu, J., and Qu, L.J. (2012). The Arabidopsis APC4 subunit of the anaphase-promoting complex/cyclosome (APC/C) is critical for both female gametogenesis and embryogenesis. Plant J *69*, 227-240.

Wang, Y.B., Hou, Y.N., Gu, H.Y., Kang, D.M., Chen, Z.L., Liu, J.J., and Qu, L.J. (2013). The Arabidopsis Anaphase-Promoting Complex/Cyclosome Subunit 1 is Critical for Both Female Gametogenesis and Embryogenesis. Journal of Integrative Plant Biology *55*, 64-74.

Wang, Z., Gerstein, M., and Snyder, M. (2009). RNA-Seq: a revolutionary tool for transcriptomics. Nat Rev Genet *10*, 57-63.

Wen, R., Newton, L., Li, G., Wang, H., and Xiao, W. (2006). Arabidopsis thaliana UBC13: implication of error-free DNA damage tolerance and Lys63-linked polyubiquitylation in plants. Plant Mol Biol *61*, 241-253.

Wen, R., Torres-Acosta, J.A., Pastushok, L., Lai, X., Pelzer, L., Wang, H., and Xiao, W. (2008). Arabidopsis UEV1D promotes Lysine-63-linked polyubiquitination and is involved in DNA damage response. Plant Cell *20*, 213-227.

Wen, R., Wang, S., Xiang, D., Venglat, P., Shi, X., Zang, Y., Datla, R., Xiao, W., and Wang, H. (2014). UBC13, an E2 enzyme for Lys63-linked ubiquitination, functions in root development by affecting auxin signaling and Aux/IAA protein stability. Plant J *80*, 424-436.

Wiborg, J., O'Shea, C., and Skriver, K. (2008). Biochemical function of typical and variant Arabidopsis thaliana U-box E3 ubiquitin-protein ligases. Biochem J *413*, 447-457.

Wickliffe, K.E., Lorenz, S., Wemmer, D.E., Kuriyan, J., and Rape, M. (2011a). The mechanism of linkage-specific ubiquitin chain elongation by a single-subunit E2. Cell *144*, 769-781.

Wickliffe, K.E., Williamson, A., Meyer, H.J., Kelly, A., and Rape, M. (2011b). K11-linked ubiquitin chains as novel regulators of cell division. Trends Cell Biol *21*, 656-663.

Wilkinson, K.D. (2005). The discovery of ubiquitin-dependent proteolysis. Proc Natl Acad Sci U S A *102*, 15280-15282.

Williamson, A., Wickliffe, K.E., Mellone, B.G., Song, L., Karpen, G.H., and Rape, M. (2009). Identification of a physiological E2 module for the human anaphase-promoting complex. Proc Natl Acad Sci U S A *106*, 18213-18218.

Williamson, B., Tudzynski, B., Tudzynski, P., and van Kan, J.A. (2007). Botrytis cinerea: the cause of grey mould disease. Mol Plant Pathol *8*, 561-580.

Wu, P.Y., Hanlon, M., Eddins, M., Tsui, C., Rogers, R.S., Jensen, J.P., Matunis, M.J., Weissman, A.M., Wolberger, C., and Pickart, C.M. (2003). A conserved catalytic residue in the ubiquitin-conjugating enzyme family. EMBO J *22*, 5241-5250.

Xu, L., Menard, R., Berr, A., Fuchs, J., Cognat, V., Meyer, D., and Shen, W.H. (2009a). The E2 ubiquitin-conjugating enzymes, AtUBC1 and AtUBC2, play redundant roles and are involved in activation of FLC expression and repression of flowering in Arabidopsis thaliana. Plant J *57*, 279-288.

Xu, P., Duong, D.M., Seyfried, N.T., Cheng, D., Xie, Y., Robert, J., Rush, J., Hochstrasser, M., Finley, D., and Peng, J. (2009b). Quantitative proteomics reveals the function of unconventional ubiquitin chains in proteasomal degradation. Cell *137*, 133-145.

Yadegari, R., and Drews, G.N. (2004). Female gametophyte development. Plant Cell *16 Suppl*, S133-141.

Yamada, K., Hara-Nishimura, I., and Nishimura, M. (2011). Unique defense strategy by the endoplasmic reticulum body in plants. Plant Cell Physiol *52*, 2039-2049.

Yan, J., Wang, J., Li, Q., Hwang, J.R., Patterson, C., and Zhang, H. (2003). AtCHIP, a U-box-containing E3 ubiquitin ligase, plays a critical role in temperature stress tolerance in Arabidopsis. Plant Physiol *132*, 861-869.

Ye, Y., and Rape, M. (2009). Building ubiquitin chains: E2 enzymes at work. Nat Rev Mol Cell Biol *10*, 755-764.

Yee, D., and Goring, D.R. (2009). The diversity of plant U-box E3 ubiquitin ligases: from upstream activators to downstream target substrates. J Exp Bot *60*, 1109-1121.

Yin, X.J., Volk, S., Ljung, K., Mehlmer, N., Dolezal, K., Ditengou, F., Hanano, S., Davis, S.J., Schmelzer, E., Sandberg, G., *et al.* (2007). Ubiquitin lysine 63 chain forming ligases regulate apical dominance in Arabidopsis. Plant Cell *19*, 1898-1911.

Yu, G., Wang, L.G., Han, Y., and He, Q.Y. (2012). clusterProfiler: an R package for comparing biological themes among gene clusters. OMICS *16*, 284-287.

Zhang, X., Dai, Y., Xiong, Y., DeFraia, C., Li, J., Dong, X., and Mou, Z. (2007). Overexpression of Arabidopsis MAP kinase kinase 7 leads to activation of plant basal and systemic acquired resistance. Plant J *52*, 1066-1079.

Zhao, Q., Tian, M., Li, Q., Cui, F., Liu, L., Yin, B., and Xie, Q. (2013). A plant-specific in vitro ubiquitination analysis system. Plant J *74*, 524-533.

Zimmermann, P., Hirsch-Hoffmann, M., Hennig, L., and Gruissem, W. (2004). GENEVESTIGATOR. Arabidopsis microarray database and analysis toolbox. Plant Physiology *136*, 2621-2632.

Zolman, B.K., Monroe-Augustus, M., Silva, I.D., and Bartel, B. (2005). Identification and functional characterization of Arabidopsis PEROXIN4 and the interacting protein PEROXIN22. Plant Cell *17*, 3422-3435.